

**A MOLECULAR DYNAMICS SIMULATION STUDY
OF MECHANICAL PROPERTIES OF DIFFERENT
CARBON NANOTUBES AND NANOCOMPOSITES**

SUBMITTED BY

NABILA TAHREEN

A Dissertation submitted to

**The Department of Industrial and Production Engineering,
Bangladesh University of Engineering and Technology,
Dhaka, Bangladesh**

**In partial fulfillment of the requirements for the degree of
M.Sc. in Industrial and Production Engineering**

September 2011

The thesis entitled as **A Molecular Dynamics Simulation study of Mechanical Properties of Different Carbon Nanotubes and Nanocomposites** submitted by Nabila Tahreen, Student No. 0409082011P, Session- April 2009, has been accepted as satisfactory in partial fulfillment of the requirement for the degree of M. Sc. in Industrial and Production Engineering on September 25, 2011.

BOARD OF EXAMINERS

1. Dr. A.K.M. Masud
Professor
Department of Industrial & Production Engineering
BUET, Dhaka
Chairman

2. Head
Department of Industrial & Production Engineering
BUET, Dhaka.
Member
(Ex-officio)

3. Dr. Abdullahil Azeem
Professor
Department of Industrial & Production Engineering
BUET, Dhaka.
Member

4. Dr. Monon Mahbub
Assistant Professor
Department of Mechanical Engineering
BUET, Dhaka.
Member

5. Dr. Mohammad Iqbal
Professor
Department of Industrial & Production Engineering
Shahjalal University of Science & Technology (SUST)
Sylhet.
Member
(External)

DECLARATION

It is hereby declared that this thesis or any part of it has not been submitted elsewhere for the award of any degree or diploma.

Nabila Tahreen

*This work is dedicated to my
loving parents*

*Quazi Fariduddin
and
Bilkis Begum*

TABLE OF CONTENTS

ABSTRACT		XIII
CHAPTER 1	INTRODUCTION	1
	Motivations	1
	Challenges	3
	Research Objectives	4
CHAPTER 2	CARBON NANOTUBES	6
2.1	History	6
2.2	Structure	9
2.3	Synthesis	10
	2.3.1 Arc Discharge	10
	2.3.2 Laser Ablation	11
	2.3.3 Chemical Vapor Deposition	11
2.4	Properties	12
	2.4.1 Electronic Properties of CNTs	12
	2.4.2 Mechanical Properties of CNTs	13
	2.4.3 Thermal Properties of CNTs	13
2.5	Some Applications of CNTs	13
CHAPTER 3	MOLECULAR DYNAMICS	16
3.1	Brief Overview of Different Simulation Method	16
3.2	Historical Background	17
3.3	Classical Mechanics	17
3.4	Integration Algorithms	20
	3.4.1 Leap-frog Algorithm	20
	3.4.2 Velocity Verlet Algorithm	21
	3.4.3 Beeman's Algorithm	21
3.5	Statistical Ensembles	21
	3.5.1 Micro-canonical Ensemble	22
	3.5.2 Canonical Ensemble	22
	3.5.3 Isothermal-isobaric Ensemble	22
3.6	Temperature	22
	3.6.1 Methods of Controlling Temperature	23
	3.6.1.1 Direct velocity scaling	23

	3.6.1.2 Berendsen method	24
	3.6.1.3 Nosé and Nosé-Hoover dynamics	24
	3.6.1.4 Andersen method	25
3.7	Pressure Control	25
	3.7.1 Methods of Controlling Pressure	25
	3.7.1.1 Berendsen method	25
	3.7.1.2 Andersen method	26
	3.7.1.3 Parrinello-Rahman method	26
CHAPTER 4	LITERATURE REVIEW	27
4.1	Forcefield	27
4.2	Periodic Boundary Condition	31
4.3	Stress	32
4.4	Strain	34
4.5	Mechanical Properties	35
4.6	Rule-of-Mixture Analysis	37
CHAPTER 5	EFFECT OF TUBE DIAMETER, LENGTH AND CHIRALITY ON MECHANICAL PROPERTIES	39
5.1	Background	39
5.2	Molecular Modeling of SWCNT	40
5.3	Molecular Dynamics Simulation of SWCNTs	42
5.4	Results and Discussion	43
CHAPTER 6	EFFECT OF RESIN ON NANOCOMPOSITES	48
6.1	Background	48
6.2	PMMA/CNT Composite System	51
	6.2.1 Building Molecular Model of Polymer Matrix	51
	6.2.2 Calculation of Mechanical Properties of the Polymer System	52
	6.2.3 Study of PMMA/CNT Composite System	53
6.3	Polystyrene (PS)/CNT Composite System	57
	6.3.1 Building Molecular Model of Polymer Matrix	57
	6.3.2 Calculation of Mechanical Properties of the Polymer System	58
	6.3.3 Study of PS/CNT Composite System	59

6.4	Nylon 6 (PA6)/CNT Composite System	62
6.4.1	Building Molecular Model of Polymer Matrix	62
6.4.2	Calculation of Mechanical Properties of the Polymer System	63
6.3.4	Study of Nylon 6/CNT Composite System	64
6.5	Polyethylene (PE)/CNT Composite System	67
6.5.1	Building Molecular Model of Polymer Matrix	67
6.5.2	Calculation of Mechanical Properties of the Polymer System	69
6.5.3	Study of PE/CNT Composite System	69
6.5.4	Experimental Evidence	72
6.6	Polypropylene (PP)/CNT Composite System	75
6.6.1	Building Molecular Model of Polymer Matrix	75
6.6.2	Calculation of Mechanical Properties of the Polymer System	76
6.6.3	Study of PP/CNT Composite System	77
6.6.4	Experimental Validation	80
6.7	Results and Discussion	82
6.7.1	PMMA/CNT Composite	82
6.7.2	PS/CNT Composite	83
6.7.3	PA6/CNT Composite	85
6.7.4	PE/CNT Composite	87
6.7.5	PP/CNT Composite	88
CHAPTER 7	CONCLUSIONS AND FUTURE WORK	90
7.1	Summary and Conclusions	90
7.2	Recommendations for Future Work	91
LIST OF REFERENCES		92

LIST OF FIGURES

Fig. 2.1: The ball like perfect structure of C60	6
Fig. 2.2: Structure of MWNT	7
Fig. 2.3: Structure of SWNT	8
Fig. 2.4: Schematic representation of the chiral vector [16]	9
Fig. 2.5: Nanotubes with different chirality	10
Fig. 2.6: MWNT bundle produced by arc discharge	10
Fig. 2.7: Crystalline structure of SWNTs obtained with laser vaporization [3]	11
Fig. 2.8: CVD grown CNTs	12
Fig. 3.1: Maxwell-Boltzmann distribution of velocity of water at various temp.	23
Fig. 4.1: Periodic boundary condition	31
Fig. 4.2: Diagram of parameters used to compute stresses in the simulations [46]	32
Fig. 4.3: Definitions of the strains applied to the composites [46]	34
Fig. 5.1: Molecular model of armchair SWNTs with different chirality	41
Fig. 5.2: Molecular model of zigzag SWNTs with different chirality	42
Fig. 5.3: Variation of MD simulated Young's modulus, bulk modulus and shear modulus of armchair SWNTs with increasing radius	45
Fig. 5.4: Variation of MD simulated Young's modulus, bulk modulus and shear modulus of zigzag SWNTs with increasing radius	45
Fig. 5.5: Variation of MD simulated Young's modulus of both armchair and zigzag SWNTs with increasing tube length	46
Fig. 6.1: Computer constructed polymer chain of PMMA	51
Fig. 6.2: PMMA amorphous cell	52
Fig. 6.3: CNT (6, 6) reinforced PMMA matrix	54
Fig. 6.4: Radial distribution function (RDF) for the PMMA/CNT composite system	54
Fig. 6.5: Computer constructed polymer chain of PS	57
Fig. 6.6: PS amorphous cell	58
Fig. 6.7: CNT (6, 6) reinforced PS matrix	60
Fig. 6.8: Radial distribution function (RDF) for the PS/CNT composite system	60
Fig. 6.9: Computer constructed polymer chain of Nylon 6 (PA6)	62
Fig. 6.10: Amorphous Nylon 6 cell	63
Fig. 6.11: CNT (6, 6) reinforced Nylon 6 matrix	65

Fig. 6.12: Radial distribution function (RDF) for the PA6/CNT composite system	65
Fig. 6.13: Computer constructed polymer chain of PE	68
Fig. 6.14: Amorphous PE cell	68
Fig. 6.15: CNT (6, 6) reinforced PE matrix	70
Fig. 6.16: Radial distribution function (RDF) for PE/CNT composite	71
Fig. 6.17: Experimental data of elastic modulus Vs. CNT volume fraction plotted in a graph	73
Fig. 6.18: Computer constructed polymer chain of PP	76
Fig. 6.19: Amorphous PP cell	76
Fig. 6.20: CNT (6, 6) reinforced PP matrix	78
Fig. 6.21: Radial distribution function (RDF) for PP/CNT composite system	79
Fig. 6.22: Mechanical reinforcement: melt-rheological investigations showing temperature dependence of Tensile modulus (E'') and $\tan\delta$ [111]	81
Fig. 6.23: Axial Young's modulus chart of CNT reinforced composite compared with PMMA polymer matrix without nanotubes and the results from the rule-of-mixture	81
Fig. 6.24: Transverse Young's modulus chart of CNT reinforced composite compared with PMMA polymer matrix without nanotubes and the results from the rule-of-mixture	82
Fig. 6.25: Axial Young's modulus chart of CNT reinforced composite compared with PS polymer matrix without nanotubes and the results from the rule-of-mixture	83
Fig. 6.26: Transverse elastic modulus chart of CNT reinforced composite compared with PS polymer matrix without nanotubes and the results from the rule-of-mixture	84
Fig. 6.27: Axial Young's modulus chart of CNT reinforced composite compared with Nylon 6 polymer matrix without nanotubes and the results from the rule-of-mixture	85
Fig. 6.28: Transverse elastic modulus chart of CNT reinforced composite compared with Nylon 6 polymer matrix without nanotubes and the results from the rule-of-mixture	86
Fig. 6.29: Axial Young's modulus chart of the CNT reinforced composite compared with PE polymer matrix without nanotubes	87

Fig. 6.30: Axial Young's modulus chart of the CNT reinforced composite compared with the results from rule of mixture and experiment	87
Fig. 6.31: Axial Young's modulus chart of the CNT reinforced composite compared with PP polymer matrix without nanotubes	88
Fig. 6.32: Axial Young's modulus chart of the CNT reinforced composite compared with the results from rule of mixture and experiment	89

LIST OF TABLES

Table 4.1: Force-field degrees of freedom	27
Table 5.1: Summary of numerical values for number of atoms, radius and length of different armchair and zigzag SWNTs	43
Table 5.2: Summary of numerical results for elastic modulus, bulk modulus, shear modulus and Poisson's ratio of different SWNTs	44
Table 6.1: Simulated properties of amorphous PMMA	53
Table 6.2: Simulated properties of PMMA/CNT composite system	55
Table 6.3: Summary of numerical results for elastic modulus of PMMA/CNT composite system	55
Table 6.4: Simulated properties of amorphous PS	59
Table 6.5: Simulated properties of PS/CNT composite system	61
Table 6.6: Summary of numerical results for elastic modulus of PS/CNT composite system	61
Table 6.7: Simulated properties of amorphous Nylon 6	64
Table 6.8: Simulated properties of Nylon 6/CNT composite system	66
Table 6.9: Summary of numerical results for elastic modulus of PA6/CNT composite system	66
Table 6.10: Simulated properties of semi-crystalline PE	69
Table 6.11: Simulated properties of PE/CNT composite system	71
Table 6.12: Summary of numerical results for elastic modulus of PE/CNT composite system	72
Table 6.13: Mechanical properties of CNT–HDPE nano-composites [108]	73
Table 6.14: Simulated properties of amorphous PP	77
Table 6.15: Simulated properties of PP/CNT composite system	79
Table 6.16: Summary of numerical results for elastic modulus of PP/CNT composite system	80

ACKNOWLEDGEMENT

I am heartily thankful to my respected supervisor, Dr. A.K.M. Masud, Professor of the Department of Industrial and Production Engineering (IPE), whose encouragement, guidance and belief in me enabled me to complete the research work. I consider it to be a great honor to work under him.

I am deeply indebted to my committee members Dr. Abdullahil Azeem, Dr. Monon Mahbub and Dr. Mohammad Iqbal for being on my M.Sc. thesis committee and providing valuable suggestions to improve the content of this thesis. A special thank goes to Dr. Monon Mahbub for his lively and insightful discussions. I appreciate the help of Abdullah Al Mamun, lecturer of IPE Department, during the setup of the molecular dynamics (MD) simulation software.

Most of all, I thank my parents, for their unconditional love and continuous support through all these years. I know it is their unprecedented sacrifice and divine love that have brought me where I am now.

Lastly, I offer my regards and blessings to all of those who supported me in any respect during the completion of the project.

ABSTRACT

Carbon nanotube is promising to revolutionize several fields in material science and is a major component of nanotechnology. Nanotubes have a wide range of unexplored potential applications in various technological areas due to their superior mechanical, thermal and electrical properties. In light of these properties, CNTs are expected to be introduced into a wide variety of new materials aimed at applications for various fields, such as high performance composites, biological and chemical sensors, magnetic recording, nano-electronic devices and flat panel displays.

In this work, carbon nanotubes of different molecular architectures have been simulated using molecular dynamics simulation. A number of mechanical properties like elastic modulus, bulk modulus, shear modulus and Poisson's ratio were analyzed to explain the effect of tube radius, tube length and tube chirality on these properties. The numerical results reveal that the value of the Young's modulus is independent of the tube length, but decreases significantly with increasing tube radius. The results also indicate that the Young's modulus is insensitive to tube chirality.

Polymer/nanotube composites have attracted a lot of attention because the polymer properties are significantly improved. In particular, intensive efforts have been directed toward synthesizing, characterizing, and understanding polymer/CNT composites. Recent investigation has revealed many novel properties of polymer/CNT systems.

In this paper, As an effort to explore the effective use of carbon nanotubes as a reinforcing material for advanced nanocomposites with polymer matrices, single-walled carbon nanotubes (MWNTs) were incorporated into five different polymer materials i.e. Polymethyl methacrylate (PMMA), Polystyrene (PS), Polyamide 6 (PA6), Polyethylene (PE) and Polypropylene (PP). Molecular dynamics (MD) simulations were used to predict the properties of these nanocomposites. The properties of interest were Young's modulus, bulk modulus, shear modulus and compressibility. The Young's modulus of polymer/CNT

composites in the axial direction increases comprehensively when the volume fraction of the CNTs is about 12-16%. The enhanced elastic modulus, bulk modulus and shear modulus of the nanocomposites suggests a strong possibility for the potential use of these nanocomposites in industrial applications. The force-field used in the MD simulation was COMPASS, and COMPASS clearly gave accurate values for the density and moduli of the amorphous polymer matrices (before incorporating CNT) as compared to experiment. In fact, the density predicted by COMPASS was in excellent agreement with reported experimental values of amorphous polymers. Finally, the effective Young's moduli of these CNT-based composites are compared with values obtained using rule-of-mixture. In case of PE and PP nanocomposites the simulation results are also compared with experimentally available values. The results are in disagreement revealing the fact that rule of-mixture is not an excellent approximate in estimating the overall response of the composite system since it assumes perfect bonding between fiber and matrix. MD simulation gives a close agreement to calculate Young's modulus of CNT based composite since the results are in good agreement with experimentally available data.

CHAPTER 1

INTRODUCTION

Motivations

The question that is very difficult to find a consistent answer for is “What is NANO?”

Generally this term is referred to nanotechnology, which deals with structures with a size of 100 nanometers or smaller. Nanotechnology is entering a new threshold of many possibilities to change the way we see things. There are materials larger than 100 nm that can pass unimpeded through human skin. Objects that are smaller than 100 nm need to be less than 70 nm before the dominant force that will hold them to a surface becomes the van der Waals force. The ability of a Gecko to climb walls and walk on ceilings is due to minute hairs attached to small hairs connected to their limbs. The thickness of the final hairs is much less than 100 nm and it is the properties of this small size that provide adhesion through the van der Waals force. The properties of gold nano-particles less than 20 nm in size provide the ability to reflect different color, which color is based on the size of the particles. Aluminum nano-particles become extremely reactive when their size is less than 20 nm. There are numerous examples of apparent change in observer properties of particles when their size is very small. This is an attractive aspect of nano. These apparently new properties provide promise for new applications that will change the world.

According to the Project on Emerging Technologies (2005), “The National Science foundation predicts that the global marketplace for goods and services using nanotechnologies will grow to \$1 trillion dollars by 2015”. A majority of the work is being done is in the health field, with the promise to revolutionize the treatment of many diseases. This new technology will provide many applications that people will experience in everyday life and will eventually improve the quality of life. This is only the start of the developments of future products. Silver nano particles are being incorporated into wound dressings. The addition of these nano-particles promotes the healing of wounds.

Gold nano-particles are being attached to molecules that have a tendency to attaching themselves to cancer cells. With the molecule attached to a cancer cell, the heating of the gold will destroy the cancer cells. There are many efforts in the health sciences to examine means of improving treatment of illness by employing various types of nanotechnology.

Carbon is a very interesting element. Its electronic structure is defined as $1s^1 2s^2 2p^2$ and the 2s electrons (4 electrons) are generally very involved in molecular bonding. This enables carbon to assemble into a wide variety of bonding configurations and allotropes as different as the brittle, hard, and insulating diamond, or the lubricant semimetal graphite.

Bucky structure were first brought to the attention of the world in 1985 when Dr. Richard Smalley and his coworkers discovered a new geometrical form of carbon, the buckminsterfullerene C_{60} , a cage-like structure of carbon atoms composed of hexagonal and pentagonal faces [1]. Over the last two decades, interest for these structures has grown, in both the research and the business communities, and sparked the discovery of carbon nanotubes (CNTs) by Ijima and his team in 1991 [2]. Dr. Smalley's work was subsequently awarded the Nobel Prize in chemistry for his work in 1996, and CNTs are today considered as one of the most considerable discovery of modern science.

After their discovery, carbon nanotubes started generating a large amount of interest in nano-scale materials research. The research was initially focused on electronic properties, due to the very extraordinary electronic structure of these new materials. Academic and industrial research thus focused on developing applications such as flat panel display, lamps, and X-ray or microwave emission sources [3].

As the technology matured, however, the possibility of using CNTs in other areas started to emerge. Nano sized mechanical devices, sensors and probes, gas storage devices or electrochemical applications such as artificial muscles or Lithium batteries all were possible applications for CNTs [4]. More attention started to be paid, also, at the fact that CNTs have mechanical properties superior to most materials. These mechanical properties have lead to an increasing amount of research being conducted in the area of nano electromechanical devices and nanotube-reinforced composite materials. In fact, nanotube based composite materials stand today as one of the major possible application for CNTs. The use of such new materials could be found in both structural and

multifunctional applications [3]. CNTs are being applied in automotive manufacturing. Toyota is replacing steel bumpers with a composite that includes CNTs. The result of this replacement is that the bumpers are lighter (fuel saving) and eight times stronger (less prone to damage). CNTs are being employed to make sports equipment stronger and lighter. Both tennis and baseball have benefited from the incorporation of CNTs. The tennis racquet incorporating CNTs is both lighter and stronger.

Baseball bats benefit with improved strength and lightness. The fact that these items are more expensive is offset by their performance and improved longevity.

CNT composites could also offer multi-functional properties, such as tailored electrical conductivity, electromagnetic interference shielding, electrostatic discharge protection or modified optoelectronic properties. Use of the non-linear optical and optical limiting properties of nanotubes has also been reported for photovoltaic application CNT based composites also show great potential for biomedical applications due to their bio-inertness and high strength. The current generation of composites used for replacement of bone and teeth are crude mixtures of filler particles that have inadequate mechanical properties.

Researchers from Rensselaer Polytechnic Institute found that composites made from MWNTs and a biodegradable polymer (polylactic acid) act more efficiently than carbon fibers for osteo-integration (growth of bone cells), especially under electrical stimulation of the composites.

Motivated by the numerous possible applications of CNTs in composite materials, this research focuses on answering some of the fundamental questions related to CNTs and the development of nanotube based composites. Specifically, it tries to understand, at the molecular level, useful mechanical and physical properties of these composites. This is accomplished thru MD simulation.

Challenges

The superior mechanical behavior of the nanotubes alone does not assure the superior mechanical properties of the resulting composite materials. CNTs unique electronic and mechanical properties in general are strongly dependent on their material structures and

bonding form, including tube length, diameter, and inclination angle. Using carbon nanotubes (CNT) as reinforcing agents to design and fabricate strong composites with desirable mechanical properties needs thorough understanding of the mechanical behavior of such nanotube [5]. The exact knowledge of the stiffness or strength of the nanotubes is important for their use as the reinforcements in the next generation composites since Young's modulus and tensile strength varies widely depending on the different CNT chiralities or lengths and different potentials employed to define the C–C bond in the plane of the grapheme sheets.

Carbon nanotubes (CNTs) are promising additives to polymeric materials due to the potential for their enhancement of the structural, mechanical and electronic properties of the resulting composite [6]. However, improvements in properties are by no means guaranteed, and the results are often sensitive to the particular polymer chosen, in addition to the quantity and quality of CNTs used in the composite. Mechanical properties widely vary depending upon the type of resin used in the particular nanocomposites. If we attempt to trace what controls the performance of materials, we can identify that properties of materials are largely dictated by the atomic structure, composition, microstructure, defects and interfaces in materials [7]. As a result, it is very important to quantitatively understand the mechanics and physics of nano-structured materials, and only then we can effectively employ them in multi-scale material design.

While theoretical predictions certainly suggest nano materials should offer exclusive material properties, experiments on nano materials, however, often showed a diverse pool of results [8]. Processing difficulties, unavailability of characterization tools and techniques, and mostly our immature knowledge in this field are often considered as the reasons why there is such a disparity between prediction and reality.

Research Objectives

The main focus of the present research is to obtain a quantitative understanding on the structural formation, structural stability, resulting mechanical and physical properties of different nano-structured materials using atomistic modelling and simulations. The objectives are:

- To investigate different mechanical properties (Young's modulus, bulk modulus, shear modulus, Poisson's ratio) of both armchair and zigzag nanotubes of different diameter, length and chirality.
- To investigate different mechanical properties (Young's modulus, bulk modulus, shear modulus, Poisson's ratio and compressibility) of different amorphous polymers and polymer/carbon nanotube composites i.e. the effect of resin on nanocomposites.

This thesis, however, will give possible suggestion of using CNTs to develop advanced materials.

CHAPTER 2

CARBON NANOTUBES

2.1 History

In 1985, Dr. Richard Smalley and his coworkers discovered a new geometrical form of carbon, the buckminsterfullerene C₆₀ [1]. The C₆₀ is a ball-like structure of carbon atoms composed of hexagonal and pentagonal faces, as shown in Figure 2.1. For their discovery, Richard Smalley, Robert Curl and Harry Kroto were awarded the Nobel Prize in 1996.

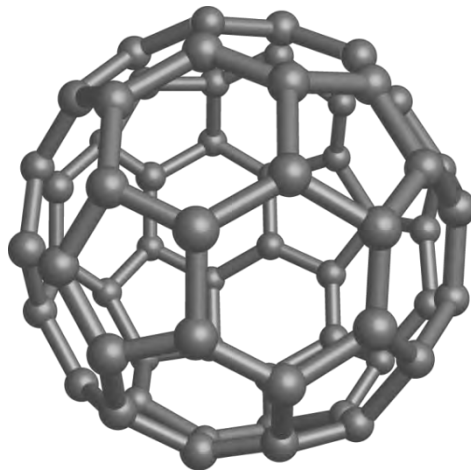


Fig. 2.1: The ball like perfect structure of C₆₀

In 2006, Marc Monthieux and Vladimir Kuznetsov described the interesting and often misstated origin of the carbon nanotube [10]. Academic and popular literature generally attributes the discovery of carbon nanotubes to Sumio Iijima of NEC in 1991 [2]. The history of nanometer sized graphitic carbon tubes, however, dates as far back as 1952. In that year, Radushkevich et al. published clear images of 50 nanometer diameter tubes made of carbon in the Russian Journal of Physical Chemistry [11]. It remains likely that carbon nanotubes were produced before 1952, but the invention of the transmission electron microscope (TEM) allowed for the direct visualization of these structures.

Mostly, the discovery went unnoticed in the West because of limited information exchange during the Cold War and because the article was published in the Russian language. Later on, in 1976, a paper published by Oberlin et al. clearly showed hollow carbon fibers with nanometer-scale diameters using a vapor-growth technique [12]. Also, in 1987, Howard G. Tennent of Hyperion Catalysis was issued a U.S. patent for the production of "cylindrical discrete carbon fibrils" with a "constant diameter between about 3.5 and about 70 nanometers..., length 102 times the diameter, and an outer region of multiple essentially continuous layers of ordered carbon atoms and a distinct inner core..." [13]. In more recent years, Endo has started being credited with discovering carbon nanotubes, and Iijima has been credited for elucidating their structure.

Either way, in 1991, the discovery by scientists at NEC corporation is what created the interest in research that is now associated with carbon nanotubes. They discovered that graphitic carbon "needles" grew on the negative carbon electrode of the arc-discharge apparatus used for the mass production of C_{60} [2]. The needles ranged up to 1 mm in length and consisted of nested concentric cylinders of rolled graphite sheets. An example of such structures is shown in Figure 2.2. These are generally referred to as multi-walls carbon nanotubes (MWNTs).

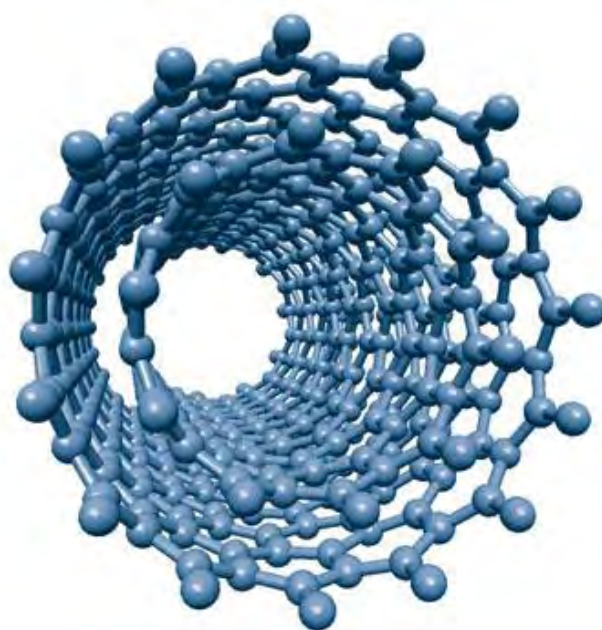


Fig. 2.2: Structure of MWNT

A short time later, Thomas Ebbesen and Pulickel Ajayan, from Iijima's lab, showed how nanotubes could be produced in bulk quantities by varying the arc evaporation conditions [14].

Finally, a major event in the development of carbon nanotubes (CNT) was the synthesis in 1993 of single-layer nanotubes [15]. The standard arc-evaporation method produces only multilayered tubes. It was found that addition of metals such as cobalt to the graphite electrodes resulted in extremely fine tube with single-layer walls. An example of single wall carbon nanotube (SWNT) is shown in Figure 2.3.

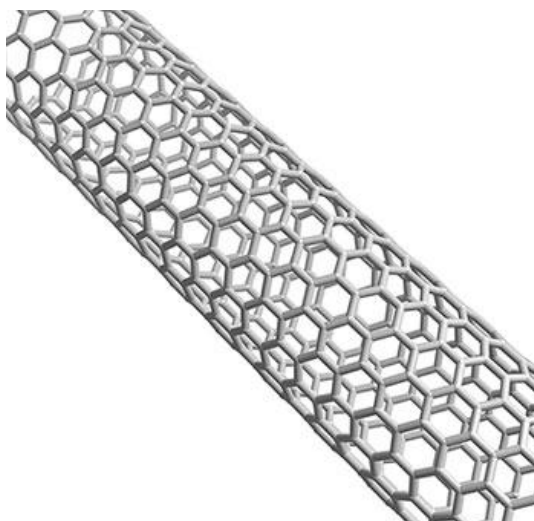


Fig. 2.3: Structure of SWNT

Since then, these intriguing structures have sparked much excitement and a large amount of research has been dedicated to their understanding. In fact, these findings paved the way to an explosion of research into the physical and chemical properties of carbon nanotubes in laboratories all over the world. Furthermore, the relatively wide availability of these structures enabled experimentalists to test some of the theoretical predictions which have been made about nanotube properties. Currently, however, the physical properties are still being discovered and disputed.

2.2 Structure

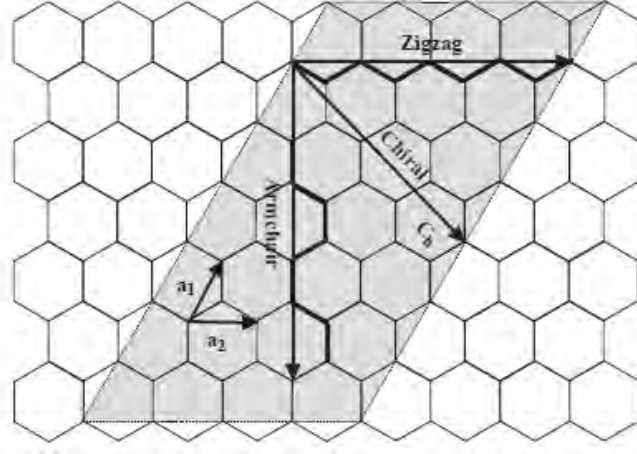


Fig. 2.4: Schematic representation of the chiral vector [16]

A SWNT can be visualized as a graphite sheet that has been rolled into a hollow cylinder. So the structure of SWNT can be described by the manner in which the graphite sheet is rolled into a tube (Fig. 2.4). To describe the structure, a chiral vector is defined as [16]

$$\mathbf{C}_h = n\mathbf{a}_1 + m\mathbf{a}_2 \quad (1)$$

where a_1 and a_2 are two unit vectors in a 2D graphite lattice. n and m are two integers. A particular integer pair (n, m) defines a chiral vector C_h , which uniquely defines the way of sheet rolling. If $n \neq 0$; $m = 0$ or $(n, 0)$; the SWNT is named a „zigzag“ SWNT. If $n = m$ or (n, n) , the SWNT is called an „armchair“ SWNT. In all other cases, the SWNT is called a „chiral“ SWNT.

The relationship between the integers (n, m) and the nanotube radius, r , and chiral angle, θ is given by

$$r = \sqrt{3}a_{c-c}(m^2 + mn + n^2)^{1/2} / 2\pi \quad (2)$$

$$\theta = \tan^{-1}[\sqrt{3}m / (m + 2n)] \quad (3)$$

where a_{c-c} is the length of the C–C bond.

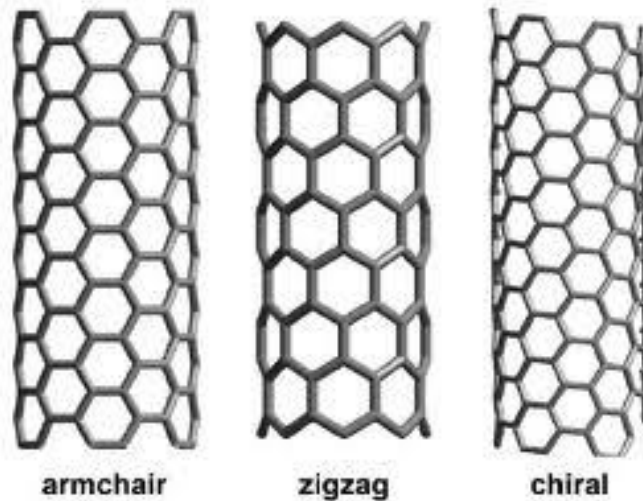


Fig. 2.5: Nanotubes with different chirality

2.3 Synthesis

2.3.1 Arc Discharge

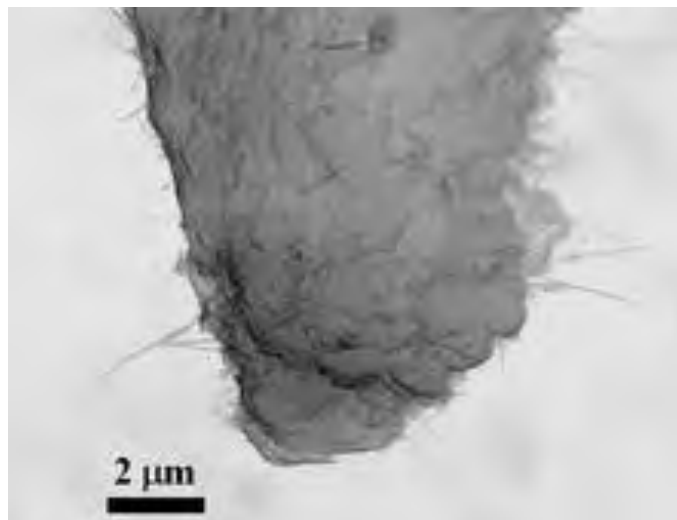


Fig. 2.6: MWNT bundle produced by arc discharge

Arc discharge [17], initially used to produce C_{60} fullerenes, is the most common and easiest way to produce CNTs. This method creates CNTs through arc-vaporization of two carbon rods placed end to end, separated by approximately 1 mm, in an enclosure that is usually filled with inert gas at low pressure. A direct current of 50 to 100 A, driven by a potential difference of approximately 20 V creates a high temperature discharge between

the two electrodes. The discharge vaporizes the surface of one of the carbon electrodes and forms a small rod-shaped deposit on other electrode.

2.3.2 Laser Ablation

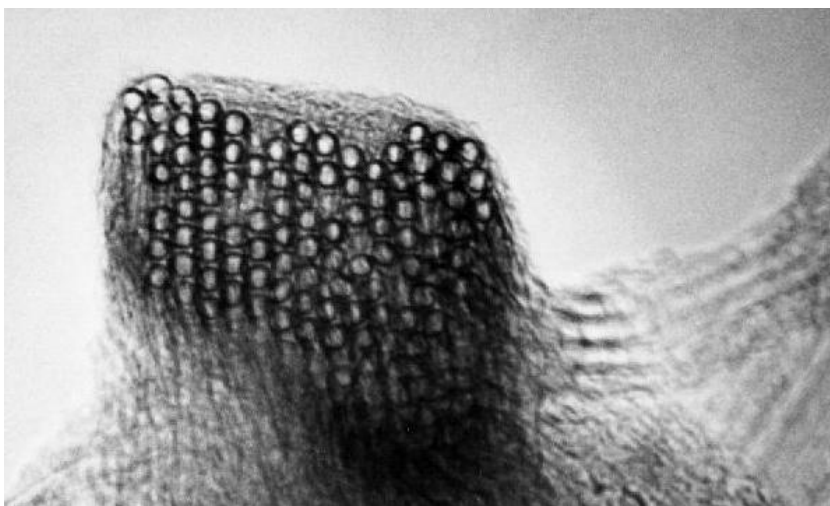


Fig. 2.7: Packed crystalline structure of SWNTs obtained with laser vaporization [3]

In Laser ablation [18] laser vaporization pulses were followed by a second pulse, to vaporize the target more uniformly. The use of two successive laser pulses minimizes the amount of carbon deposited as soot. The second laser pulse breaks up the larger particles ablated by the first one, and feeds them into the growing nanotubes structure. The material produced by this method appears as a mat of “ropes”, 10-20 nm in diameter and upto 100 μm or more in length.

2.3.3 Chemical Vapor Deposition

Chemical Vapor Deposition [19] of hydrocarbons over a metal catalyst is a classical method that has been used to produce various carbon materials like carbon fibers and filaments. Large amount of CNTs can be formed by catalytic CVD of acetylene over cobalt and iron catalysts supported on silica or zeolite. High yields of single walled nanotubes have been obtained by catalytic decomposition of H_2/CH_4 mixture all over well dispersed metal particles such as cobalt, nickel and iron on magnesium oxide at 1000° C.

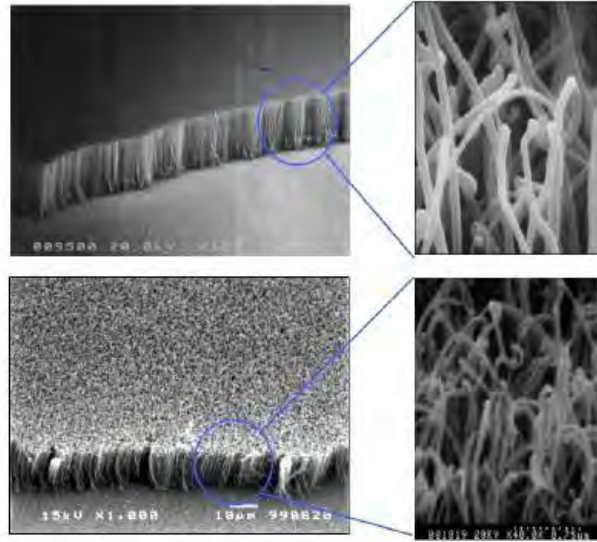


Fig. 2.8: CVD grown CNTs

The reduction produces very small transition metal particles at a temperature of usually $>800^{\circ}\text{C}$. The decomposition of CH_4 over the freshly formed nano-particles prevents their further growth and thus results in a very high proportion of SWNTs and few MWNTs.

2.4 Properties

2.4.1 Electronic Properties of CNTs

The nanometer dimensions of the CNTs, together with the unique electronic structure of a graphene sheet, make the electronic properties of these one-dimensional structures highly unusual. The electronic properties of the CNTs are very sensitive to their geometric structure. Although graphene is a zero-gap semiconductor, the CNTs can be metals or semiconductors with different sized energy gaps, depending very sensitively on the diameter and helicity of the tubes, i.e. on the indices (n,m) . The general rules for the metallicity of the SWNTs are as follows: (n,n) tubes are metals; (n,m) tubes with $n - m = 3j$, where j is a non-zero integer, are very tiny gap semiconductors; and all others are large-gap semiconductors. The $n - m = 3j$ tubes would all be metals but, because of tube curvature effects, a tiny gap opens for the case that j is non-zero. Hence, CNTs come in three varieties: large gap, tiny gap and zero gap. The (n,n) tubes, also known as armchair tubes, are always metallic. As the tube radius, R , increases, the band gaps of the large-gap and tiny-gap varieties decrease with a $1/R$ and $1/R^2$ dependence, respectively. Thus, for

most experimentally observed carbon nanotube sizes, the gap in the tiny-gap variety, which arises from curvature effects, is so small that, for most practical purposes, all the $n-m = 3j$ tubes can be considered as metallic at room temperature. Thus, a (7, 1) tube would be metallic, whereas a (8, 0) tube would be semiconducting; the (5, 5) armchair tube would always be metallic [20].

2.4.2 Mechanical Properties of CNTs

The carbon-carbon chemical bond in a graphene layer is probably the strongest chemical bond in an extended system known in nature. Since CNTs are nothing but seamlessly rolled-up graphene layers, from the time of their discovery it has been speculated that these nanostructures have exceptional mechanical properties, and to quantify these properties has become a topic of great interest in the field of nanotechnology. Many of the envisaged applications of nanotubes, such as composite reinforcement or lubrication, are related in one way or another to their mechanical properties, and therefore a great deal of experimental and theoretical studies have been devoted to their characterization [20].

2.4.3 Thermal Properties of CNTs

In graphite, the thermal conductivity is generally dominated by phonons, and limited by the small crystallite size within a sample. The apparent long-range crystallinity of nanotubes and long phonon mean free path led to the speculation (Ruoff & Lorents 1995) that the longitudinal thermal conductivity of nanotubes could possibly exceed the in-plane thermal conductivity of graphite—the material, together with diamond, that has the highest 3D thermal conductivity. The thermal conductivity, along with the specific heat, provides a sensitive tool for probing the interesting low-energy phonon structure of nanotubes, and also has the potential for practical applications that exploit the high thermal conductivity of these nanostructures [20].

2.5 Some Applications of CNTs

- Nanotubes bound to an antibody that is produced by chickens have been shown to be useful in lab tests to destroy breast cancer tumors. The antibody carrying nanotubes are attracted to proteins produced by a one type of breast cancer cell.

Then the nanotubes absorb light from an infrared laser, incinerating the nanotubes and the tumor they are attached to.

- Lightweight windmill blades are made with an epoxy containing carbon nanotubes. The strength and low weight provided by the use of nanotube filled epoxy allows longer windmill blades to be used. This increases the amount of electricity generated by each windmill.
- Aircraft is using carbon nanotubes to increase strength and flexibility in highly stressed components.
- Nanotube is used as electrodes in thermo-cells that generate electricity from waste heat.
- Inexpensive nanotube based sensor detects bacteria in drinking water. Antibodies sensitive to the particular bacteria are bound to the nanotubes, which are then deposited onto a paper strip. When the bacteria is present it attaches to the antibodies, changing the spacing between the nanotubes and the resistance of the paper strip containing the nanotubes.
- Carbon nanotubes, bucky-balls and polymers are combined to produce inexpensive solar cells that can be formed by simply painting a surface.
- A lightweight, low power anti-icing system is using carbon nanotubes in a layer coated onto aircraft wing surfaces.
- Gold tipped carbon nanotubes are used to trap oil drops polluting water.
- Building transistors from carbon nanotubes to enable minimum transistor dimensions of a few nanometers and developing techniques to manufacture integrated circuits are built with nanotube transistors.
- Using nanotubes as a cellular scale needle to deliver quantum dots and proteins into cancer cells.
- Ultra-capacitors are using nanotubes that may do even better than batteries in hybrid cars.
- Stronger bicycle components are made by adding carbon nanotubes to a matrix of carbon fibers.
- Improve the healing process for broken bones by providing a carbon nanotube scaffold for new bone material to grow on.
- Sensors are using carbon nanotube detection elements capable of detecting a range of chemical vapors. These sensors depend upon the fact that the resistance of a carbon nanotube changes in the presence of a chemical vapor.

- Static dissipative plastic molding compounds containing nanotubes can be used to make parts such as automobile fenders that can be electro-statically painted.
- Strong, lightweight composites of carbon nanotubes and other materials can be used to build lightweight spacecraft.
- Cables made from carbon nanotubes are strong enough to be used for the Space Elevator to drastically reduce the cost of lifting people and materials into orbit.
- Carbon nanotubes are used to direct electrons to illuminate pixels, resulting in a lightweight, millimeter thick "nano-emissive" display panel.
- Printable electronics devices are using nanotube "ink" in inkjet printers
- Transparent, flexible electronics devices are using arrays of nanotubes.

CHAPTER 3

MOLECULAR DYNAMICS

3.1 Brief Overview of Different Simulation Method

Computer simulation is a powerful and modern tool for solving scientific problems as numerical experiments can be performed for new materials without synthesizing them. One of the aims of computer simulation is to reproduce experiment to elucidate the invisible microscopic details and further explain experiments. On the other hand, simulation can also be used as a useful predictive tool. The most widely used simulation methods for molecular systems are Monte Carlo, Brownian dynamics and molecular dynamics [21].

The Monte Carlo method is a stochastic strategy that relies on probabilities (Sadus, 1999). The Monte Carlo sampling technique generates large numbers of configurations or microstates of equilibrated systems by stepping from one microstate to the next in a particular statistical ensemble. Random changes are made to the positions of the species present, together with their orientations and conformations where appropriate. Quantities of interest can be averaged over these microstates. The advantages of the Monte Carlo simulation technique include the ease of extending it to simulate different ensembles, flexibility in the choice of sampling functions and the underlying matrix or trial move which must satisfy the principle of microscopic reversibility as well as timesaving as only the potential energy is required.

Brownian dynamics is an efficient approach for simulations of large polymer molecules or colloidal particles in a small molecule solvent. In this approach, the solvent is treated as a viscous continuum which dissipates energy as macromolecules or particles move through it. The Brownian motion of the macromolecules produced by random collisions with solvent molecules is mimicked by a stochastic force generated by pseudo-random numbers.

Molecular dynamics is the most detailed molecular simulation method which computes the motions of individual molecules. Coupled Newton's equations of motion, which

describe the positions and momenta, are solved for a large number of particles in an isolated cluster or in the bulk using periodic boundary conditions. The equations of motion for these particles which interact with each other via intra- and inter-molecular potentials can be solved accurately using various numerical integration methods such as the common predictor-corrector or Verlet methods. Molecular dynamics efficiently evaluates different configurational properties and dynamic quantities which cannot generally be obtained by Monte Carlo.

3.2 Historical Background

The molecular dynamics method was first introduced by Alder and Wainwright in the late 1950's to study the interactions of hard spheres [22]. Many important insights concerning the behavior of simple liquids emerged from their studies. The next major advance was in 1964, when Rahman carried out the first simulation using a realistic potential for liquid argon [23]. The first molecular dynamics simulation of a realistic system was done by Rahman and Stillinger in their simulation of liquid water in 1974 [24]. The first protein simulations appeared in 1977 with the simulation of the bovine pancreatic trypsin inhibitor (BPTI) [25]. Today in the literature, one routinely finds molecular dynamics simulations of solvated proteins, protein-DNA complexes as well as lipid systems addressing a variety of issues including the thermodynamics of ligand binding and the folding of small proteins. The number of simulation techniques has greatly expanded; there exist now many specialized techniques for particular problems, including mixed quantum mechanical - classical simulations that are being employed to study enzymatic reactions in the context of the full protein. Molecular dynamics simulation techniques are widely used in experimental procedures such as X-ray crystallography and NMR structure determination.

3.3 Classical Mechanics

The molecular dynamics simulation method is based on Newton's second law or the equation of motion, $F=ma$, where F is the force exerted on the particle, m is its mass and a is its acceleration. From knowledge of the force on each atom, it is possible to determine the acceleration of each atom in the system. Integration of the equations of motion then yields a trajectory that describes the positions, velocities and accelerations of

the particles as they vary with time. From this trajectory, the average values of properties can be determined. The method is deterministic; once the positions and velocities of each atom are known, the state of the system can be predicted at any time in the future or the past.

Newton's equation of motion is given by [26],

$$F_i = m_i a_i$$

where F_i is the force exerted on particle i , m_i is the mass of particle i and a_i is the acceleration of particle i . The force can also be expressed as the gradient of the potential energy,

$$F_i = -\nabla_i V$$

Combining these two equations yields,

$$-\frac{dV}{dr_i} = m_i \frac{d^2 r_i}{dt^2}$$

where V is the potential energy of the system. Newton's equation of motion can then relate the derivative of the potential energy to the changes in position as a function of time.

$$F = ma = m \cdot \frac{dv}{dt} = m \cdot \frac{d^2 x}{dt^2}$$

Taking the simple case where the acceleration is constant,

$$a = \frac{dv}{dt}$$

we obtain an expression for the velocity after integration,

$$v = at + v_0$$

and since

$$v = \frac{dx}{dt}$$

we can once again integrate to obtain [27]

$$x = v.t + x_0$$

Combining this equation with the expression for the velocity, we obtain the following relation which gives the value of x at time t as a function of the acceleration, a , the initial position, x_0 , and the initial velocity, v_0 .

$$x = a.t^2 + v_0.t + x_0$$

The acceleration is given as the derivative of the potential energy with respect to the position, r ,

$$a = -\frac{1}{m} \frac{dE}{dr}$$

Therefore, to calculate a trajectory, one only needs the initial positions of the atoms, an initial distribution of velocities and the acceleration, which is determined by the gradient of the potential energy function. The equations of motion are deterministic, e.g., the positions and the velocities at time zero determine the positions and velocities at all other times, t .

The initial distribution of velocities are usually determined from a random distribution with the magnitudes conforming to the required temperature and corrected so there is no overall momentum, i.e.,

$$P = \sum_{i=1}^N m_i v_i = 0$$

The velocities, v_i , are often chosen randomly from a Maxwell-Boltzmann or Gaussian distribution at a given temperature, which gives the probability that an atom i has a velocity v_x in the x direction at a temperature T .

$$p(v_{ix}) = \left(\frac{m_i}{2\pi k_B T} \right)^{1/2} \exp \left[-\frac{1}{2} \frac{m_i v_{ix}^2}{k_B T} \right] \quad (4)$$

The temperature can be calculated from the velocities using the relation [28],

$$T = \frac{1}{(3N)} \sum_{i=1}^N \frac{|p_i|}{2m_i} \quad (5)$$

where N is the number of atoms in the system.

3.4 Integration Algorithms

The potential energy is a function of the atomic positions ($3N$) of all the atoms in the system. Due to the complicated nature of this function, there is no analytical solution to the equations of motion; they must be solved numerically.

Numerous numerical algorithms have been developed for integrating the equations of motion like leap-frog algorithm [29], velocity verlet algorithm [30], Beeman's algorithm [31]. Molecular dynamics is usually applied to a large model. Energy evaluation is time consuming and the memory requirement is large. To generate the correct statistical ensembles, energy conservation is also important. Thus, the basic criteria for a good integrator for molecular simulations are as follows:

- It should be fast, ideally requiring only one energy evaluation per time-step.
- It should require little computer memory.
- It should permit the use of a relatively long time-step.
- It must show good conservation of energy.

3.4.1 The Leap-Frog Algorithm

$$\begin{aligned} r(t + \delta t) &= r(t) + v\left(t + \frac{1}{2}\delta t\right)\delta t \\ v\left(t + \frac{1}{2}\delta t\right) &= v\left(t - \frac{1}{2}\delta t\right) + a(t)\delta t \end{aligned} \quad (6)$$

In this algorithm, the velocities are first calculated at time $t + 1/2\delta t$; these are used to calculate the positions, r , at time $t + \delta t$. In this way, the velocities leap over the positions, and then the positions leap over the velocities. The advantage of this algorithm is that the velocities are explicitly calculated, however, the disadvantage is that they are not

calculated at the same time as the positions. The velocities at time t can be approximated by the relationship:

$$v(t + \delta t) = v(t) + v(t)\delta t + \frac{1}{3}a(t)\delta t + \frac{5}{6}a(t)\delta t - \frac{1}{6}a(t - \delta t)\delta t \quad (7)$$

3.4.2 The Velocity Verlet Algorithm

This algorithm yields positions, velocities and accelerations at time t . There is no compromise on precision.

$$r(t + \delta t) = r(t) + v(t)\delta t + \frac{1}{2}a(t)\delta t^2 \quad (8)$$

$$v(t + \delta t) = v(t) + \frac{1}{2}[a(t) + a(t + \delta t)]\delta t \quad (9)$$

3.4.3 Beeman's Algorithm

This algorithm is closely related to the Verlet algorithm;

$$r(t + \delta t) = r(t) + v(t)\delta t + \frac{2}{3}a(t)\delta t^2 - \frac{1}{6}a(t - \delta t)\delta t^2 \quad (10)$$

$$v(t + \delta t) = v(t) + v(t)\delta t + \frac{1}{3}a(t)\delta t + \frac{5}{6}a(t)\delta t - \frac{1}{6}a(t - \delta t)\delta t \quad (11)$$

The advantage of this algorithm is that it provides a more accurate expression for the velocities and better energy conservation. The disadvantage is that the more complex expressions make the calculation more expensive.

3.5 Statistical Ensembles

Integrating Newton's equations of motion allow us to explore the constant-energy surface of a system. However, most natural phenomena occur under conditions where the system is exposed to external pressure and/or exchanges heat with the environment. Under these conditions, the total energy of the system is no longer conserved and extended forms of molecular dynamics are required [32].

3.5.1 Micro-canonical Ensemble (NVE)

The constant-energy, constant-volume ensemble (NVE), also known as the *microcanonical ensemble* [33], is obtained by solving the standard Newton equation without any temperature and pressure control. Energy is conserved when this (adiabatic) ensemble is generated. However, because of rounding and truncation errors during the integration process, there is always a slight fluctuation, or drift in energy.

3.5.2 Canonical Ensemble (NVT)

The constant-temperature, constant-volume ensemble (NVT), also referred to as the *canonical ensemble* [33], is obtained by controlling the thermodynamic temperature. It is also sometimes called constant temperature molecular dynamics (CTMD). In NVT, the energy of endothermic and exothermic processes is exchanged with a thermostat. This is the appropriate choice when conformational searches of models are carried out in vacuum without periodic boundary conditions.

3.5.3 Isothermal-Isobaric (NPT) Ensemble

The constant-temperature, constant-pressure ensemble (NPT) [33] allows control over both the temperature and pressure. The unit cell vectors are allowed to change, and the pressure is adjusted by adjusting the volume (that is, the size and, in some programs, the shape of the unit cell). NPT is the ensemble of choice when the correct pressure, volume, and densities are important in the simulation. This ensemble can also be used during equilibration to achieve the desired temperature and pressure before changing to the constant-volume or constant-energy ensemble when data collection starts.

3.6 Temperature

Temperature is a state variable that specifies the thermodynamic state of the system. It is also an important concept in dynamics simulations. This macroscopic quantity is related to the microscopic description of simulations through the kinetic energy, which is calculated from the atomic velocities.

The temperature and the distribution of atomic velocities in a system are related through the Maxwell-Boltzmann equation [33]:

$$f(v) = \left(\frac{m}{2\pi k_B T} \right)^{3/2} \exp\left(-\frac{mv^2}{2k_B T} \right) 4\pi v^3 \quad (12)$$

This well known formula expresses the probability $f(v)$ that a molecule of mass m has a velocity of v when it is at temperature T . Figure 3.1 shows this distribution at various temperatures.

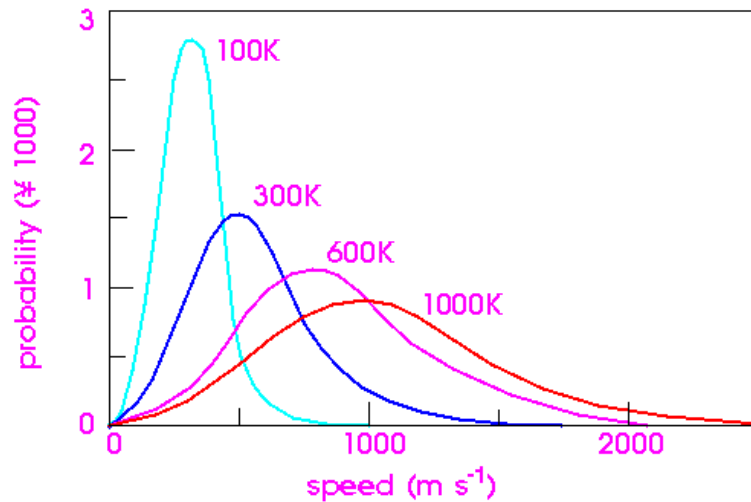


Fig. 3.1: Maxwell-Boltzmann distribution of velocity of water at various temperatures.

The x , y , z components of the velocities have Gaussian distributions [33]:

$$g(v_x) dv_x = \left(\frac{m}{2\pi k_B T} \right)^{1/2} e^{-\frac{mv_x^2}{2k_B T}} dv_x \quad (13)$$

The initial velocities are generated from the Gaussian distribution of v_x , v_y , and v_z .

3.6.1 Methods of Controlling Temperature

The temperature-control methods, or thermostats are: direct velocity scaling, Berendsen, Nosé and Andersen.

3.6.1.1 Direct velocity scaling

Direct velocity scaling [33] is a drastic way to change the velocities of the atoms so that the target temperature can be exactly matched whenever the system temperature is higher

or lower than the target by some user-defined amount. It can be used to bring a system to equilibrium quickly. The velocities of all atoms are scaled uniformly as follows [33]:

$$\left(\frac{v_{new}}{v_{old}}\right)^2 = \frac{T_{target}}{T_{system}} \quad (14)$$

3.6.1.2 Berendsen method of temperature-bath coupling

After equilibration, a more gentle exchange of thermal energy between the system and a heat bath can be introduced through the Berendsen method [34], in which each velocity is multiplied by a factor λ given by:

$$\lambda = \left[1 - \frac{\Delta t}{\tau} \left(\frac{T - T_0}{T}\right)\right]^{1/2} \quad (15)$$

where Δt is the time-step size, τ is a characteristic relaxation time, T_0 is the target temperature, and T the instantaneous temperature.

To a good approximation, this treatment gives a constant-temperature ensemble that can be controlled, both by adjusting the target temperature T_0 and by changing the relaxation time τ .

3.6.1.3 Nosé and Nosé-Hoover dynamics

Nosé dynamics [35] is a method for performing constant-temperature dynamics that produces true canonical ensembles in both coordinate space and momentum space. The Nosé-Hoover formalism is based on a simplified reformulation by Hoover [36], which eliminates time scaling and therefore yields trajectories in real time and with evenly spaced time points. The method is also called the Nosé-Hoover thermostat.

The main idea behind Nosé-Hoover dynamics is that an additional (fictitious) degree of freedom is added to the structure, to represent the interaction of the structure with the heat bath. This fictitious degree of freedom is given a mass Q . The equations of motion for the extended (that is, structure plus fictitious) system are solved. If the potential chosen for that degree of freedom is correct, the constant-energy dynamics (or the micro-canonical dynamics, NVE) of the extended system produces the canonical ensemble (NVT) of the real structure.

The Hamiltonian H^* of the extended system is:

$$H^* = \sum_i \frac{p_i^2}{2m_i} + \phi(q) + \frac{Q}{2} \zeta^2 + gkT \ln S \quad (16)$$

The choice of the fictitious mass Q of that additional degree of freedom is arbitrary but is critical to the success of a run. If Q is too small, the frequency of the harmonic motion of the extended degree of freedom is too high. This forces a smaller time-step to be used in integration. However, if Q is too large, the thermalization process is not efficient; as Q approaches infinity, there is no energy exchange between the heat bath and the structure.

The choice of Q should therefore be based on a balance between the stability of the solution and the highest-frequency motions of the structure.

Q should be different for different models. Nosé (1991) suggests that Q should be proportional to $gk_B T$, where g is the number of degrees of freedom in the structure, k_B is the Boltzmann constant, and T is the temperature.

3.6.1.4 Andersen method

One version of the Andersen method [37] of temperature control involves randomizing the velocities of all atoms at a predefined collision period. The other version involves choosing atom collision times from a Poisson distribution at each time-step and changing their velocities according to the Boltzmann distribution.

3.7 Pressure Control

3.7.1 Methods of Controlling Pressure

With the Berendsen and Andersen methods the volume can change, but there is no change in the shape of the cell. Therefore, only the pressure is controlled. With the Parrinello-Rahman method, the cell shape can change and therefore both pressure and stress can be controlled.

3.7.1.1 Berendsen method of pressure control

The pressure can be changed by changing the coordinates of the particles and the size of the unit cell under periodic boundary conditions.

The Berendsen method [34] couples the system to a pressure bath to maintain the pressure at a certain target. The strength of coupling is determined by both the compressibility of the system (using a user-defined variable γ) and a relaxation time constant (a user-defined variable τ). At each step, the x, y, and z coordinates of each atom are scaled by the factor:

$$\mu = \left[1 - \frac{\Delta t}{\tau} \gamma [P - P_0] \right]^{1/3} \quad (17)$$

where Δt is the time step, P is the instantaneous pressure, and P_0 is the target pressure. The Cartesian components of the unit cell vectors are scaled by the same factor.

3.7.1.2 Andersen method of pressure control

In the Andersen method [37] of pressure control, the volume of the cell can change, but its shape is preserved by allowing the cell to change isotropically.

The Andersen method is useful for liquid simulations since the box could become quite elongated in the absence of restoring forces if the shape of the cell were allowed to change. A constant shape also makes the dynamics analysis easier.

The basic idea is to treat the volume V of the cell as a dynamic variable in the system. The Lagrangian of the system is modified so that it contains a kinetic energy term with a user-defined mass M and a potential term which is the pV potential derived from an external pressure P_{ext} acting on volume V of the system.

3.7.1.3 Parrinello-Rahman method of pressure and stress control

The Parrinello-Rahman [38] method of pressure and stress control can allow simulation of a structure under externally applied stress. This is useful for studying the stress-strain relationship of materials. Both the shape and the volume of the cell can change, so that the internal stress of the system can match the externally applied stress.

CHAPTER 4


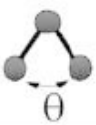
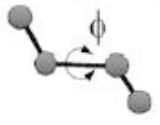
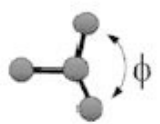

LITERATURE REVIEW

4.1 Forcefield

Many of the molecular modeling force-fields in use for molecular systems can be interpreted in terms of simple four-component of the intra- and inter- molecular forces within the system. The types of forces involved are derived from the following phenomena:

- Deviation from equilibrium bond configurations
- Deviation from equilibrium angle configurations
- Energetic function for bond rotations
- Interaction between non-bonded parts of the system

Table 4.1: Force-field degrees of freedom [9]

Bond stretching	
Bond Angle Bending	
Bond Torsion	
Improper Bond Torsion	
Non-Bonded Interactions	

More sophisticated force-fields have more than four components of course, but they invariably relate to these four. In our work, the condensed phase optimization molecular potentials for atomistic simulation studies (COMPASS) is used. It is a new molecular

mechanics class 2 forcefield, parameterized from ab initio computations of model compounds and optimized using condensed-phase properties of polymers and low molecular-weight compounds. The COMPASS force-field was parameterized for the most common organic and inorganic small molecules and for polymers. It was based on the Polymer Consistent Force Field (PCFF) [39-41]. Although the exact parameters of this force-field are proprietary (hence unavailable), it is known and referenced that it was parameterized, tested and validated for most of the common organic and inorganic materials [42-44].

The total potential energies calculated by the COMPASS force-field can be broken down into the following terms:

$$E_{opt} = E_{valence} + E_{nonbond}$$

$$E_{valence} = E_{diagonal} + E_{coupling}$$

$$E_{diagonal} = E_{bond} + E_{angle} + E_{torsion} + E_{out-of-plane}$$

$$E_{nonbond} = E_{elec} + E_{vdW}$$

where $E_{valence}$ is the valence component energy.

$E_{diagonal}$ is the diagonal term energy.

$E_{coupling}$ is the coupling term energy.

E_{bond} is the bond stretching energy.

E_{angle} is the angle energy.

$E_{torsion}$ is the torsion energy.

$E_{out-of-plane}$ is the out-of plane deformation energy.

$E_{nonbond}$ is the non-bond energy between atoms in different molecules and atoms separated by three or more bonded atoms.

E_{elec} is the term for Coulombic electrostatic interaction

E_{vdW} is the term for Van der waals energies.

These terms can be further decomposed in the following manner:

$$E_{bond} = \sum_b \left[{}^2K_b (b-b_0)^2 + {}^3K_b (b-b_0)^3 + {}^4K_b (b-b_0)^4 \right] \quad (18)$$

$$E_{angle} = \sum_\theta \left[{}^2K_\theta (\theta-\theta_0)^2 + {}^3K_\theta (\theta-\theta_0)^3 + {}^4K_\theta (\theta-\theta_0)^4 \right] \quad (19)$$

$$E_{torsion} = \sum_\phi \left[{}^1K_\phi (1-\cos\phi) + {}^2K_\phi (1-\cos 2\phi) + {}^3K_\phi (1-\cos 3\phi) \right] \quad (20)$$

$$E_{out-of-plane} = \sum_\chi K_\chi \chi^2 \quad (21)$$

$$\begin{aligned} E_{coupling} = & \sum_b \sum_{b'} K_{bb'} (b-b_0)(b'-b_0) \\ & + \sum_b \sum_g K_{bg} (b-b_0)(\theta-\theta_0) \\ & + \sum_b \sum_\phi K_{b\phi} (b-b_0) (F_{b\phi}^1 (\cos\phi) + F_{b\phi}^2 (\cos 2\phi) + F_{b\phi}^3 (\cos 3\phi)) \\ & + \sum_\theta \sum_{\theta'} K_{\theta\theta'} (\theta-\theta_0)(\theta'-\theta'_0) \\ & + \sum_\theta \sum_\phi (\theta-\theta_0) (F_{\theta\phi}^1 \cos\phi + F_{\theta\phi}^2 \cos 2\phi + F_{\theta\phi}^3 \cos 3\phi) \\ & + \sum_\theta \sum_{\theta'} \sum_\phi (\theta-\theta_0)(\theta'-\theta'_0)(\phi-\phi_0) \end{aligned} \quad (22)$$

$$E_{elect} = \sum_{i,j} \frac{q_i q_j}{r_{ij}} \quad (23)$$

$$E_{vdW} = \sum_{i,j} \varepsilon_{ij} \left[2 \left(\frac{r_{ij}^0}{r_{ij}} \right)^9 - 3 \left(\frac{r_{ij}^0}{r_{ij}} \right)^6 \right] \quad (24)$$

where 2K is the quadratic force-field parameter.

3K is the cubic force-field parameter

4K is the quartic force-field parameter

b is the bond length

b_0 is the reference value of the bond length (min. energy state)

θ_0 is the reference value of the bond angle

Φ is the torsion angle

χ is the out-of-plane coordinates

q_i is the atomic partial charge on atom i

r_{ij} is the distance between atom i and atom j

B_{ij} is the minimum Van de Waals interaction energy

r_{0ij} is the distance where B_{ij} occurs

r_{0ij} and B_{ij} are computed from the individual atomic parameters by the Waldman-Hagler combination rules [45]. This rule is an approximation (combination rule) aimed at reducing extensive calculations related to non-bond interactions. With this rule, van der Waals interaction parameters that are defined for the heterogeneous atom pairs are named off-diagonal parameters. When off-diagonal parameters are not available for such atom pairs, they are calculated by averaging individual values for each of the two atom types using the 6th-power combination rule.

$$r_{i,j}^0 = \left(\frac{(r_i^0)^6 + (r_j^0)^6}{2} \right)^{\frac{1}{6}} \quad (25)$$

$$\varepsilon_{i,j} = 2\sqrt{\varepsilon_i \cdot \varepsilon_j} \left(\frac{(r_i^0)^3 \cdot (r_j^0)^3}{(r_i^0)^6 + (r_j^0)^6} \right) \quad (26)$$

where B_i , B_j , r_{0j} and r_{0i} are the individual atomic parameters.

Finally, the energy summation also has a significant dependence on the number of atoms in the system. To reduce the computational efforts, non-bond interactions are simply calculated to a cutoff distance only. Interactions beyond this distance are ignored.

Choosing a time-step is also an important part of correctly running a molecular dynamics simulation algorithm. Unfortunately, there are no hard rules for calculating the most appropriate time-step. It is simply known that if the time-step is too small, the particles' trajectory will only cover a limited proportion of the phase space (computational wastes), and if it is too large, instabilities will arise in the integration algorithm due to high energy overlaps between atoms. Such instabilities generally lead to violations of energy or numerical overflow.

4.2 Periodic Boundary Condition

The term Periodic boundary condition [21] refers to the simulation of structures consisting of a periodic lattice of identical subunits. By applying periodic boundaries to simulations, the influence, for example, of bulk solvent or crystalline environments can be included, thereby improving the rigor and realism of a structure.

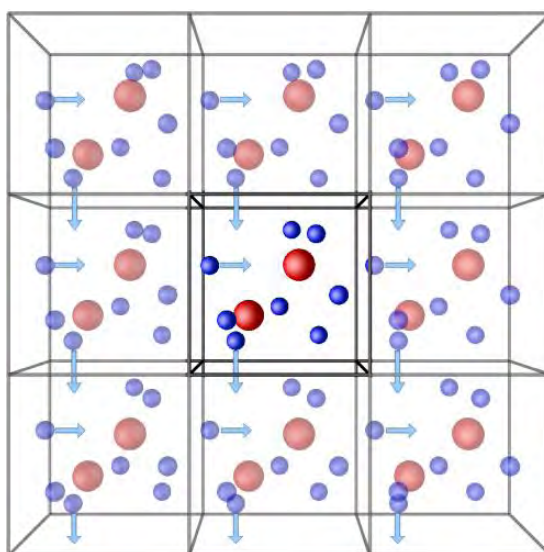


Fig 4.1: Periodic boundary condition

Small sample size means that, unless surface effects are of particular interest, periodic boundary conditions need to be used. If we consider 1000 atoms arranged in a $10 \times 10 \times 10$ cube, nearly half the atoms are on the outer faces, and these will have a large effect on the measured properties. Even for $10^6 = 100^3$ atoms, the surface atoms amount to 6% of the total, which is still nontrivial. Surrounding the cube with replicas of itself takes care of this problem. Provided the potential range is not too long, we can adopt the minimum

image convention that each atom interacts with the nearest atom or image in the periodic array. In the course of the simulation, if an atom leaves the basic simulation box, attention can be switched to the incoming image. This is shown in Figure 4.1.

In any periodic system containing polymers, it is clear that the atoms from the same molecule may lie in different cells. All polymer chains whose tailmost backbone atoms lie in the central cell are referred to as parent molecules and all others as image molecules. Moreover, when discussing dynamics simulations, the term parent is used to refer to those molecules whose tailmost backbone atoms are contained within the central cell at the beginning of the simulation, even if they subsequently drift into neighboring cells during the course of the simulation. In addition, since it is occasionally necessary to refer to atoms rather than molecules, all atoms that initially lie within the central cell are referred to as parent atoms, and all other atoms as images. One of the characteristics of a periodic system is that, during a dynamics simulation, all image atoms move in exactly the same manner as their parent atoms (that is, with the same velocity vectors, etc.). Consequently, when an atom leaves the central cell through one side (face), its image simply enters through the opposite side (face).

4.3 Stress

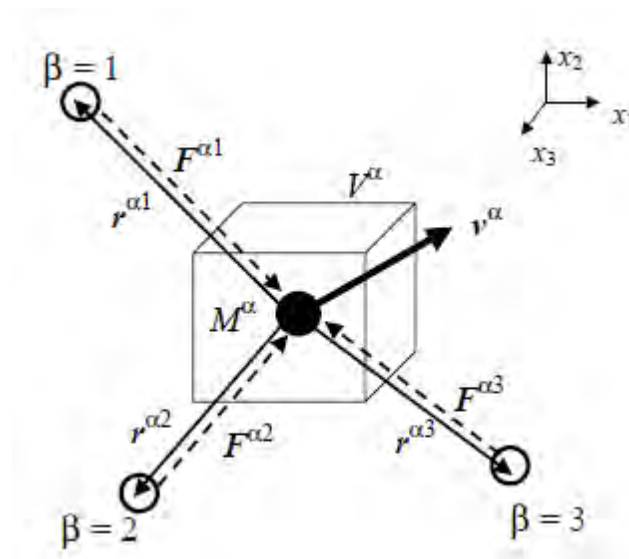


Fig 4.2: Diagram of parameters used to compute stresses in the simulations [46]

In general, the stress in a solid (or a group of interacting particles in the form of a solid) is defined as the change in the internal energy (in the thermodynamic sense) with respect to the strain per unit volume. For example, at the continuum level, the stress tensor, ζ_{ij} , for a linear-elastic material is [47]

$$\sigma_{ij} = \frac{1}{V} \left(\frac{\partial E}{\partial \varepsilon_{ij}} \right)_S \quad (27)$$

where V is the volume of the solid, E is the total internal energy, ε_{ij} is the strain tensor, and the subscript S denotes constant entropy. When the internal energy is equal to the strain energy of the solid, then Hooke's law may be derived from Eq. (27). Furthermore, if the strain energy is expressed in terms of an applied force acting over the surface area of a solid, then a more familiar form of stress as force per unit area is derived.

At the atomic level, the total internal energy given in Eq. (27) can be expressed as the summation of the energies of the individual atoms E^α that compose the solid:

$$E^\alpha = T^\alpha + U^\alpha = \frac{1}{2} M^\alpha (v^\alpha)^2 + \Phi^\alpha(r) \quad (28)$$

where for each atom α , T^α is the kinetic energy, U^α is the potential energy, M^α is the mass, v^α is the magnitude of its velocity, and $\Phi^\alpha(r)$ is the potential energy at the atom location r . Using a Hamiltonian based on these individual energy contributions, E^α , it has been shown that the stress contribution, ζ_{ij}^α , for a given atom is,

$$\sigma_{ij}^\alpha = -\frac{1}{V^\alpha} \left(M^\alpha v_i^\alpha v_j^\alpha + \sum_{\beta} F_i^{\alpha\beta} r_j^{\alpha\beta} \right) \quad (29)$$

where V^α is the atomic volume of atom α , v_i^α is the i -component of the velocity of atom α , v_j^α is the j -component of the velocity of atom α , $F_i^{\alpha\beta}$ is the i -component of the force between atoms α and β obtainable from the derivative of the potential $\Phi(r)$, and $r_j^{\alpha\beta}$ is the j -component of the separation of atoms α and β [48,49]. These parameters are shown in Fig. 4.2 as well.

4.4 Strain

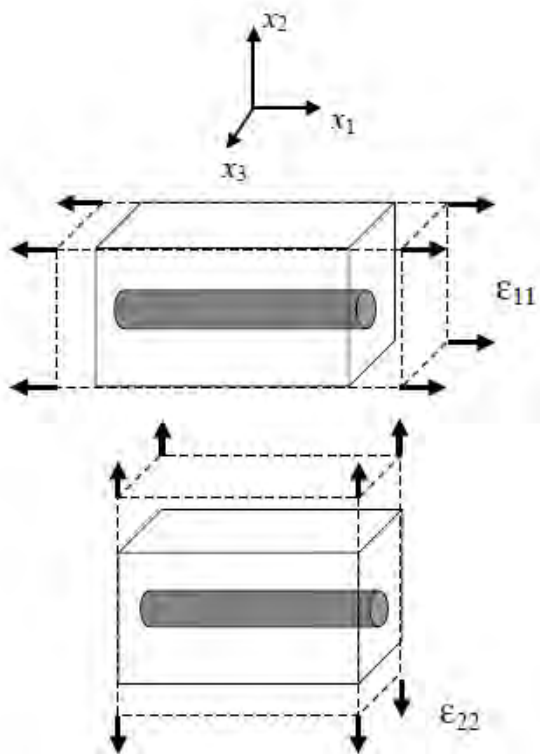


Fig. 4.3: Definitions of the strains applied to the composites [46]

For each increment of applied deformation, a uniform strain was prescribed on the entire MD model. For the longitudinal and transverse deformations, pure states of the strains ϵ_{11} and ϵ_{22} , respectively, were initially applied (Fig. 4.3). The application of strain was accomplished by uniformly expanding the dimensions of the MD cell in the direction of the deformation and re-scaling the new coordinates of the atoms to fit within the new dimensions.

After this initial deformation, the MD simulation was continued and the atoms were allowed to equilibrate within the new MD cell dimensions. This process was carried out for the subsequent increments of deformation [46].

4.5 Mechanical Properties

Any body or element thereof, which is acted on by external forces is in a state of stress. Moreover, if the body is in equilibrium, the external stress must be exactly balanced by internal forces. In general, stress is a second rank tensor with nine components as follows:

$$\begin{bmatrix} \sigma_{11} & \sigma_{12} & \sigma_{13} \\ \sigma_{21} & \sigma_{22} & \sigma_{23} \\ \sigma_{31} & \sigma_{32} & \sigma_{33} \end{bmatrix}$$

The application of stress to a body results in a change in the relative positions of particles within the body, expressed quantitatively via the strain tensor [33]:

$$\begin{bmatrix} \varepsilon_{11} & \varepsilon_{12} & \varepsilon_{13} \\ \varepsilon_{21} & \varepsilon_{22} & \varepsilon_{23} \\ \varepsilon_{31} & \varepsilon_{32} & \varepsilon_{33} \end{bmatrix}$$

For a parallelepiped (for example, a periodic simulation cell) characterized in some reference state by the three column vectors a_0 , b_0 , c_0 , and by the vectors a , b , c in the deformed state, the strain tensor is given by [33]:

$$\varepsilon = \frac{1}{2} \left[\left(h_0^T \right)^{-1} G h_0^{-1} - 1 \right] \quad (30)$$

where h_0 denotes the matrix formed from the three column vectors a_0 , b_0 , c_0 , h denotes the corresponding matrix formed from a , b , c , T denotes the matrix transpose, and G denotes the metric tensor $h^T h$.

The elastic stiffness coefficients, relating the various components of stress and strain are defined by [33]:

$$C_{lmnk} = \left. \frac{\partial \sigma_{lm}}{\partial \varepsilon_{nk}} \right|_T = \left. \frac{1}{V_0} \frac{\partial^2 A}{\partial \varepsilon_{lm} \partial \varepsilon_{nk}} \right|_T \quad (31)$$

where A denotes the Helmholtz free energy. For small deformations, the relationship between the stresses and strains may be expressed in terms of a generalized Hooke's law:

$$\sigma_{lm} = C_{lmnk} \varepsilon_{nk} \quad (32)$$

or, alternatively:

$$\varepsilon_{lm} = S_{lmnk} \sigma_{nk} \quad (33)$$

where S_{lmnk} denotes the compliance components.

In view of the fact that both the stress and strain tensors are symmetric, it is often convenient to simplify these expressions by making use of the Voigt vector notation.

Stress is represented as [33]:

$$\begin{bmatrix} \sigma_{11} & \sigma_{12} & \sigma_{13} \\ \sigma_{21} & \sigma_{22} & \sigma_{23} \\ \sigma_{31} & \sigma_{32} & \sigma_{33} \end{bmatrix} \rightarrow \begin{bmatrix} \sigma_1 & \sigma_6 & \sigma_5 \\ \sigma_6 & \sigma_2 & \sigma_4 \\ \sigma_5 & \sigma_4 & \sigma_3 \end{bmatrix}$$

For example:

$$\sigma = [\sigma_{11} \sigma_{22} \sigma_{33} \sigma_{23} \sigma_{13} \sigma_{12}]^T$$

while strain is represented as [33]:

$$\begin{bmatrix} \varepsilon_{11} & \varepsilon_{12} & \varepsilon_{13} \\ \varepsilon_{21} & \varepsilon_{22} & \varepsilon_{23} \\ \varepsilon_{31} & \varepsilon_{32} & \varepsilon_{33} \end{bmatrix} \rightarrow \begin{bmatrix} \varepsilon_1 & \varepsilon_6/2 & \varepsilon_5/2 \\ \varepsilon_6/2 & \varepsilon_2 & \varepsilon_4/2 \\ \varepsilon_5/2 & \varepsilon_4/2 & \varepsilon_3 \end{bmatrix}$$

For example:

$$\varepsilon = [\varepsilon_{11} \varepsilon_{22} \varepsilon_{33} \varepsilon_{23} \varepsilon_{13} \varepsilon_{12}]^T$$

The generalized Hooke's law is thus often written as [33]:

$$\sigma_i = C_{ij} \varepsilon_j \quad (34)$$

For an isotropic material, the stress-strain behavior can be fully described by specifying only two independent coefficients. The resulting stiffness matrix may be written as [33]:

$$\begin{bmatrix} \lambda+2\mu & \lambda & \lambda & 0 & 0 & 0 \\ \lambda & \lambda+2\mu & \lambda & 0 & 0 & 0 \\ \lambda & \lambda & \lambda+2\mu & 0 & 0 & 0 \\ 0 & 0 & 0 & \mu & 0 & 0 \\ 0 & 0 & 0 & 0 & \mu & 0 \\ 0 & 0 & 0 & 0 & 0 & \mu \end{bmatrix}$$

where λ and μ are referred to as the Lamé coefficients. For the isotropic case, the familiar elastic moduli may be written in terms of the Lamé coefficients as follows [33]:

$$\text{Young's Modulus,} \quad E = \mu \left(\frac{3\lambda + 2\mu}{\lambda + \mu} \right) \quad (35)$$

$$\text{Poisson's Ratio,} \quad \nu = \frac{\lambda}{2(\mu + \lambda)} \quad (36)$$

$$\text{Bulk Modulus,} \quad K = \lambda + \frac{2}{3}\mu \quad (37)$$

$$\text{Shear Modulus,} \quad G = \mu \quad (38)$$

4.6 Rule-of-Mixture Analysis

For a nanocomposite under uniaxial loading, the dependence of the elastic modulus on the CNT volume fraction can be estimated by the rule of mixtures [50]. The longitudinal elastic modulus, Y , of the composite cell with long CNTs under isostrain conditions is:

$$Y = Y_{CNT} f_{CNT} + Y_m f_m \quad (39)$$

where Y_{CNT} and Y_m are the effective longitudinal elastic modulus of the CNT and the polymer matrix, respectively, and f_{CNT} and f_m are the volume fractions occupied by the CNT and the polymer matrix, respectively. The volume fractions satisfy

$$f_{CNT} + f_m = 1 \quad (40)$$

The CNT volume fraction is an important variable in determining the composite mechanical properties. Since the polymer matrix does not penetrate the CNTs, and the (6,6) SWNT used in the present work has a radius small enough to be thought of as a solid beam [51]. Therefore its effective volume fraction, f_{CNT} , includes the entire CNT cross-section and is defined by,

$$f_{CNT} = \frac{\pi \left(R_{CNT} + \frac{h_{vdW}}{2} \right)^2}{A_{cell}} \quad (41)$$

where h_{vdW} is the equilibrium van der Waals separation distance between the CNT and the matrix, and A_{cell} is the cross-sectional area of the unit cell transverse to the nanotube axis. The van der Waals separation distance depends on the nature of the CNT–polymer interfacial interactions.

CHAPTER 5

EFFECT OF TUBE DIAMETER, LENGTH AND CHIRALITY ON MECHANICAL PROPERTIES

5.1 Background

Carbon nanotubes (CNTs) have been the subject of intense research due to their exceptional mechanical, thermal and electrical properties [52–55]. The mechanical load carrying capacities of CNTs in nanocomposites have also been demonstrated on some experiments [56–58]. Qian et al. [56] have reported that an addition of just 1 wt% CNTs resulted in a 25% increase in the tensile strength for polystyrene based composite films. In general, an accurate assessment of the properties of individual CNTs is essential for the development of CNT-based reinforced composites.

Experiment methods for measuring the mechanical properties are based mainly on the techniques of transmission electron microscopy (TEM) and atomic force microscopy (AFM). The first experimental measurement of the elastic modulus in multi-walled carbon nanotubes (MWNTs) has given a value 1.8 ± 0.9 TPa obtained by measuring thermal vibration method [59]. Later, a slightly lower value of 1.28 ± 0.59 TPa was been obtained by Wong et al. [60] using the tip of AFM to bend anchored MWNTs. Yu et al. [61] have found the tensile strength and modulus of single walled carbon nanotubes (SWNTs) to be in the range from 11 to 63 GPa and 0.27 to 0.95 TPa respectively. Krishnan et al. [62] have measured the elastic modulus of SWNTs in the diameter range 1.0–1.5 nm. The mean value of 27 nanotubes has been estimated to be around 1.25 TPa. These experiments have contributed to confirming that CNTs have exceptional mechanical properties. Due to the experimental error bars, however, it is rather difficult to directly state the dependence of chirality on the strength of CNTs.

The theoretical [63-73] and experimental [74-77] results obtained for the Young's moduli of CNTs vary widely. Using an empirical force-constant model, Lu [63] established an average Young's modulus of approximately 1 TPa for a series of single-walled carbon nanotubes (SWNTs) and concluded that the modulus is insensitive to the tube's structural

parameters, e.g. its radius and helicity. Yakobson et al [64] simulated the structural instability of SWNTs under axial compression and obtained Young's moduli ranging from 1.4 to 5.5 TPa.

Robertson et al [65] reported that the Young's modulus for a nanotube is smaller than that of a graphene sheet. Cornwell and Wille [66] developed a simple mathematical formula to approximate the Young's modulus of nanotubes with a wide range of tube radii.

Quantum mechanical-based methods such as the ab initio and tight-binding (TB) schemes have also been employed to predict the Young's moduli of nanotubes [67–70]. Sánchez-Portal [68] performed ab initio calculations based on pseudo-potential density function theory and established that the Young's moduli of SWNTs range from 0.95 to 1.10 TPa. The numerical results indicated that the Young's modulus of graphene was smaller than that of a (5, 5) nanotube. Similar findings were also reported by Peralta-Inga et al [70], who used a density functional tight-binding (DFTB) approach to study the elastic properties of a series of SWNTs with diameters ranging from 0.55 to 1.08 nm. The results showed that the Young's modulus decreased with increasing tube radius and approached the modulus of a graphene sheet in the limiting case.

Computational simulation for predicting mechanical properties of CNTs has been regarded as a powerful tool relative to the experimental difficulty. To perform the complicated calculation, however, an available computational power of computer hardware and simulation software is demanded for the MD and quantum mechanics methods. Therefore, a well established nano scale continuum model between molecular and solid mechanics is a challenging task for computer simulation in engineering.

5.2 Molecular Modeling of SWCNT

The molecular models of SWNTs with different diameters and chirality were established with use of Materials Studio 4.3[®]. The electronic structures of the all carbon atoms in the SWNT models were sp^2 hybridization. The unsaturated boundary effect was avoided by adding hydrogen atoms at the ends of the SWNTs. Each C-C bond length was 1.42 Å and each C-H bond length was 1.14 Å. The hydrogen atoms had charges of +0.1268 e and the carbon atoms connecting hydrogen atoms had charges of -0.1268 e, thus the neutrally charged SWNTs were constructed. The computer graphics picture of (5, 5) (6, 6) (7, 7) (8,

8) (9, 9) (10, 10) and (7, 0) (8, 0) (9, 0) (10, 0) (11, 0) (12, 0) SWNT models are shown in Figure 5.1 and Figure 5.2 respectively.

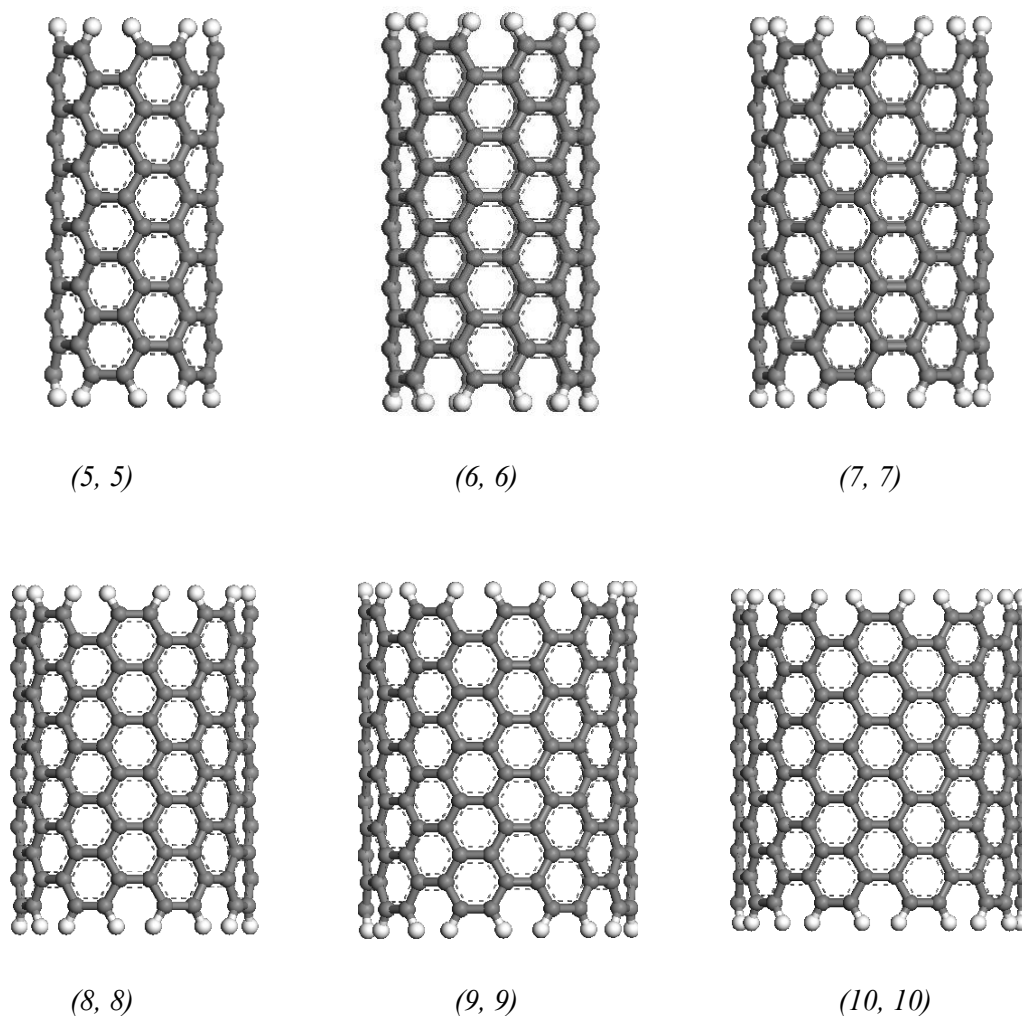
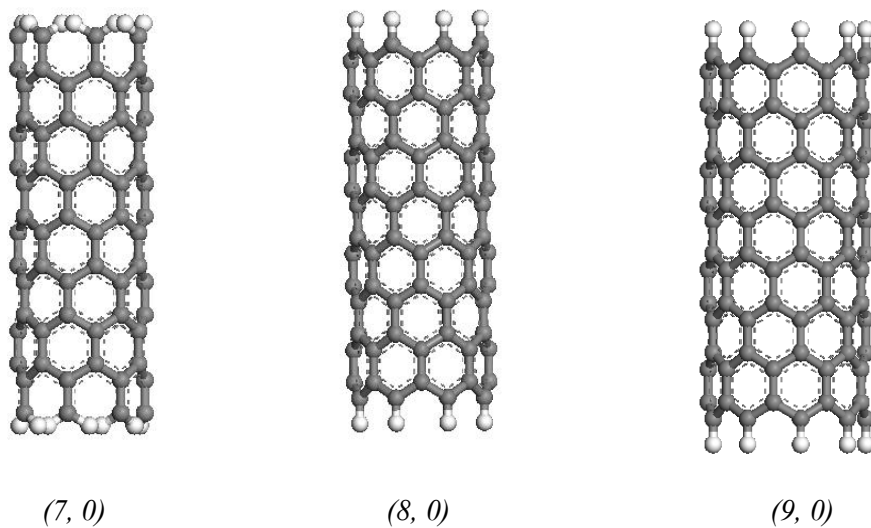


Fig. 5.1: Molecular model of armchair SWNTs with different chirality



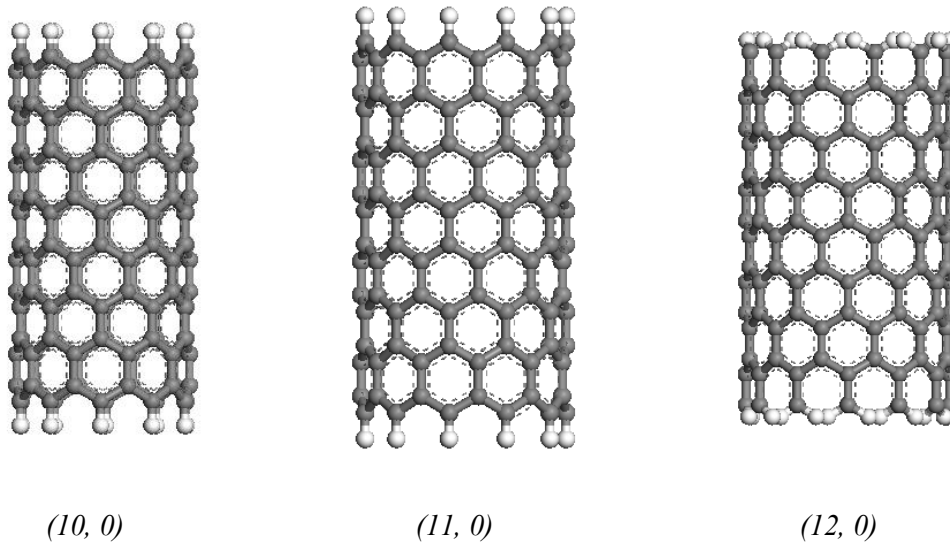


Fig. 5.2: Molecular model of zigzag SWCNTs with different chirality

5.3 Molecular Dynamics Simulation of SWCNTs

One of the primary aims of the present study is to determine the elastic constant of single-wall carbon nanotubes of different chirality. Molecular dynamics simulation runs of SWCNT with different chirality were carried out under the constant number of particle, constant pressure and constant temperature (NPT) ensemble.

The aspect ratio of the nanotubes, which is the length-to-radius ratio, is set to be greater than 10 to ensure that edge effects can be neglected.

At first, an energy minimization was performed to obtain a minimum energy state of the nanotube without any applied deformation. The first step consists of a conjugate gradients minimization of the periodic system, after which the energy attained a constant minimum value. Following this initial stage, the constant-strain energy minimization method was applied to calculate the elastic moduli of the periodic system. In general, the stress in a solid (or a group of interacting particles in the form of a solid) is defined as the change in the internal energy per unit volume with respect to the strain. Small strains were applied to a periodic structure at an energy minimum. The application of strain was accomplished by uniformly expanding the dimensions of the simulation cell in the direction of the deformation and re-scaling the new coordinates of the atoms to fit within the new dimensions. The structure was then re-minimized keeping the lattice parameters

fixed, and the resultant stress in the minimized structure was measured. This was repeated for a series of strains. The variation of the measured stress as a function of applied strain was used to derive the stiffness matrix.

5.4 Results and Discussion

Six zigzag and six armchair nanotubes with increasing radiuses were selected to consider the effects of radius and chirality.

Table 5.1: Summary of numerical values for number of atoms, radius and length of different armchair and zigzag SWNTs

Nanotubes	No. of atoms	Radius (nm)	Length (nm)
Armchair (5, 5)	300	0.34	3.44
Armchair (6, 6)	432	0.41	4.18
Armchair (7, 7)	560	0.47	4.67
Armchair (8, 8)	736	0.54	5.41
Armchair (9, 9)	936	0.61	6.15
Armchair (10, 10)	1160	0.68	6.89
Zigzag (7, 0)	210	0.27	2.98
Zigzag (8, 0)	272	0.31	3.41
Zigzag (9, 0)	342	0.35	3.83
Zigzag (10, 0)	420	0.39	4.26
Zigzag (11, 0)	506	0.43	4.68
Zigzag (12, 0)	600	0.47	5.11

Different mechanical properties of these SWNTs derived from MD simulations are listed in Table 5.2:

Table 5.2: Summary of numerical results for elastic modulus, bulk modulus, shear modulus and Poisson's ratio of different SWNTs

Nanotubes	Young's Modulus (TPa)	Bulk Modulus (GPa)	Shear Modulus (GPa)	Poisson's Ratio
Armchair (5, 5)	0.974	137	66	0.32
Armchair (6, 6)	0.911	133	62	0.33
Armchair (7, 7)	0.852	127	57	0.33
Armchair (8, 8)	0.796	120	54	0.38
Armchair (9, 9)	0.748	113	50	0.40
Armchair (10, 10)	0.707	105	47	0.26
Zigzag (7, 0)	1.023	141	71	0.29
Zigzag (8, 0)	0.990	138	68	0.32
Zigzag (9, 0)	0.956	136	65	0.29
Zigzag (10, 0)	0.920	133	62	0.33
Zigzag (11, 0)	0.885	130	60	0.32
Zigzag (12, 0)	0.852	127	58	0.23

Different graphs are plotted taking Young's modulus vs. nanotube radius, bulk modulus vs. nanotube radius and shear modulus vs. nanotube radius.

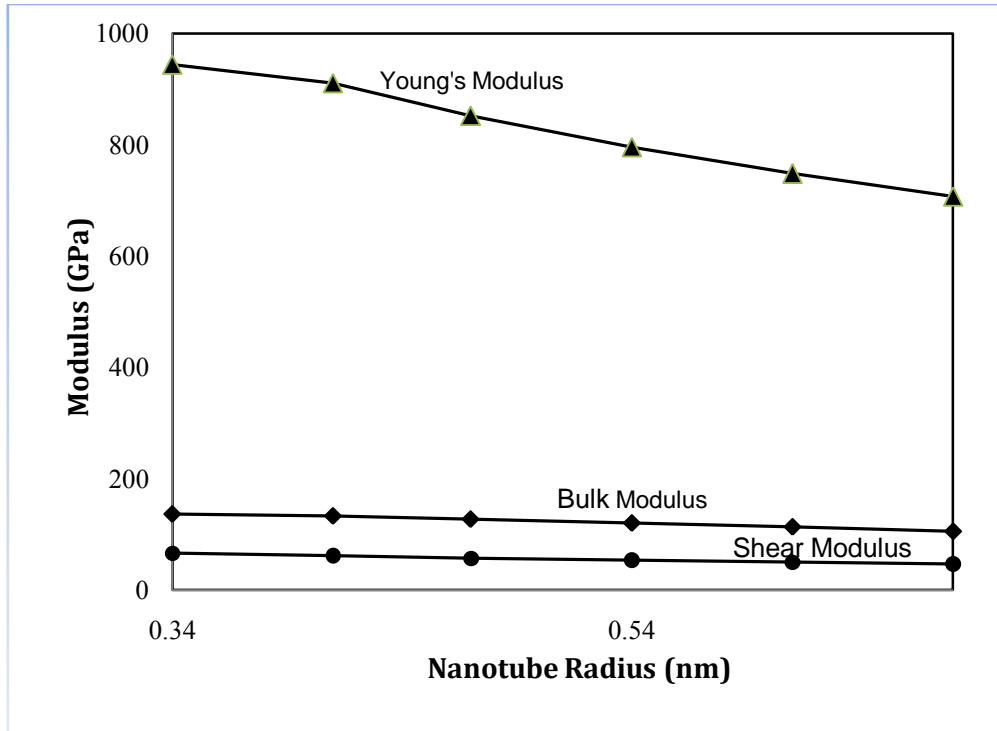


Fig. 5.3: Variation of MD simulated Young's modulus, bulk modulus and shear modulus of armchair SWNTs with increasing radius

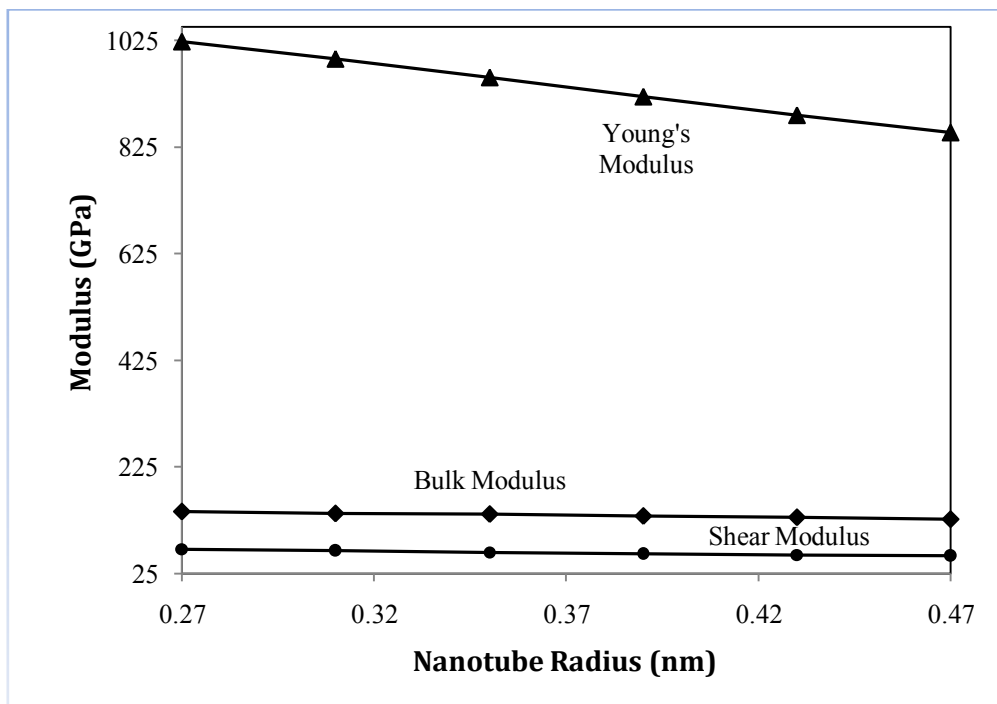


Fig. 5.4: Variation of MD simulated Young's modulus, bulk modulus and shear modulus of zigzag SWNTs with increasing radius

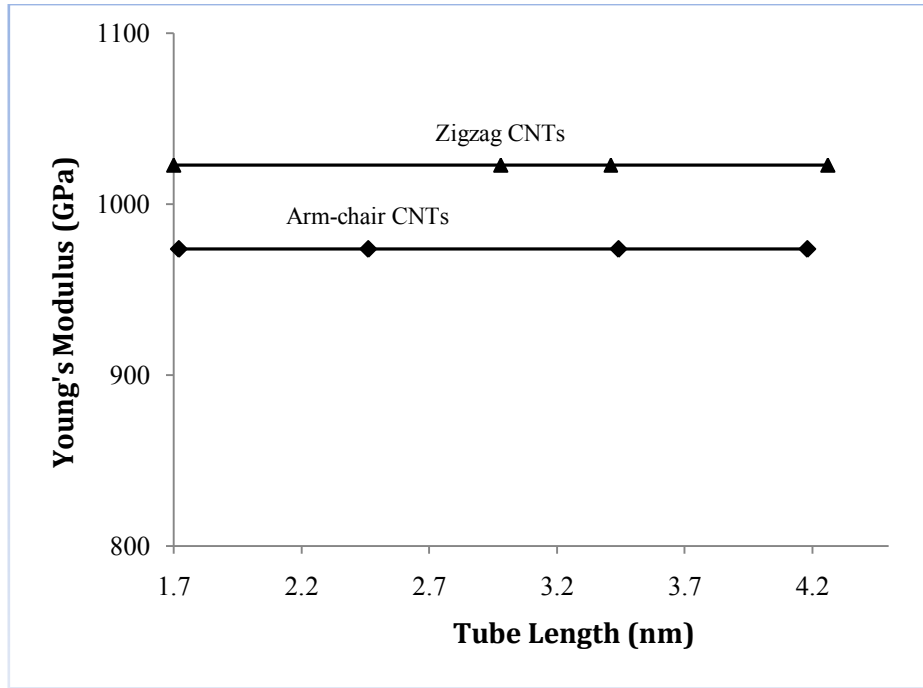


Fig. 5.5: Variation of MD simulated Young's modulus of both armchair and zigzag SWNTs with increasing tube length

The axial Young's modulus of arm-chair SWNT with (5, 5) chirality is 0.974 GPa whereas the axial Young's modulus of zigzag SWNT with (7, 0) chirality is 1023 GPa (more than 1 TPa). These are in good agreement with experimentally obtained values by other researchers [78-82]. As the tube radius increases the Young's modulus also seems to decrease. The arm-chair (10, 10) SWNT which has a radius of 0.68 nm has a Young's modulus of 0.707 GPa and zigzag (12, 0) SWNT which has a radius of 0.47 nm has a Young's modulus of 0.852 GPa. From computation it can be said that, the axial Young's modulus of both arm-chair and zigzag SWNTs decreases with increasing diameter of the nanotubes. There seems a clear diameter dependent trend in agreement with experimental observation.

The MD result shows the axial Young's modulus of armchair (7, 7) SWCNT, whose radius is approximately equal to that of the zigzag (12, 0) SWCNT is very similar to that of the zigzag (12, 0) SWCNT. Therefore, it can be concluded that the elastic modulus of a SWCNT is insensitive to its helicity i.e. tube chirality.

The arm-chair (5, 5) CNTs of different length (1.72 nm, 2.46 nm, 3.44 nm, 4.18 nm) and zigzag (7, 0) CNTs of different length (1.7 nm, 2.98 nm, 3.41 nm, 4.26 nm) are taken and

Young's Modulus is estimated from MD simulation. For both arm-chair and zigzag CNTs, the value of Young's modulus is identical irrespective of the tube length. Therefore, it can be inferred that the Young's modulus of the nanotube is independent of the tube length.

Similarly, the Figure 5.5 shows that, both the bulk modulus and shear modulus also decrease linearly with increasing tube radius. But the Poisson's ratio shows no such relation with the CNT diameters.

CHAPTER 6

EFFECT OF RESIN ON NANOCOMPOSITES

6.1 Background

Carbon nanotubes (CNTs) are potential additives to polymeric materials due to the potential for their enhancement of the structural, mechanical and electronic properties of the resulting composite [6]. However, improvements in properties are by no means guaranteed, and the results are often sensitive to the particular polymer chosen, in addition to the quantity and quality of CNTs used in the composite. If we attempt to trace what controls the performance of materials, we can identify that properties of materials are largely dictated by the atomic structure, composition, microstructure, defects and interfaces in materials [83]. As a result, it is very important to quantitatively understand the mechanics and physics of nano-structured materials, and only then we can effectively employ them in multi-scale material design.

S. B. Sane, T. Cagin, W. A. Goddard and W. G. Knauss studied the bulk response of amorphous PMMA using molecular dynamics simulation [84]. Later, Y. Han and J. Elliott [6] estimated the elastic properties of polymer/carbon nanotube composites for different volume fraction of CNT. The simulation results support the idea that it is possible to use CNTs to mechanically reinforce an appropriate polymer matrix, especially in the longitudinal direction of the nanotube. In addition, the results show that detailed interfacial ordering effects cannot be ignored when interactions between the nanotube and polymer matrix are strong. The comparison of the simulation results with the macroscopic rule-of-mixtures for composite systems showed that for strong interfacial interactions, there can be large deviations of the results from the rule-of mixtures.

Adnan et al. [85] studied the effect of filler size on the elastic properties of particle reinforced polymer nanocomposites. Linear elastic constant and bulk modulus are evaluated by assuming isotropic materials symmetry for both PE neat and nanocomposites. A simulation result demonstrates that elastic properties of nanocomposites are significantly improved with the reduction of bucky-ball size.

Odegard et al. [86] modeled the mechanical properties of nanocomposites using silica nanoparticle. A continuum-based elastic micromechanics model is developed for silica nanoparticle/polyimide composites with various nanoparticle/polyimide interfacial treatments. It is found that specific silica nanoparticle/polyimide interface conditions have a significant effect on the composite mechanical properties.

Gou et al. [87] used molecular mechanics and molecular dynamics simulations to study the molecular interaction and load transfer in presence of single-walled carbon nanotube ropes. The simulation result showed that individual nanotubes had stronger interactions with epoxy resins and, therefore, provided better load transfer than the nanotube rope.

Zhu et al. [88] studied the stress-strain behavior of carbon-nanotube reinforced Epon-862 composites using molecular dynamics simulation. The result shows that with increasing strain in the longitudinal direction the Young's modulus of CNT increases whilst that of the EPON 862 composite or matrix decreases. Furthermore, a long CNT can greatly improve the Young's modulus of the EPON 862 composite. The MD simulated stress-strain relation is also compared to that predicted based on simple the rule of mixture. While the two curves are very close to each other at low strain level, the curve from rule-of-mixture is always above from MD.

Al-Ostaz et al. [89] employed MD simulation of SWNT-polymer composite using PE as polymer matrix. Results obtained from various types of loadings applied to SWCNT show that SWCNTs are transversely isotropic. Elastic constants are the same for SWCNT under various loadings. Thus, SWCNT behaves as a linear elastic material. The simulation of various SWCNT clusters establishes the fact that clusters of nanotubes have lower transverse properties when compared to individual nanotubes. SWCNTs lose their circularity when a polymer chain is placed in their vicinity. This shows that their transverse properties are comparatively poor.

Frankland et al. [90] used molecular dynamics (MD) simulations to generate the stress-strain behavior of polymer-carbon nanotube (NT) composites mechanically loaded in both the longitudinal and transverse directions. Molecular dynamics (MD) simulations were used to generate the stress-strain behavior of polymer-carbon nanotube (NT) composites mechanically loaded in both the longitudinal and transverse directions. Two NT geometries, long continuous fibers and short discontinuous fibers, were investigated.

The simulated stress-strain curves were compared with results calculated from the rule of mixtures. The stiffest behavior, and the one closest to approaching the stiffness obtained by using the rule of mixtures, was observed for the longitudinally loaded, long continuous NT composite. An increase in the aspect ratio of the NT in this composite is anticipated to lead to further enhancement of the stress–strain curve and greater differences between the longitudinal and transverse stress–strain behavior.

Yang et al. [91] performed molecular dynamics simulations of polyethylene/fullerene (PE/C60) nanocomposites with different fullerene contents. The simulation results show that, as the C60 content increases, the crystallinity of the ultimate structures of PE/C60 nanocomposites decreases.

Chowdhury et al. [92] investigated the effects of the matrix density, chemical cross-links in the interface and geometrical defect in the CNT on the interfacial shear strength (ISS) of CNT reinforced polyethylene composites. For this purpose, CNT pull-out from the polymer matrix has been simulated by the molecular dynamics method. The result shows that, with the increase of matrix density ISS increases and the presence of chemical cross-links in the interface increases the ISS of CNT–polymer composites.

Yang et al. [93] studied the mechanical properties of carbon nanotube embedded gold composite using MD simulation. The computational results show that the increase in Young's modulus of the long CNT-embedded gold composite over pure gold is much large. From the simulation, we also find that the yield stress and the yield strain of short CNT-embedded gold composite are evidently less than that of the nano-single crystal gold.

My research work will present classical molecular dynamics (MD) simulations of model polymer/CNT composites constructed by embedding a single wall (6, 6) CNT into five different amorphous polymer matrices: poly(methyl methacrylate) (PMMA), polypropylene (PP), polyethylene (PE), Polystyrene (PS) and Nylon 6 (PA6) respectively. A constant-strain energy minimization method was then applied to calculate the axial elastic modulus, bulk modulus, shear modulus and compressibility of the composite system.

6.2 PMMA/CNT Composite System

6.2.1 Building Molecular Model of the Polymer Matrix

Polymethyl methacrylate (PMMA), which is widely used in engineering and for many utility items, has been chosen as the matrix material for construction of the composite. An amorphous polymer matrices of PMMA free from finite size effects and any residual stresses is built taking two chains of syndiotactic PMMA with fifty monomer units per chain. The simulation cell was then subjected to periodic boundary condition. The periodic box is constructed using COMPASS force field parameter with initial density of 0.1 g/cm^3 . The equilibrium state in MD requires fulfillment of two major criteria – to achieve energy stabilized state at a prescribed temperature and to obtain minimum stress state for the periodic box. The stable state was achieved by subjecting the model to NVT ensemble simulation. In the second step, the unit cell size was adjusted to minimize the initial stresses using NPT ensembles for several thousand steps depending on the molecular model and cell size. At the end of these steps, the molecular model was believed to be relaxed at 298 K with minimum initial stress. During NPT dynamics the density of the matrix is increased by reducing the lengths of the unit cell. The density of the final matrix was 1.18 g/cm^3 which is the experimental density value of amorphous PMMA at a temperature of 298 K and a pressure of 1 atm. A time step of 1 fs is used for all the simulations. A single polymer chain of PMMA and an amorphous PMMA matrix with correct density and residuals stresses are shown in Figure 6.1 and 6.2 respectively.

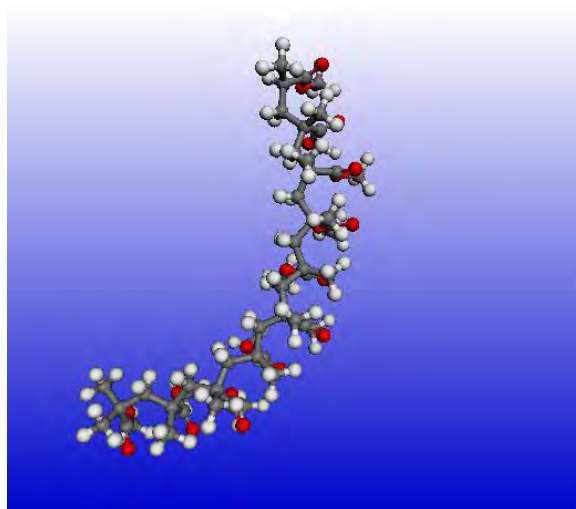


Fig. 6.1: Computer constructed polymer chain of PMMA

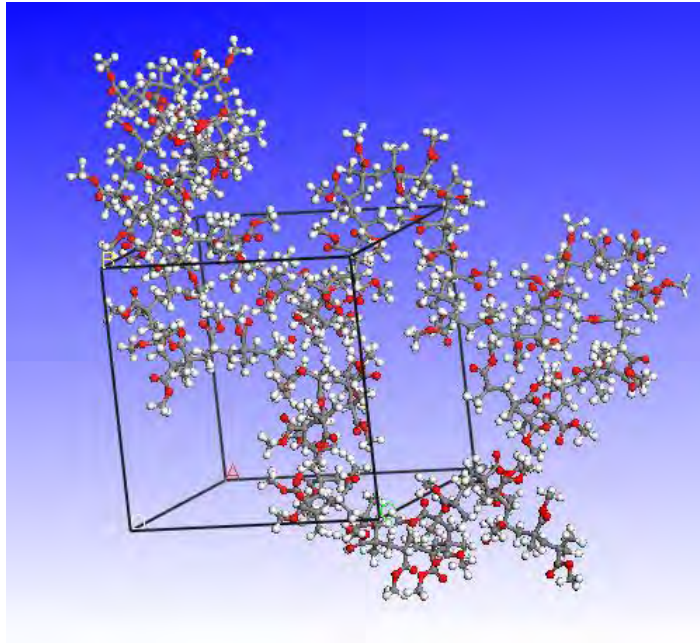


Fig 6.2: PMMA amorphous cell

6.2.2 Calculation of Mechanical Properties of the Polymer System

The constant-strain energy minimization method was applied to calculate the elastic moduli of the amorphous polymer. In general, the stress in a solid (or a group of interacting particles in the form of a solid) is defined as the change in the internal energy per unit volume with respect to the strain. Small strains were applied to a periodic structure at an energy minimum. The application of strain was accomplished by uniformly expanding the dimensions of the simulation cell in the direction of the deformation and re-scaling the new coordinates of the atoms to fit within the new dimensions. The structure was then re-minimized keeping the lattice parameters fixed, and the resultant stress in the minimized structure was measured. This was repeated for a series of strains. The variation of the measured stress as a function of applied strain was used to derive the stiffness matrix. Since the periodic computation cell is triclinic, the system is not isotropic. Thus the Young's modulus of the PMMA matrix constructed was calculated by taking the average value in the x , y and z directions. The final mechanical properties of the simulated system are shown in the Table 6.1.

Table 6.1: Simulated properties of amorphous PMMA

Amorphous PMMA	
Density	1.184 g/cm ³
Young's Modulus	2.727 GPa
Bulk Modulus	1.608 GPa
Shear Modulus	1.120 GPa
Poisson's Ratio	0.37

These values are in good agreement with experimentally established values [6][84][94-95].

6.2.3 Study of PMMA/CNT Composite System

Atomic scale modeling of a polymer/CNT composite system is rather challenging because of the significant number of atoms involved, and equilibration times for the polymer that are orders of magnitude longer than a few nanoseconds, which is typically the limit of large classical molecular dynamics simulations. Thus, the present simulation work is focused on composite systems with a large CNT volume fraction (>10%) in order to reduce the total size of the model. Although experimental systems typically contain much lower volume fractions of CNTs, this simulation results can help to understand interfacial behavior on an atomic scale, and can make useful predictions for lower CNT volume fraction enhancement by extrapolation.

The simulation cell for the composite consists of single (6, 6) SWCNT embedded in PMMA matrix. The dimension of the simulation cell was maintained as $2.4127 \text{ nm} \times 2.4127 \text{ nm} \times 2.4127 \text{ nm}$.

Then the energy of the polymer/CNT composite system is minimized using conjugate gradient method. The energy minimization is followed by a long time NVT dynamics process to obtain a stable CNT reinforced PMMA composite. The periodic boundary condition is applied to replicate the cell in all three directions and that the simulation is carried out at temperature of 298 K with a 1 fs time step.

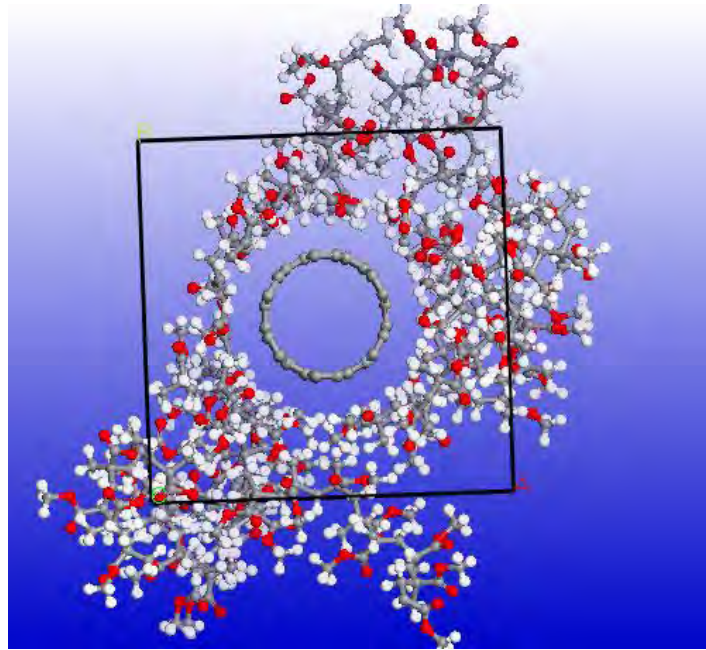


Fig. 6.3: CNT (6, 6) reinforced PMMA matrix

After the forgoing procedures, the radial distribution function (RDF) $g(r)$ was calculated for all non-bonded VDW atom pairs which comprise atoms that contribute to non-bonded energy. These $g(r)$ functions were then utilized to estimate VDW separation distance or gap (h_{vdw}), henceforth referred here as VDW zone was also calculated for comparison.

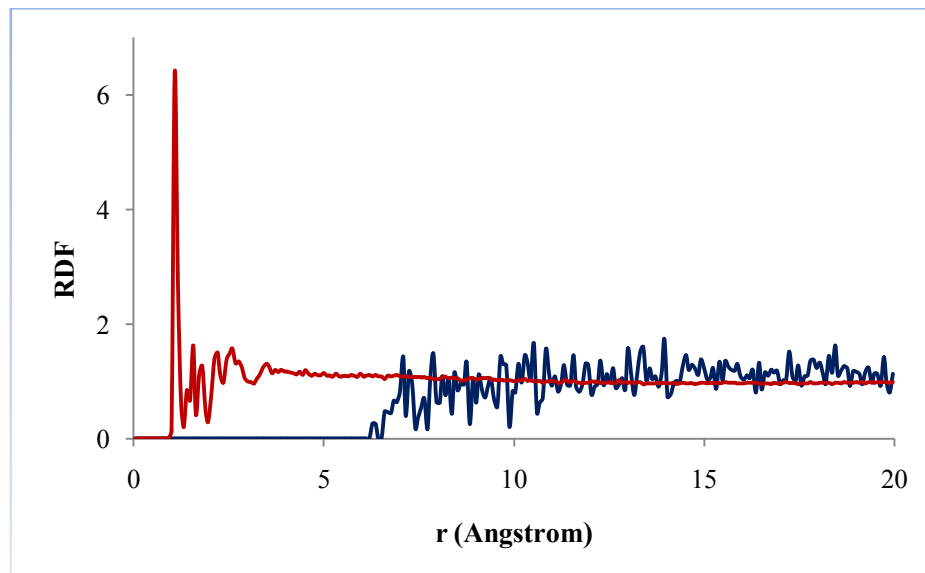


Fig. 6.4: Radial distribution function (RDF) for the PMMA/CNT composite system.

Following equilibration, the amorphous model of PMMA/CNT composite was then subjected to constant-strain minimization for the calculation of mechanical properties. The position of the CNT was kept unchanged in order to maintain the unreformed shape of the CNT. Using this technique a uniform strain field (0.5%) was applied to the periodic cell. Various strain components resulting from applied strains were recorded to derive the stiffness matrix.

The final mechanical properties of the polymer/composite system are shown in the Table 6.2.

Table 6.2: Simulated properties of PMMA/CNT composite system

PMMA/CNT composite system	
Young's Modulus	95.017 GPa
Bulk Modulus	34.81 GPa
Shear Modulus	6.97 GPa
Compressibility	41.3 TPa ⁻¹

After MD minimization the VDW separation distance between the CNT and the PMMA matrix is found to be about 0.226 nm and the volume fraction of the CNT (f_{CNT}) is calculated as 14.6%.

Table 6.3: Summary of numerical results for elastic modulus of PMMA/CNT composite system

	Molecular dynamics results	Rule of mixtures
Longitudinal Young's modulus (GPa)	95.017	104.5
Transverse Young's modulus (GPa)	3.804	3.15

From the Table 6.3, we can see that subjected to transverse loading condition, there is no strong reinforcement of the matrix. This is because the matrix material sustains most of the load in the transverse direction, and also the Young's modulus for SWNTs in the transverse direction (30 GPa in the present calculation) is very small compared with that

of the longitudinal direction (700 GPa in the present calculation). However, in the longitudinal direction, the Young's modulus clearly increases since the CNTs carried most of the load in this direction.

A longitudinal modulus of 700 GPa and transverse modulus of 30 GPa for (6, 6) SWNT were used here. These modulus values were calculated via constant strain energy minimization method for a hexagonal, infinitely periodic SWNT bundle. The 2D unit cell formed by the centers of adjacent SWNTs in the bundle therefore defined the transverse cross-sectional area per tube. A value of 700 GPa calculated using this method is equivalent to about 1 TPa when considering an isolated single wall nanotube modeled as a solid beam. This value is within the range of most of the theoretical and experimental results [6].

6.3 Polystyrene (PS)/CNT Composite System

6.3.1 Building Molecular Model of the Polymer Matrix

The matrix utilized in this simulation is polystyrene. Polystyrene is a vinyl polymer. Structurally, it is a long hydrocarbon chain, with a phenyl group attached to every other carbon atom. Polystyrene is produced by free radical vinyl polymerization, from the monomer styrene. A chain of polystyrene was first created with 50 repeat units. A periodic cell was then constructed with two chains of the atactic polystyrene molecule with initial density of 0.1 g/cm^3 using the COMPASS force field parameters. The equilibrium state in MD requires fulfillment of two major criteria – to achieve energy stabilized state at a prescribed temperature and to obtain minimum stress state for the periodic box. The stable state was achieved by subjecting the model to NVT ensemble simulation for 50 ps. In the second step, the unit cell size was adjusted to minimize the initial stresses using NPT ensembles for several thousand steps depending on the molecular model and cell size. At the end of these steps, the molecular model was believed to be relaxed at 298 K with minimum initial stress. During NPT dynamics the density of the matrix is increased by reducing the lengths of the unit cell. The density of the final matrix was 1.03 g/cm^3 which is very close to the experimental value of 1.05 g/cm^3 at a temperature and pressure of 298 K and 1 atm respectively. A time step of 1 fs is used for all the simulations. A single polymer chain of atactic polystyrene and an amorphous polymer matrix of PS with correct density and zero residuals stresses are shown in the Figure 6.5 and 6.6 respectively.

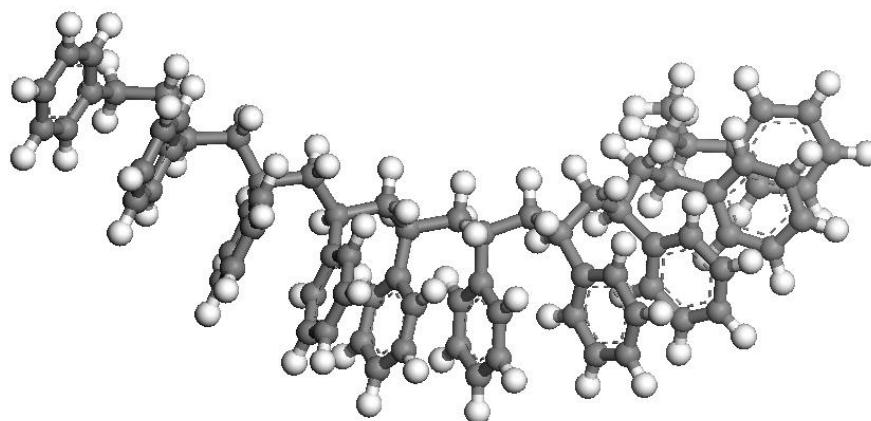


Fig. 6.5: Computer constructed polymer chain of PS

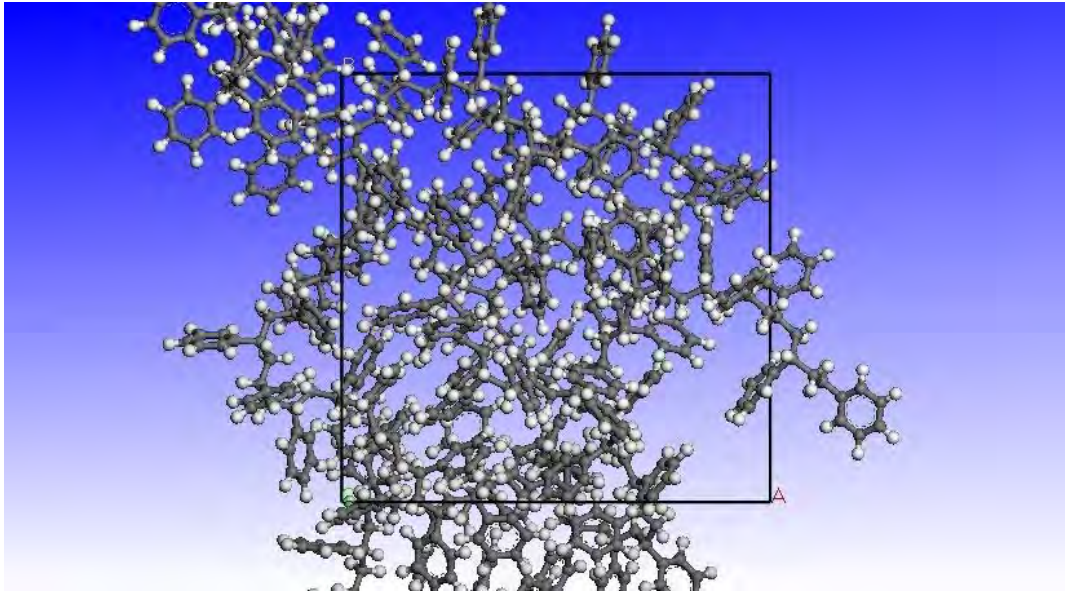


Fig 6.6: PS amorphous cell

6.3.2 Calculation of Mechanical Properties of the Polymer System

The constant-strain energy minimization method was applied to calculate the elastic moduli of the amorphous polymer. In general, the stress in a solid (or a group of interacting particles in the form of a solid) is defined as the change in the internal energy per unit volume with respect to the strain. Small strains were applied to a periodic structure at an energy minimum. The application of strain was accomplished by uniformly expanding the dimensions of the simulation cell in the direction of the deformation and re-scaling the new coordinates of the atoms to fit within the new dimensions. The structure was then re-minimized keeping the lattice parameters fixed, and the resultant stress in the minimized structure was measured. This was repeated for a series of strains. The variation of the measured stress as a function of applied strain was used to derive the stiffness matrix. Since the periodic computation cell is triclinic, the system is not isotropic. Thus the Young's modulus of the PS matrix constructed was calculated by taking the average value in the x , y and z directions. The final mechanical properties of the simulated system are shown in the Table 6.4.

Table 6.4: Simulated properties of amorphous PS

Amorphous PS	
Density	1.03 g/cm ³
Young's Modulus	3.217 GPa
Bulk Modulus	2.495 GPa
Shear Modulus	1.252 GPa
Poisson's Ratio	0.29

These values are in good agreement with experimentally established values [94-97].

6.3.3 Study of PS/CNT Composite System

A (6, 6) SWNT was placed in the centre of the periodic simulation cell. Thus, after the addition of the SWNT the composite cell is composed of a fragment of SWNT fully embedded inside the polystyrene. The dimension of the simulation cell was maintained as $2.529 \text{ nm} \times 2.529 \text{ nm} \times 2.529 \text{ nm}$.

Then the energy of the PS/CNT composite system is minimized using conjugate gradient method. The energy minimization is followed by a long time NVT dynamics process to obtain a stable CNT reinforced PS composite. We also remark that, the periodic boundary condition is applied to replicate the cell in all three directions and that the simulation is carried out at temperature of 298 K with a 1 fs time step.

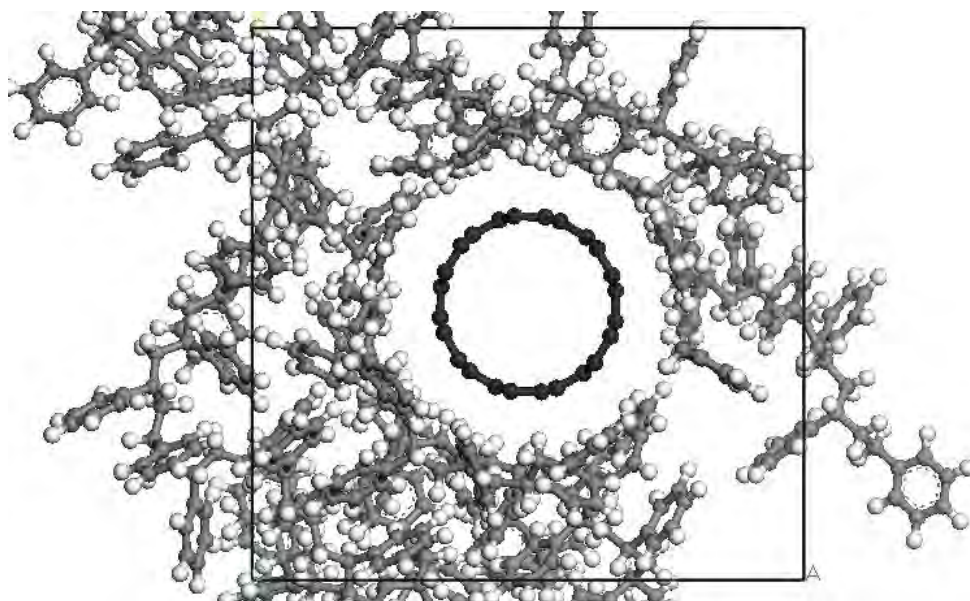


Fig. 6.7: CNT (6, 6) reinforced PS matrix

After the forgoing procedures, the radial distribution function (RDF) $g(r)$ was calculated for all non-bonded VDW atom pairs which comprise atoms that contribute to non-bonded energy. There $g(r)$ functions were then utilized to estimate VDW separation distance or gap (h_{vdw}), henceforth referred here as VDW zone was also calculated for comparison.

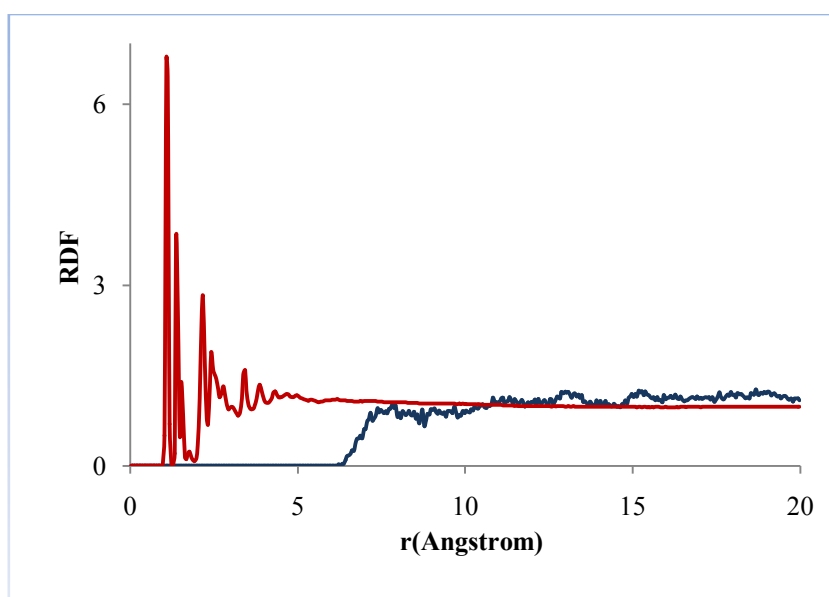


Fig. 6.8: Radial distribution function (RDF) for the PS/CNT composite system.

Following equilibration, the PS/CNT composite was then subjected to constant-strain minimization for the calculation of mechanical properties. The position of the CNT was kept unchanged in order to maintain the unreformed shape of the CNT. Using this technique a uniform strain field (0.5%) was applied to the periodic cell. Various strain components resulting from applied strains were recorded to derive the stiffness matrix.

The final mechanical properties of the polymer/composite system are shown in Table 6.5.

Table 6.5: Simulated properties of PS/CNT composite system

PS/CNT composite system	
Young's Modulus	110.8 GPa
Bulk Modulus	12.1 GPa
Shear Modulus	5.41 GPa
Compressibility	215 TPa ⁻¹

After MD minimization the VDW separation distance between the CNT and the PS matrix is found to be about 0.25 nm and the volume fraction of the CNT (f_{CNT}) is calculated as 14.1%.

Table 6.6: Summary of numerical results for elastic modulus of PS/CNT composite system

	Molecular dynamics results	Rule of mixtures
Longitudinal elastic modulus (GPa)	110.8	101.5
Transverse elastic modulus (GPa)	3.37	3.68

From the Table 6.6, we can see that subjected to transverse loading condition, there is no strong reinforcement of the matrix. This is because the matrix material sustains most of the load in the transverse direction, and also the Young's modulus for SWNTs in the transverse direction (30 GPa) is very small compared with that of the longitudinal direction (700 GPa). However, in the longitudinal direction, the Young's modulus clearly increases since the CNTs carried most of the load in this direction.

6.4 Nylon 6 (PA6)/CNT Composite System

6.4.1 Building Molecular Model of the Polymer Matrix

The matrix utilized in this simulation is Nylon 6. Nylon 6 is a thermoplastic polyamide 6 (PA6). A chain of PA6 was first created with 25 repeat units. A periodic cell was then constructed with three chains of the isotactic nylon 6 molecule with initial density of 0.1 g/cm^3 using the COMPASS force field parameters. The equilibrium state in MD requires fulfillment of two major criteria – to achieve energy stabilized state at a prescribed temperature and to obtain minimum stress state for the periodic box. The stable state was achieved by subjecting the model to NVT ensemble simulation for 50 ps. In the second step, the unit cell size was adjusted to minimize the initial stresses using NPT ensembles for several thousand steps depending on the molecular model and cell size. At the end of these steps, the molecular model was believed to be relaxed at 298 K with minimum initial stress. During NPT dynamics the density of the matrix is increased by reducing the lengths of the unit cell. The density of the final matrix was 1.082 g/cm^3 which is very close to the experimental value of 1.084 g/cm^3 at a temperature and pressure of 298 K and 1 atm respectively. A time step of 1 fs is used for all the simulations. A single polymer chain of PA6 and an amorphous polymer matrix of PA6 with correct density and zero residuals stresses are shown in the Figure 6.9 and 6.10 respectively.

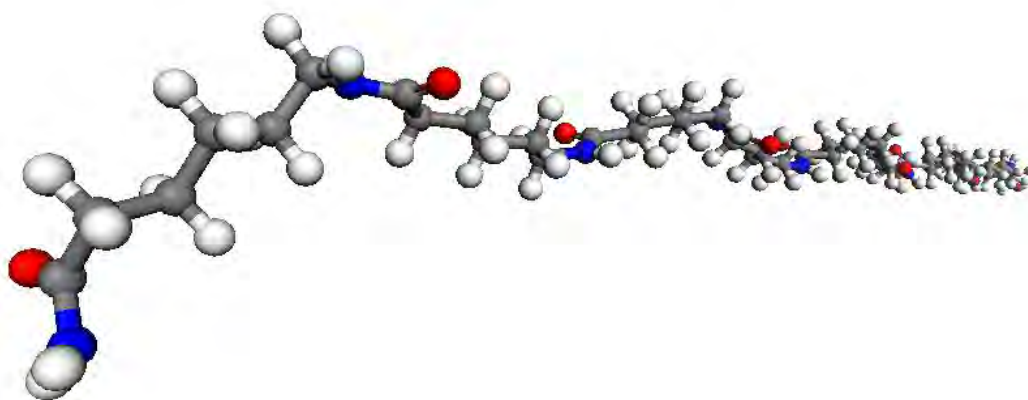


Fig. 6.9: Computer constructed polymer chain of Nylon 6 (PA6)

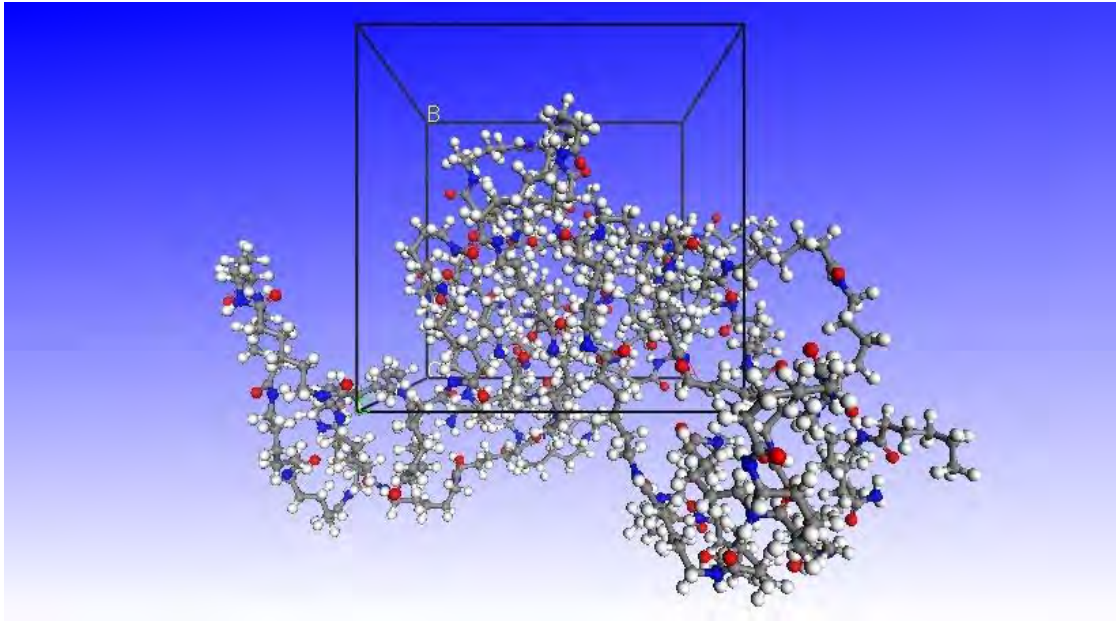


Fig. 6.10: Amorphous Nylon 6 cell

6.4.2 Calculation of Mechanical Properties of the Polymer System

The constant-strain energy minimization method was applied to calculate the elastic moduli of the amorphous polymer. In general, the stress in a solid (or a group of interacting particles in the form of a solid) is defined as the change in the internal energy per unit volume with respect to the strain. Small strains were applied to a periodic structure at an energy minimum. The application of strain was accomplished by uniformly expanding the dimensions of the simulation cell in the direction of the deformation and re-scaling the new coordinates of the atoms to fit within the new dimensions. The structure was then re-minimized keeping the lattice parameters fixed, and the resultant stress in the minimized structure was measured. This was repeated for a series of strains. The variation of the measured stress as a function of applied strain was used to derive the stiffness matrix. Since the periodic computation cell is triclinic, the system is not isotropic. Thus the Young's modulus of the Nylon 6 matrix constructed was calculated by taking the average value in the x , y and z directions. The final mechanical properties of the simulated system are shown in the Table 6.8.

Table 6.7: Simulated properties of amorphous Nylon 6

Amorphous Nylon 6	
Density	1.082 g/cm ³
Young's Modulus	2.28 GPa
Bulk Modulus	3.73 GPa
Shear Modulus	0.816 GPa
Poisson's Ratio	0.398

These values are in good agreement with experimentally established values [94-95][97-99].

6.4.3 Study of Nylon 6/CNT Composite System

A (6, 6) SWNT was placed in the centre of the periodic simulation cell. Thus, after the addition of the SWNT the composite cell is composed of a fragment of SWNT fully embedded inside the polyamide 6. The dimension of the simulation cell was maintained as $2.353 \text{ nm} \times 2.353 \text{ nm} \times 2.353 \text{ nm}$.

Then the energy of the Nylon 6/CNT composite system is minimized using conjugate gradient method. The energy minimization is followed by a long time NVT dynamics process to obtain a stable CNT reinforced Nylon 6 composite. We also remark that, the periodic boundary condition is applied to replicate the cell in all three directions and that the simulation is carried out at temperature of 298 K with a 1 fs time step.

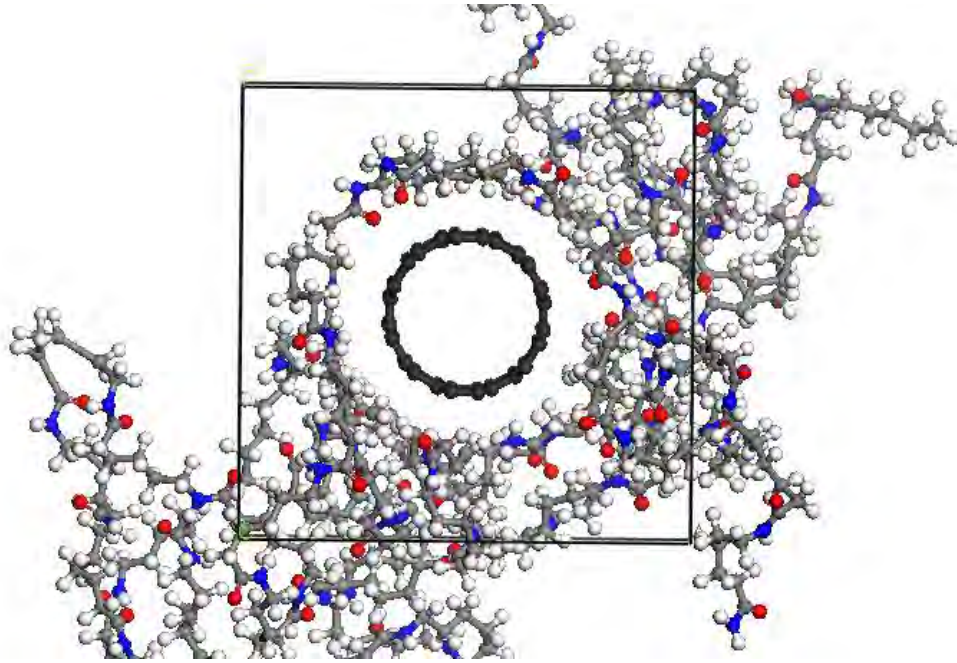


Fig. 6.11: CNT (6, 6) reinforced Nylon 6 matrix

After the forgoing procedures, the radial distribution function (RDF) $g(r)$ was calculated for all non-bonded VDW atom pairs which comprise atoms that contribute to non-bonded energy. There $g(r)$ functions were then utilized to estimate VDW separation distance or gap (h_{vdw}), henceforth referred here as VDW zone was also calculated for comparison.

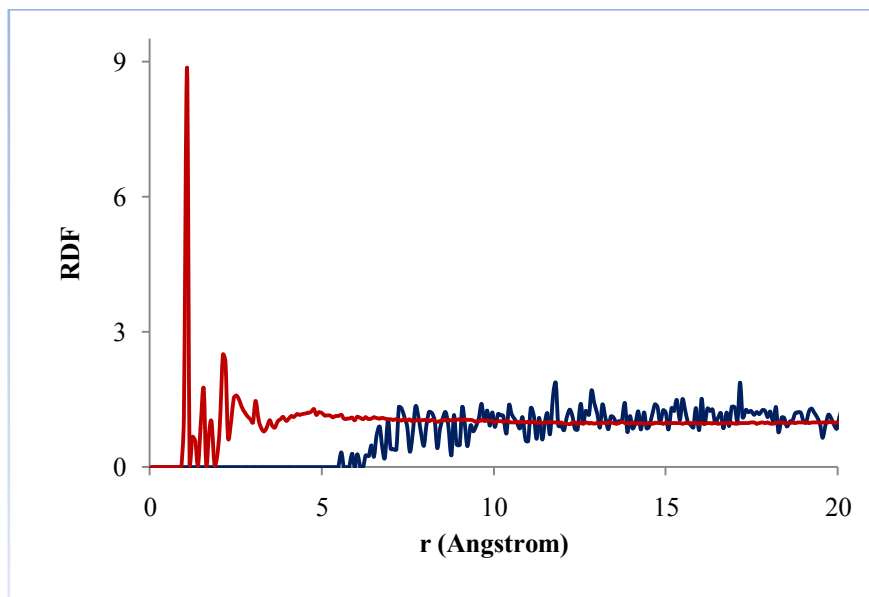


Fig. 6.12: Radial distribution function (RDF) for the Nylon 6/CNT composite system.

Following equilibration, the Nylon 6/CNT composite was then subjected to constant-strain minimization for the calculation of mechanical properties. The position of the CNT was kept unchanged in order to maintain the unreformed shape of the CNT. Using this technique a uniform strain field (0.5%) was applied to the periodic cell. Various strain components resulting from applied strains were recorded to derive the stiffness matrix.

The final mechanical properties of the PA6/composite system are shown in the Table 6.8.

Table 6.8: Simulated properties of Nylon 6/CNT composite system

Nylon 6/CNT composite system	
Young's Modulus	50.84 GPa
Bulk Modulus	10.52 GPa
Shear Modulus	2.5 GPa
Compressibility	112 TPa ⁻¹

After MD minimization the VDW separation distance between the CNT and the Nylon 6 matrix is found to be about 0.149 nm and the volume fraction of the CNT (f_{CNT}) is calculated as 13.16%.

Table 6.9: Summary of numerical results for elastic modulus of PA6/CNT composite system

	Molecular dynamics results	Rule of mixtures
Longitudinal tensile modulus (GPa)	50.84	94
Transverse tensile modulus (GPa)	5.9	2.6

From the Table 6.9, we can see that subjected to transverse loading condition, there is no strong reinforcement of the matrix. This is because the matrix material sustains most of the load in the transverse direction, and also the Young's modulus for SWNTs in the transverse direction (30 GPa in the present calculation) is very small compared with that of the longitudinal direction (700 GPa in the present calculation). However, in the longitudinal direction, the Young's modulus clearly increases since the CNTs carried most of the load in this direction.

6.5 Polyethylene (PE)/CNT Composite System

6.5.1 Building Molecular Model of the Polymer Matrix

The matrix utilized in this simulation is Polyethylene (PE). Polyethylene is a thermoplastic commodity polymer created through polymerization of ethylene. The ethylene molecule, C_2H_4 is $CH_2=CH_2$, two CH_2 connected by a double bond. A chain of polyethylene was first created with 50 repeat units. A periodic cell was then constructed with five chains of the polyethylene molecule with initial density of 0.1 g/cm^3 using the COMPASS force field parameters.

Polyethylene is characterized as a semi-crystalline polymer, made up of crystalline regions and amorphous regions. Crystalline regions are those of highly ordered, neatly folded, layered and densely packed molecular chains. These occur only when chains branching off the sides of the primary chains are small in number. Within crystalline regions, molecules have properties that are locally directionally dependent. Where tangled molecular chains branching off the molecular trunk chains interfere with or inhibit the close and layered packing of the trunks, the random resulting arrangement is of lesser density, and termed amorphous. An abundance of closely packed polymer chains results in a tough material of moderate stiffness.

High-density polyethylene resin has a greater proportion of crystalline regions than low-density polyethylene. Hypothetically, a completely crystalline polyethylene would be too brittle to be functional and a completely amorphous polyethylene would be waxlike, much like paraffin. Upon heating, the ordered crystalline structure regresses to the disordered amorphous state; with cooling, the partially crystalline structure is recovered.

This initial periodic model was subjected to the molecular dynamics simulation where an equilibration sequence was performed. The equilibrium state in MD requires fulfillment of two major criteria – to achieve energy stabilized state at a prescribed temperature and to obtain minimum stress state for the periodic box. Initially, the simulation ran for 10,000 time-steps ($\Delta t=1 \text{ fs}$) using NVT dynamics at 500 K followed by relaxation for 50,000 time-steps ($\Delta t=1 \text{ fs}$) using NPT dynamics at 500 K. The next relaxation cooled the structure down to the desired temperature for 50,000 time-steps followed by further relaxation of 50,000 time-steps at the desired temperature.

The density of the final semi-crystalline polymer matrix was 0.91 g/cm^3 which falls within the range of experimental values for low density polyethylene ($0.91\text{-}0.94 \text{ g/cm}^3$), which contains a high degree of short and long chain branching [100]. A single polymer chain of polyethylene and an amorphous polymer matrix of PE with correct density and zero residuals stresses are shown in the Figure 6.13 and 6.14 respectively.

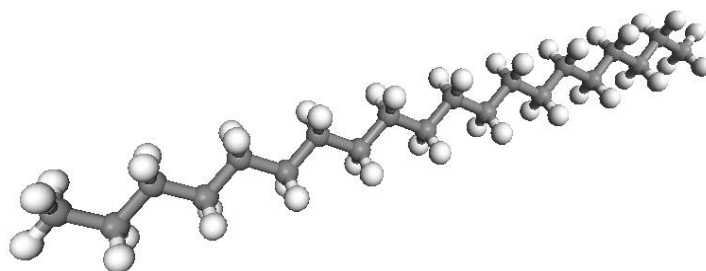


Fig. 6.13: Computer constructed polymer chain of PE

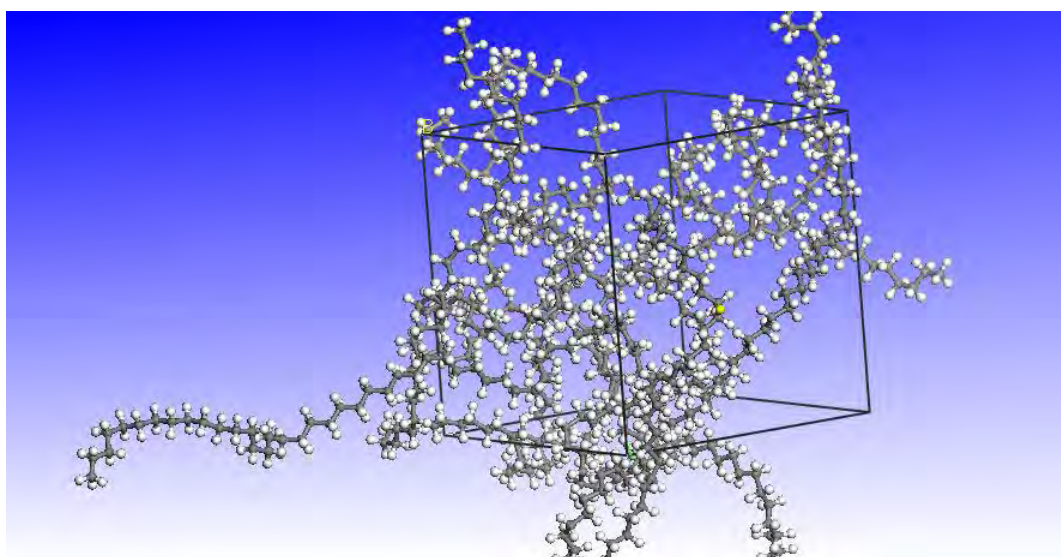


Fig. 6.14: Amorphous PE cell

6.5.2 Calculation of Mechanical Properties of the Polymer System

The constant-strain energy minimization method was applied to calculate the elastic moduli of the polymer. In general, the stress in a solid (or a group of interacting particles in the form of a solid) is defined as the change in the internal energy per unit volume with respect to the strain. Small strains were applied to a periodic structure at an energy minimum. The application of strain was accomplished by uniformly expanding the dimensions of the simulation cell in the direction of the deformation and re-scaling the new coordinates of the atoms to fit within the new dimensions. The structure was then re-minimized keeping the lattice parameters fixed, and the resultant stress in the minimized structure was measured. This was repeated for a series of strains. The variation of the measured stress as a function of applied strain was used to derive the stiffness matrix. Since the periodic computation cell is triclinic, the system is not isotropic. Thus the Young's modulus of the PE matrix constructed was calculated by taking the average value in the x , y and z directions. The final mechanical properties of the simulated system are shown in the Table 6.10.

Table 6.10: Simulated properties of semi-crystalline PE

Semi-crystalline PE Matrix	
Density	0.91 g/cm ³
Young's Modulus	0.9873 GPa
Bulk Modulus	0.897 GPa
Shear Modulus	0.374 GPa
Poisson's Ratio	0.32

These values are in good agreement with experimentally established values [95][100-103].

6.5.3 Study of PE/CNT Composite System

Atomic scale modeling of a polymer/CNT composite system is rather challenging because of the significant number of atoms involved, and equilibration times for the polymer that are orders of magnitude longer than a few nanoseconds, which is typically

the limit of large classical molecular dynamics simulations. Thus, the present simulation work is focused on composite systems with a large CNT volume fraction ($>10\%$) in order to reduce the total size of the model. Although experimental systems typically contain much lower volume fractions of CNTs, this simulation results can help to understand interfacial behavior on an atomic scale, and can make useful predictions for lower CNT volume fraction enhancement by extrapolation.

A (6, 6) SWNT was placed in the centre of the periodic simulation cell. Thus, after the addition of the SWNT the composite cell is composed of a fragment of SWNT fully embedded inside the polyethylene matrix. The dimension of the simulation cell was maintained as $2.36 \text{ nm} \times 2.36 \text{ nm} \times 2.36 \text{ nm}$.

Then the energy of the PE/CNT composite system is minimized using conjugate gradient method. The energy minimization is followed by a long time NVT dynamics process to obtain a stable CNT reinforced PE composite. We also remark that, the periodic boundary condition is applied to replicate the cell in all three directions and that the simulation is carried out at temperature of 298 K with a 1 fs time step.

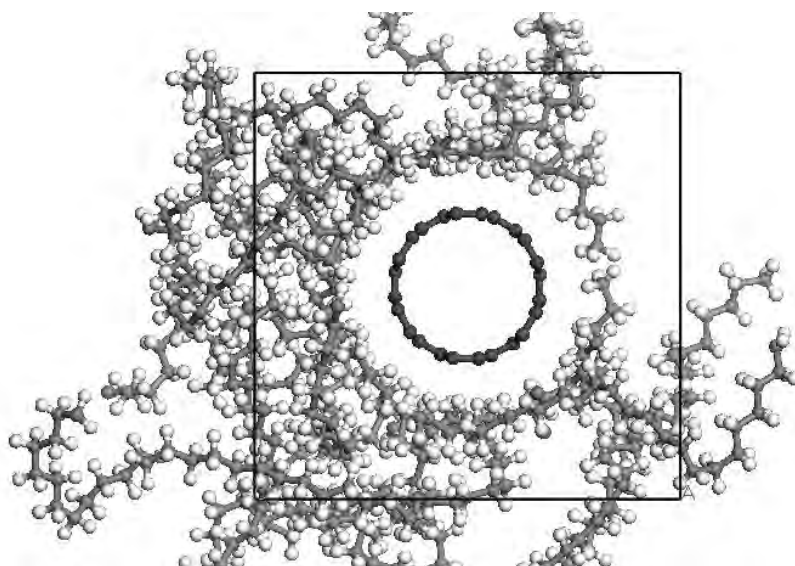


Fig. 6.15: CNT (6, 6) reinforced PE matrix

After the forgoing procedures, the radial distribution function (RDF) $g(r)$ was calculated for all non-bonded VDW atom pairs which comprise atoms that contribute to non-bonded

energy. These $g(r)$ functions were then utilized to estimate VDW separation distance or gap (h_{vdw}), henceforth referred here as VDW zone was also calculated for comparison.

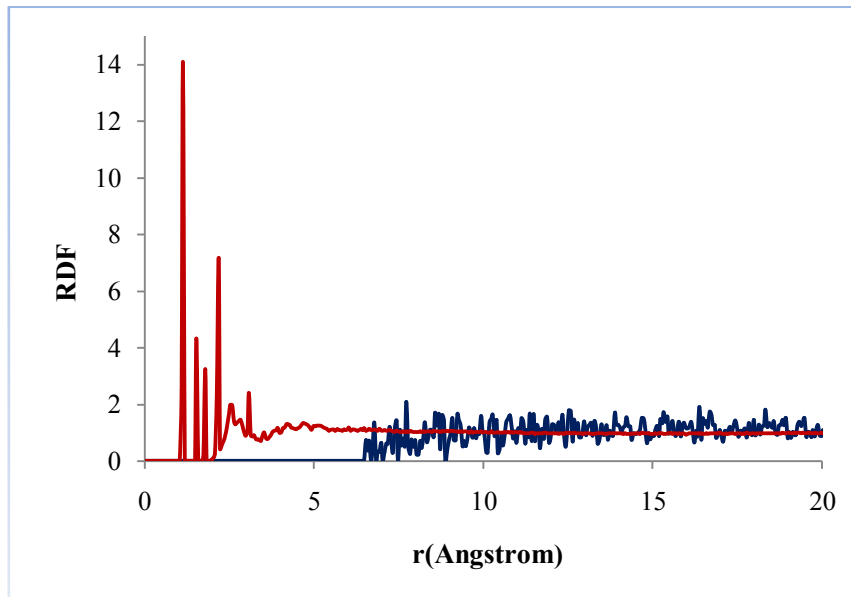


Fig. 6.16: Radial distribution function (RDF) for PE/CNT composite

Following equilibration, the PE/CNT composite was then subjected to constant-strain minimization for the calculation of mechanical properties. The position of the CNT was kept unchanged in order to maintain the unreformed shape of the CNT. Using this technique a uniform strain field (0.5%) was applied to the periodic cell. Various strain components resulting from applied strains were recorded to derive the stiffness matrix.

The final mechanical properties of the PE/composite system are shown in the Table 6.11.

Table 6.11: Simulated properties of PE/CNT composite system

PE/CNT composite system	
Young's Modulus	46.5 GPa
Bulk Modulus	14.2 GPa
Shear Modulus	3.27 GPa
Compressibility	77 TPa ⁻¹

After MD minimization the VDW separation distance between the CNT and the PE matrix is found to be about 0.245 nm and the volume fraction of the CNT (f_{CNT}) is calculated as 15.8% .

Table 6.12: Summary of numerical results for elastic modulus of PE/CNT composite system

	Molecular dynamics results	Rule of mixtures
Longitudinal elastic modulus (GPa)	46.5	111

6.5.4 Experimental Evidence

The promising area of composite research involves an enhancement of mechanical properties of polymer using CNTs as a reinforcing material. Although several studies have been focused on producing nano-composites, many practical challenges concerning their fabrication still remain, compromising the full realization of their enormous potential. Dispersing nanotubes individually and uniformly into the polymer matrix seems to be fundamental when producing composites with enhanced and reproducible properties. One of the most significant challenges toward improving the properties of nanocomposites based on carbon nanotubes is to obtain a uniform dispersion of nanotubes within the polymer matrix. Because of their small size, carbon nanotubes will tend to agglomerate when dispersed in a polymeric resin. To achieve good reinforcement in a composite, it is critical to have uniform dispersion within the polymer matrix. In addition to slipping of tubes that are not adhered to the matrix, aggregates of nanotube bundles effectively reduce the aspect ratio (length/diameter) of the reinforcement. Agglomeration is significant in CVD-grown nanotubes, since entanglement of the tubes occurs during nanotube growth [105]

Ji et al. [106] have discussed the difficulties obtained to get uniform dispersion of CNTs in a polymer matrix. Zou et al. [107] found that HDPE/CNT composites fabricated at higher screw speed give uniform dispersion of CNT in HDPE. Thostenson and Chou [105] studied mechanical properties of aligned and random oriented nano-composites using DMA and observed an improvement on Young's modulus with an addition of CNTs. Moreover, in the aligned composites, Young's modulus could be observed five times greater than that of randomly oriented composites.

S. Kanagaraj, Fátima R. Varanda, Tatiana V. Zhil'tsova, Mónica S.A. Oliveira, José A.O. Simões in an experiment, prepared CNT-HDPE composites and investigated the effect of CNT loading on mechanical properties [108]. The experiment is reported in “Mechanical properties of high density polyethylene/carbon nanotube composites” *Composites Science and Technology*, vol, 67, p. 3071–3077, 2007. Their experimental data are given in Table 6.13 below.

Table 6.13: Mechanical properties of CNT–HDPE nano-composites [108]

Volume fraction CNT concentration (%)	Young's modulus (GPa)
0.00	1.095
0.11	1.169
0.22	1.228
0.33	1.287
0.44	1.338

If the data of Table 6.13 are plotted in a graph, we get:

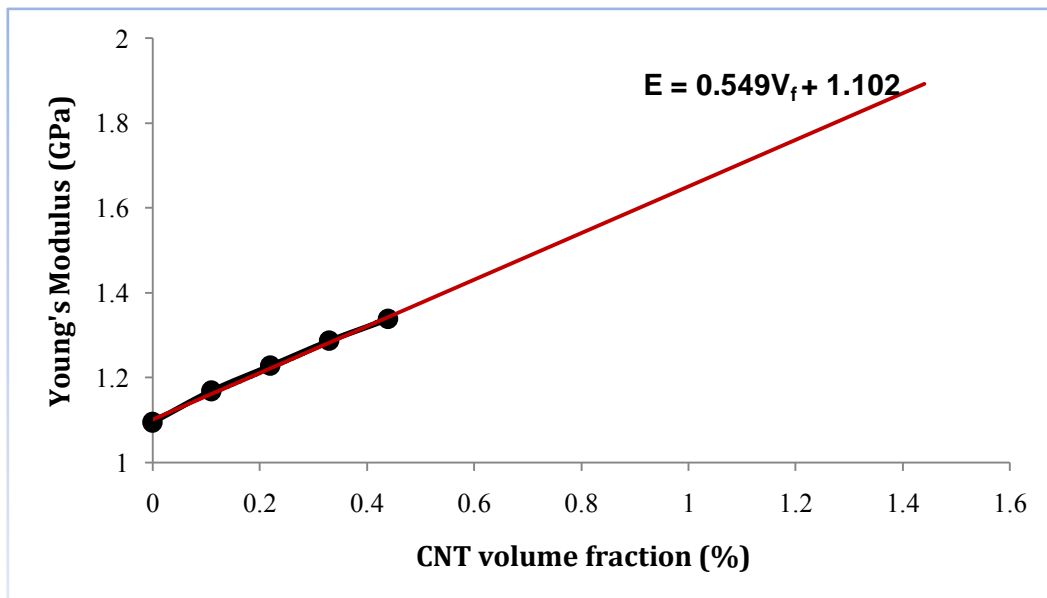


Fig. 6.17: Experimental data of elastic modulus Vs. CNT volume fraction plotted in a graph

The experimental values of stiffness show a linear increase of modulus with volume fraction of CNTs. In case of CNT–HDPE composites, it is considered as randomly oriented short fiber arrangement.

By extrapolation, at a CNT Volume fraction of 15.8%, we observe the Young's modulus of the CNT-HDPE composite will be 9.79 GPa. Since, addition of nanotube increases the tensile modulus of the polymer films, and the improvement in elastic modulus with the aligned nanotube composite is five times greater than the improvement for the randomly oriented composite [105], in an aligned composite with CNT volume fraction of 15.8%, the Young's modulus of the composite is expected to be around 48.96 GPa.

In the experimental work, CVD-grown multi-walled nanotubes were dispersed randomly in a HDPE thermoplastic matrix whereas; in our simulation we embedded SWCNT inside LDPE thermoplastic matrix. From the results of our simulation, the measure of reinforcement for CNT–LDPE composites at 15.8% volume fraction comes about 46.5 GPa which has very close agreement with the results obtained in the experimental study.

6.6 Polypropylene (PP)/CNT Composite System

6.6.1 Building Molecular Model of the Polymer Matrix

The matrix utilized in this simulation is Polypropylene (PP). Polypropylene is a thermoplastic polymer created through polymerization of propylene. It is a linear structure based on the monomer C_nH_{2n} . It is manufactured from propylene gas in presence of a catalyst such as titanium chloride. Beside, PP is a by-product of oil refining processes. A chain of isotactic polypropylene was first created with 25 repeat units. A periodic cell was then constructed with three chains of the polypropylene molecule with initial density of 0.1 g/cm^3 using the COMPASS force field parameters. The equilibrium state in MD requires fulfillment of two major criteria – to achieve energy stabilized state at a prescribed temperature and to obtain minimum stress state for the periodic box. The stable state was achieved by subjecting the model to NVT ensemble simulation for 50 ps. In the second step, the unit cell size was adjusted to minimize the initial stresses using NPT ensembles for several thousand steps depending on the molecular model and cell size. At the end of these steps, the molecular model was believed to be relaxed at 298 K with minimum initial stress. During NPT dynamics the density of the matrix is increased by reducing the lengths of the unit cell. The density of the final matrix was 0.853 g/cm^3 which is very close to the experimental value of 0.855 g/cm^3 at a temperature and pressure of 298 K and 1 atm respectively. A time step of 1 fs is used for all the simulations. A single polymer chain of isotactic polypropylene and an amorphous polymer matrix of PP with correct density and zero residuals stresses are shown in the Figure 6.18 and 6.19 respectively.

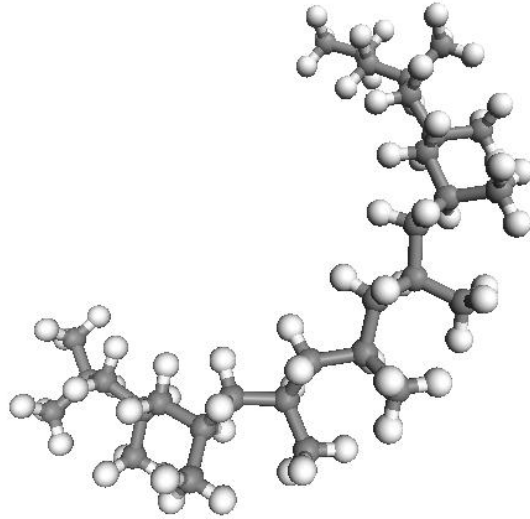


Fig. 6.18: Computer constructed polymer chain of PP

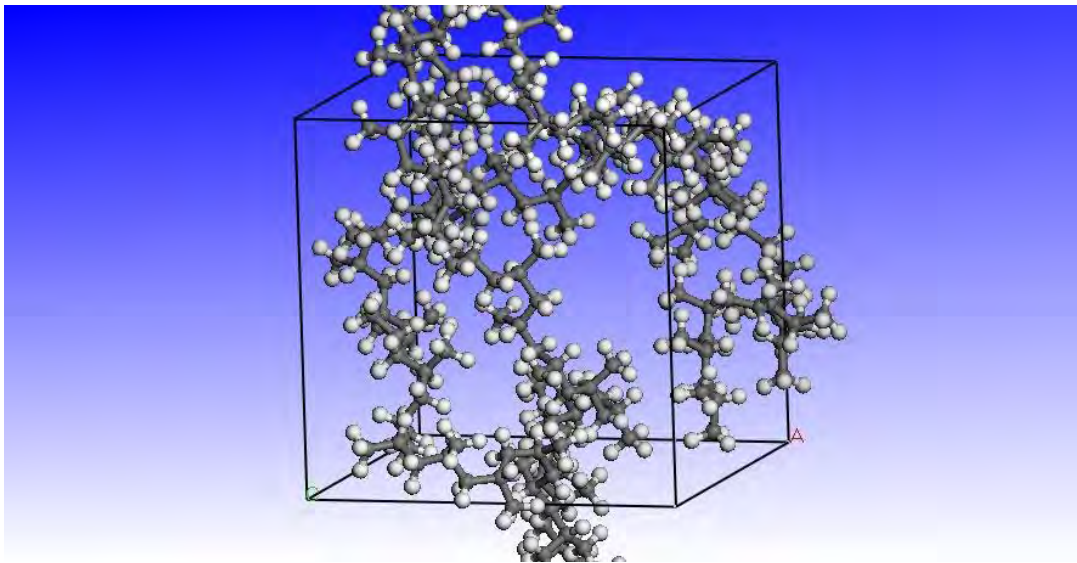


Fig. 6.19: Amorphous PP cell

6.6.2 Calculation of Mechanical Properties of the Polymer System

The constant-strain energy minimization method was applied to calculate the elastic moduli of the amorphous polymer. In general, the stress in a solid (or a group of interacting particles in the form of a solid) is defined as the change in the internal energy per unit volume with respect to the strain. Small strains were applied to a periodic

structure at an energy minimum. The application of strain was accomplished by uniformly expanding the dimensions of the simulation cell in the direction of the deformation and re-scaling the new coordinates of the atoms to fit within the new dimensions. The structure was then re-minimized keeping the lattice parameters fixed, and the resultant stress in the minimized structure was measured. This was repeated for a series of strains. The variation of the measured stress as a function of applied strain was used to derive the stiffness matrix. Since the periodic computation cell is triclinic, the system is not isotropic. Thus the Young's modulus of the PP matrix constructed was calculated by taking the average value in the x , y and z directions. The final mechanical properties of the simulated system are shown in the Table 6.14.

Table 6.14: Simulated properties of amorphous PP

Amorphous PP	
Density	0.853 g/cm ³
Young's Modulus	1.435 GPa
Bulk Modulus	0.708 GPa
Shear Modulus	0.617 GPa
Poisson's Ratio	0.40

These values are in good agreement with experimentally established values [94-95][109-110].

6.6.3 Study of PP/CNT Composite System

Atomic scale modeling of a polymer/CNT composite system is rather challenging because of the significant number of atoms involved, and equilibration times for the polymer that are orders of magnitude longer than a few nanoseconds, which is typically the limit of large classical molecular dynamics simulations. Thus, the present simulation work is focused on composite systems with a large CNT volume fraction (>10%) in order to reduce the total size of the model. Although experimental systems typically contain much lower volume fractions of CNTs, this simulation results can help to understand

interfacial behavior on an atomic scale, and can make useful predictions for lower CNT volume fraction enhancement by extrapolation.

The simulation cell for the composite consists of single (6, 6) SWCNT embedded in PP matrix. The dimension of the simulation cell was maintained as $1.833 \text{ nm} \times 1.833 \text{ nm} \times 1.833 \text{ nm}$.

Then the energy of the polymer/CNT composite system is minimized using conjugate gradient method. The energy minimization is followed by a long time NVT dynamics process to obtain a stable CNT reinforced PP composite. We also remark that, the periodic boundary condition is applied to replicate the cell in all three directions and that the simulation is carried out at temperature of 298 K with a 1 fs time step.

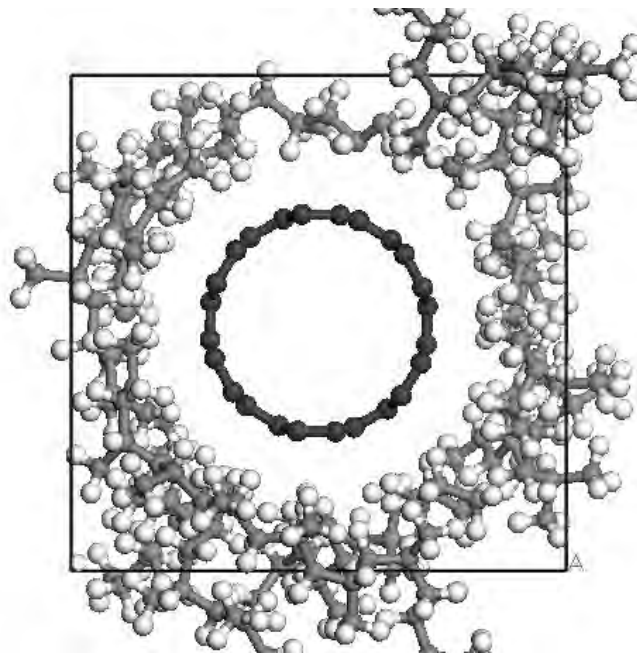


Fig. 6.20: CNT (6, 6) reinforced PP matrix

After the forgoing procedures, the radial distribution function (RDF) $g(r)$ was calculated for all non-bonded VDW atom pairs which comprise atoms that contribute to non-bonded energy. There $g(r)$ functions were then utilized to estimate VDW separation distance or gap (h_{vdw}), henceforth referred here as VDW zone was also calculated for comparison.

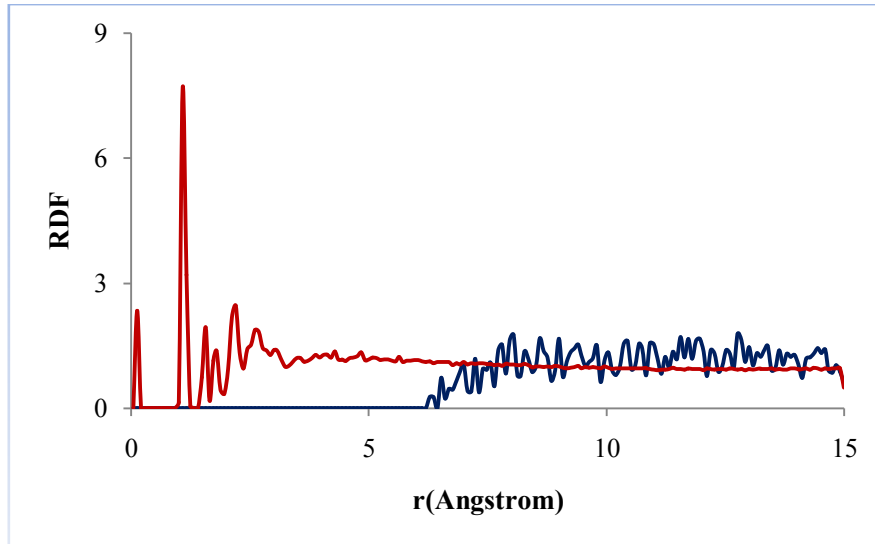


Fig. 6.21: Radial distribution function (RDF) for PP/CNT composite system

Following equilibration, the PP/CNT composite was then subjected to constant-strain minimization for the calculation of mechanical properties. The position of the CNT was kept unchanged in order to maintain the unreformed shape of the CNT. Using this technique a uniform strain field (0.5%) was applied to the periodic cell. Various strain components resulting from applied strains were recorded to derive the stiffness matrix. The final mechanical properties of the polymer/composite system are shown in the Table 6.15.

Table 6.15: Simulated properties of PP/CNT composite system

PP/CNT composite system	
Young's Modulus	39.5 GPa
Bulk Modulus	17.6 GPa
Shear Modulus	4.48 GPa
Compressibility	43.8 TPa ⁻¹

After MD minimization the VDW separation distance between the CNT and the PP matrix is found to be about 0.21 nm and the volume fraction of the CNT (f_{CNT}) is calculated as 24%.

Table 6.16: Summary of numerical results for elastic modulus of PP/CNT composite system

	Molecular dynamics results	Rule of mixtures
Longitudinal elastic modulus (GPa)	39.5	169

6.6.4 Experimental Validation

Tensile performance is an important criterion for practical application of polymer products. In order to achieve excellent tensile properties, main attentions were devoted to improve CNT's dispersion and interfacial interaction of CNTs/matrix. A well dispersion of CNTs in polymer is benefit for eliminating stress concentration (defeats of consistent system), while a strong interfacial adhesion is favorable to stress transfer from CNTs to basal polymer.

Martin Ganß, Bhabani K. Satapathy, Mahendra Thunga, Roland Weidisch, Petra Pötschke and Dieter Jehnichen in an experimental work, studied the deformation and crack resistance behavior of polypropylene (PP) multi-walled carbon nanotube (MWNT) composites [111]. Their experimental work is available in "Structural interpretations of deformation and fracture behavior of polypropylene/multi-walled carbon nanotube composites" *Acta Materialia*, vol. 56, p. 2247–2261, 2008. Polymer nanocomposites containing 0.5, 1, 1.5, 2, 2.5, 3 and 5 wt.% MWNT were prepared by melt-mixing from premixtures of PP powder. Tensile tests were performed with a testing machine at room temperature.

The stiffness E' vs. temperature as plotted in Figure 6.22 shows an enhancement of the modulus (stiffness) with the increase in the amount of MWNT, an observation which is well in accordance with literature. The extent of increase of tensile modulus is relatively high with increasing MWNT content. For example, at room temperature the increase of E' of the nanocomposite with 5 wt % MWNT is 23% compared to pure PP.

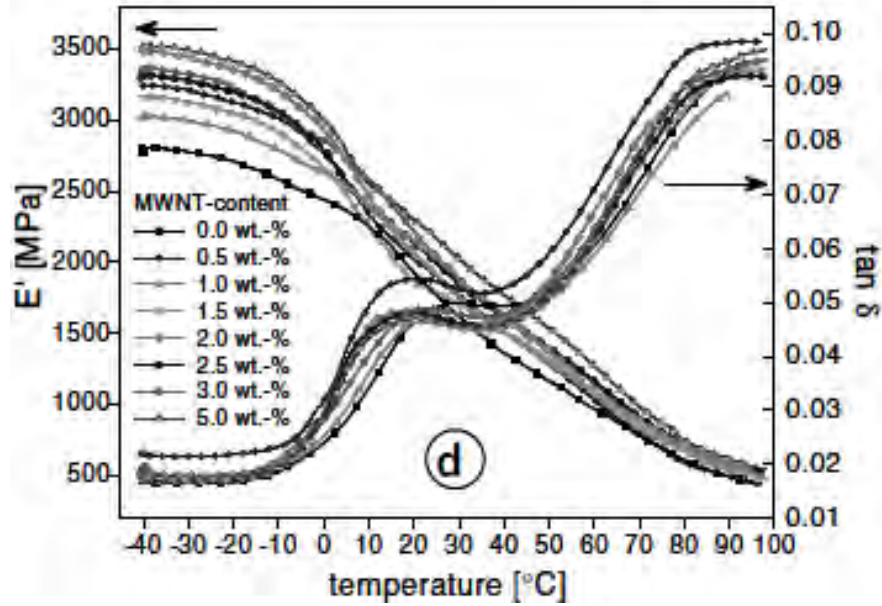


Fig. 6.22: Mechanical reinforcement: melt-rheological investigations showing temperature dependence of Tensile modulus (E') and $\tan\delta$ [111]

In the simulation study, polymer nanocomposite containing 91 wt% SWNT is investigated. By extrapolation, at 91 wt% SWNT, we observe the Young's modulus of the CNT-PP composite will be 7.43 GPa. Since, addition of nanotubes increase the tensile modulus of the polymer films, and the improvement in elastic modulus with the aligned nanotube composite is five times greater than the improvement for the randomly oriented composite [105], in an aligned composite with 91 wt% CNT, the Young's modulus of the composite is expected to be around 37 GPa.

In the experimental work, multi-walled nanotubes are dispersed randomly in PP matrix whereas; in our simulation we embedded SWCNT in an aligned direction inside PP thermoplastic matrix. From the results of our simulation, the measure of reinforcement for SWNT-PP composites at 91 wt% comes about 39.5 GPa which has very close agreement with the results obtained in the experimental study.

6.7 Results and Discussion

6.7.1 PMMA/CNT Composite

In case of CNT (6, 6) reinforced PMMA composite the following graphs are derived from the above reported studies:

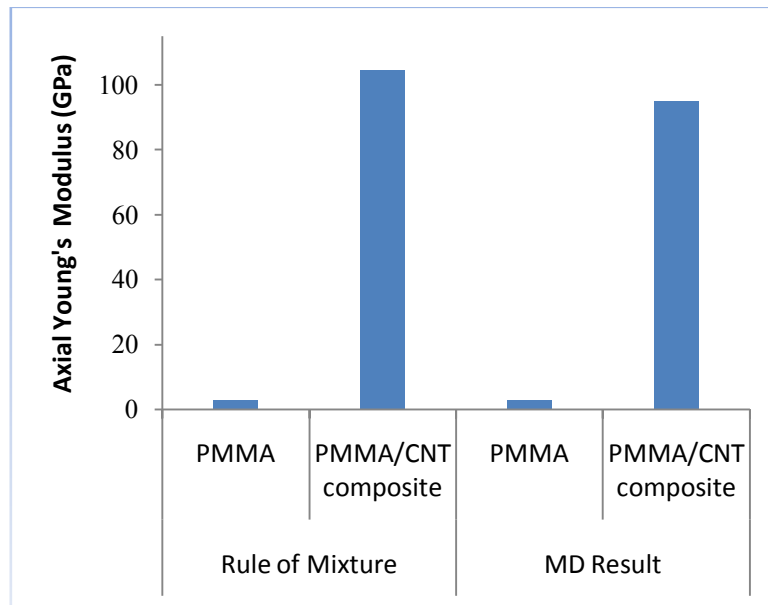


Fig. 6.23: Axial Young's modulus chart of CNT reinforced composite compared with PMMA polymer matrix without nanotubes and the results from the rule-of-mixture.

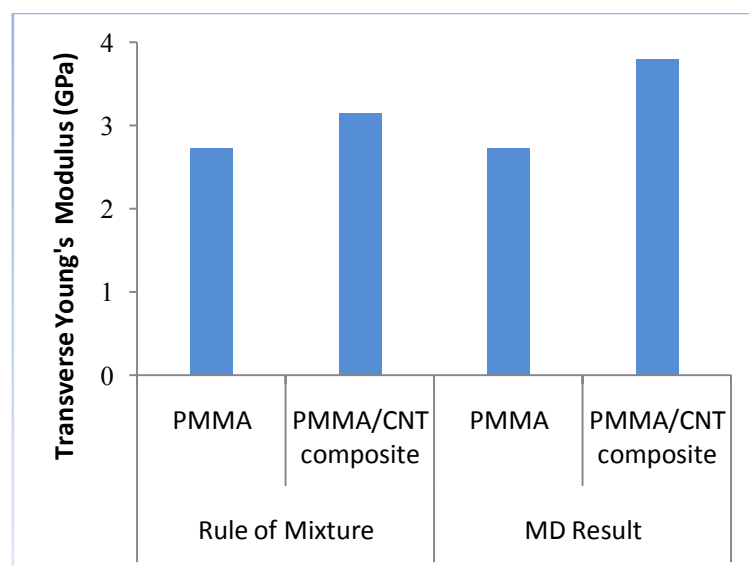


Fig. 6.24: Transverse Young's modulus chart of CNT reinforced composite compared with PMMA polymer matrix without nanotubes and the results from the rule-of-mixture.

The following conclusions can be stated from the Figures 6.23 and 6.24:

1. CNT can substantially enhance the stiffness of CNT/PMMA composite in the direction parallel to the fiber axis.
2. CNT can also improve the stiffness of the composite in transverse direction although not as significant as that in the longitudinal direction.
3. Rule-of-mixture predicted a larger axial elastic modulus than MD, indicating that the perfect interface condition used in the rule-of-mixture needs to be modified to accommodate the real imperfect interface behaviors.

6.7.2 PS/CNT Composite

In case of CNT (6, 6) reinforced PS composite the following graphs are derived from the above reported studies:

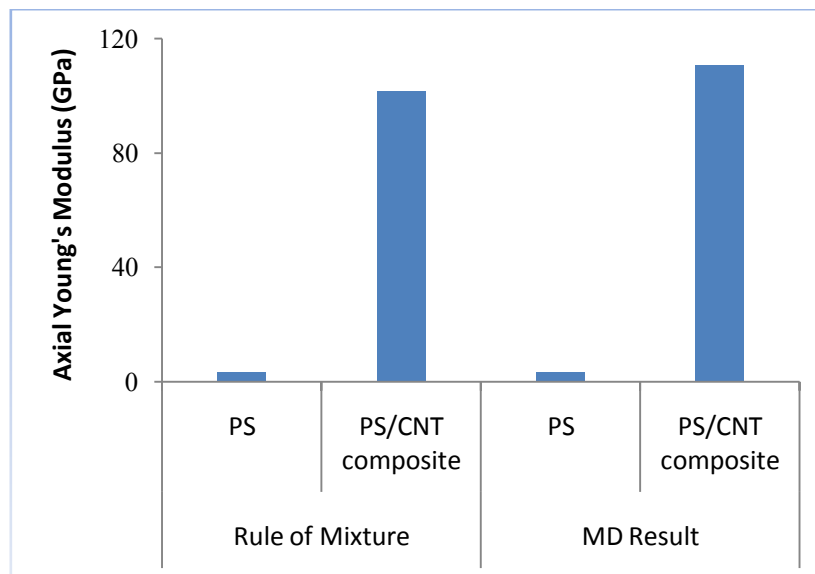


Fig. 6.25: Axial Young's modulus chart of CNT reinforced composite compared with PS polymer matrix without nanotubes and the results from the rule-of-mixture.

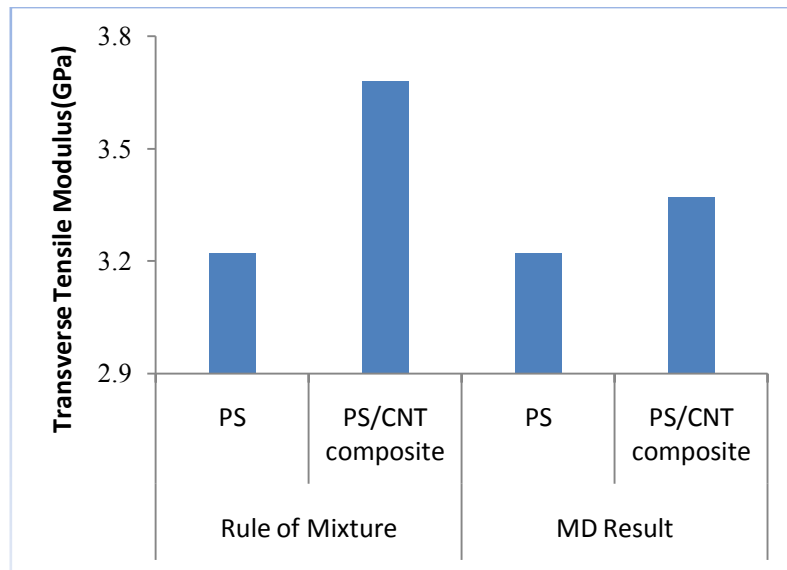


Fig. 6.26: Transverse Young's modulus chart of CNT reinforced composite compared with PS polymer matrix without nanotubes and the results from the rule-of-mixture.

The following conclusions can be stated from the Figures 6.25 and 6.26:

1. CNT can significantly enhance the stiffness of CNT/PS composite in the direction parallel to the fiber axis.
2. CNT can also improve the stiffness of the composite in transverse direction although not as significant as that in the longitudinal direction.
3. MD predicted a larger axial elastic modulus than rule-of-mixture. This could be explained by the interfacial shear stress of the CNT/PS composite system. Fiber-matrix interfacial shear stress is a critical parameter controlling the efficiency of stress transfer and hence some of the important mechanical properties of the composite such as elastic modulus, tensile strength, and fracture toughness. Results of a CNT pullout simulation suggests that the interfacial shear stress of the CNT-PS system is about 160 MPa, significantly higher than most carbon fiber reinforced polymer composite systems [112]. In term of interfacial shear stress, a value for CNT/Epon862 system is given by the work of Gou [113] 75 MPa, a value for CNT/PE system is given by Frankland et al. [114] 2.8 MPa. Zheng et al. [115] found that for PS the interaction is much stronger and increases more rapidly than that of PE and PP. PS is a polymer with aromatic rings, which is therefore expected to possess a strong attractive interaction with the surface of the SWNTs and may play an important role in providing effective adhesion [116]. The

assumption of conventional rule-of mixtures was that the whole system is continuum and the interfaces between the matrix and filler material remain fully intact. In general, the macroscopic rule-of-mixture which takes only the CNT volume fraction into account in determining composite modulus appears to break down for polymer/CNT composites where there are strong interfacial interactions [6].

6.7.3 PA6/CNT Composite

In case of CNT (6, 6) reinforced Nylon 6 composite the following graphs are derived from the above reported studies:

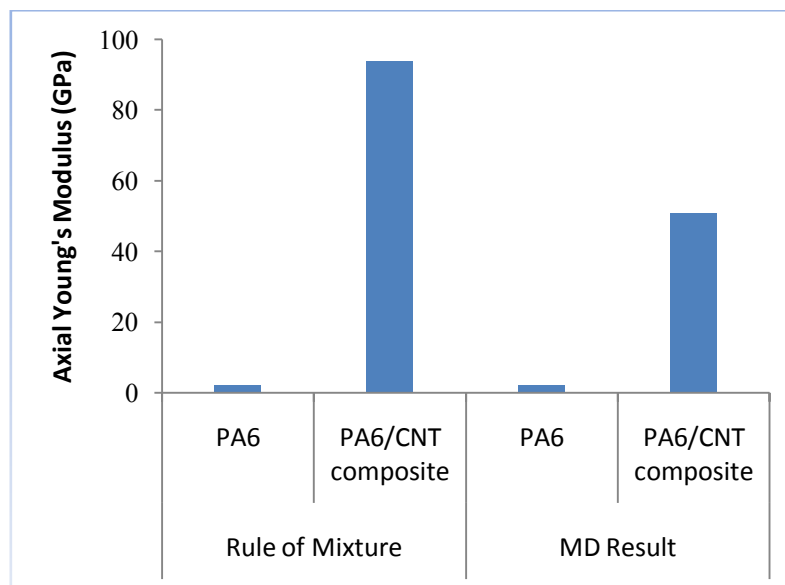


Fig. 6.27: Axial Young's modulus chart of CNT reinforced composite compared with Nylon 6 polymer matrix without nanotubes and the results from the rule-of-mixture.

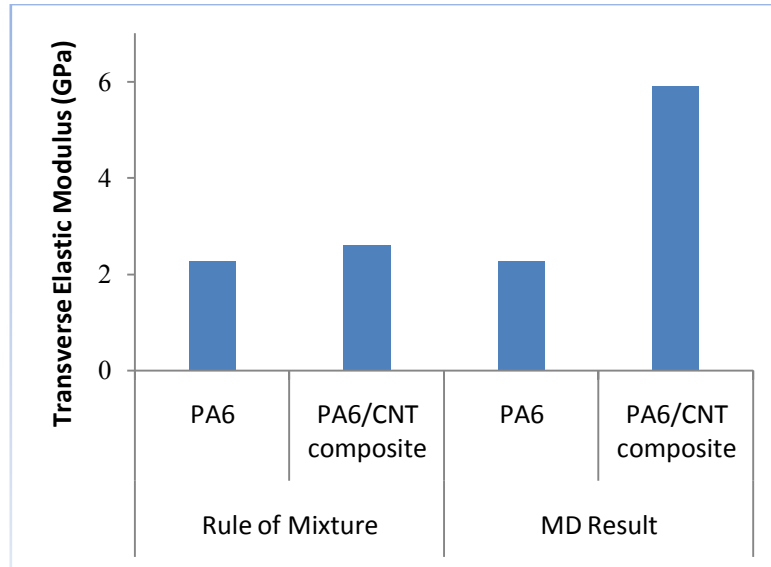


Fig. 6.28: Transverse elastic modulus chart of CNT reinforced composite compared with Nylon 6 polymer matrix without nanotubes and the results from the rule-of-mixture.

The following conclusions can be stated from the Figures 6.27 and 6.28:

1. CNT can substantially enhance the stiffness of CNT/PA6 composite in the direction parallel to the fiber axis.
2. CNT can also improve the stiffness of the composite in transverse direction although not as significant as that in the longitudinal direction.
3. Rule-of-mixture predicted a larger axial elastic modulus than MD, indicating that the perfect interface condition used in the rule-of-mixture needs to be modified to accommodate the real imperfect interface behaviors.

6.7.4 PE/CNT Composite

In case of CNT (6, 6) reinforced PE composite the following graphs are derived from the above reported studies:

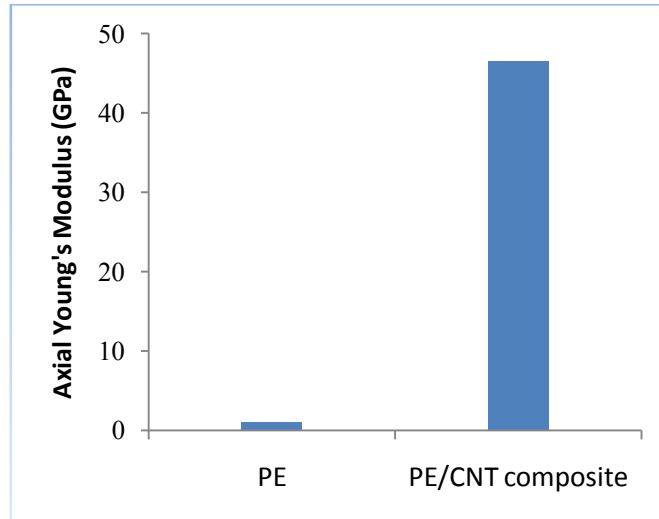


Fig. 6.29: Axial Young's modulus chart of the CNT reinforced composite compared with PE polymer matrix without nanotubes.

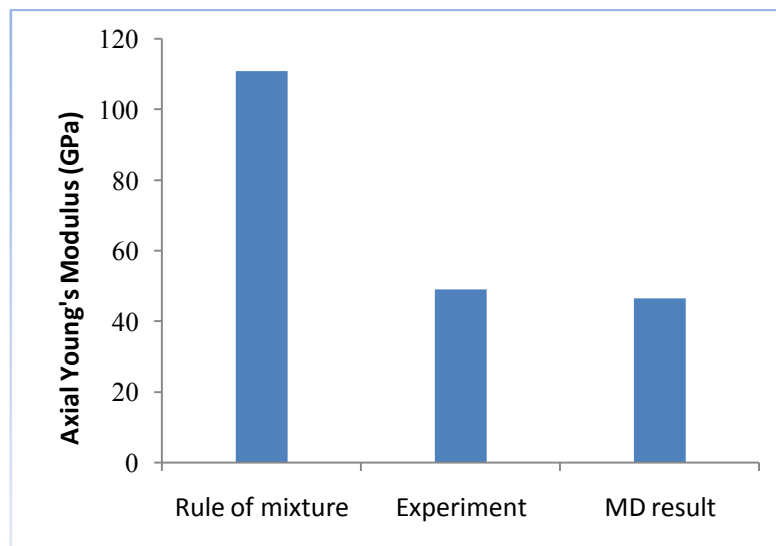


Fig. 6.30: Axial Young's modulus chart of the CNT reinforced composite compared with the results from rule of mixture and experiment.

The following conclusions can be stated from the Figures 6.29 and 6.30:

1. CNT–PE composite shows a good enhancement of mechanical properties with addition of SWNT as fiber in semi-crystalline PE matrix. This improvement of properties is observed in parallel to the fiber direction.
2. MD simulation gives a close agreement to calculate Young’s modulus of CNT–PE composites.
3. Rule-of-mixture predicted a larger elastic modulus than that based on the MD. A large stiffness in the effective property from the rule-of-mixture is perhaps due to the fact that in the rule-of-mixture, the interface between the CNT and the matrix is assumed to be perfectly bonded, whilst the interaction between these two materials could be weak.

6.7.5 PP/CNT Composite

In case of CNT (6, 6) reinforced PP composite the following graphs are derived from the above reported studies:

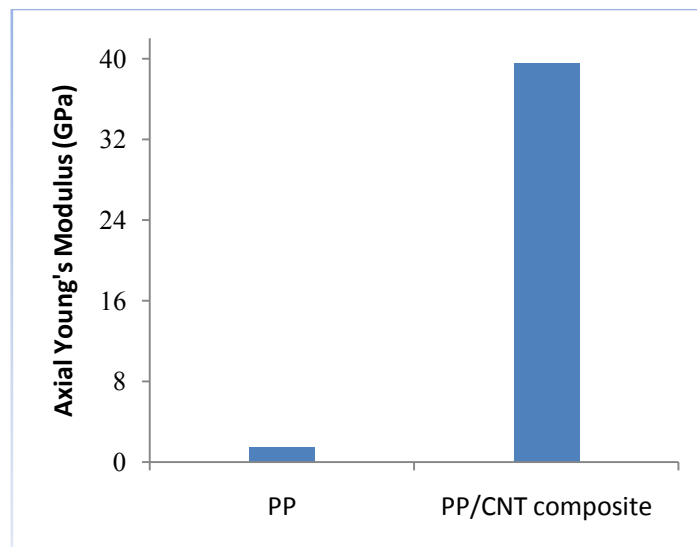


Fig. 6.31: Axial Young’s modulus chart of the CNT reinforced composite compared with PP polymer matrix without nanotubes.

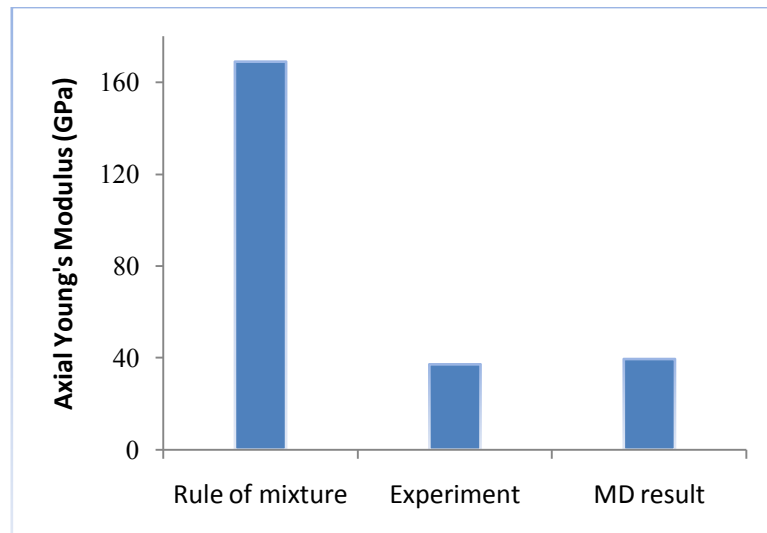


Fig. 6.32: Axial Young's modulus chart of the CNT reinforced composite compared with the results from rule of mixture and experiment.

The following conclusions can be stated from the Figures 6.31 and 6.32:

1. CNT–PP composite shows a good enhancement of mechanical properties with addition of SWNT as fiber in amorphous PP matrix. This improvement of properties is observed in parallel to the fiber direction.
2. MD simulation gives a close agreement to calculate Young's modulus of CNT–PP composites.
3. Rule-of-mixture predicted a larger elastic modulus than that based on the MD. A large stiffness in the effective property from the rule-of-mixture is perhaps due to the fact that in the rule-of-mixture, the interface between the CNT and the matrix is assumed to be perfectly bonded, whilst the interaction between these two materials could be weak.

Chapter 7

Conclusions and Future Work

7.1 Summary and Conclusions

In this work, both SWCNT and MWCNT based composite materials have been studied. In Chapter 5, molecular dynamics simulations of various armchair and zigzag nanotubes were performed to estimate various mechanical properties like Young's modulus, shear modulus, bulk modulus, Poisson's ratio. Our study was motivated from the fact that an accurate assessment of the properties of individual CNTs is essential for the development of CNT-based reinforced composites. Six zigzag and six armchair nanotubes with increasing diameter were chosen to investigate the effects of diameter and chirality. Nanoscale molecular dynamics simulations of the Young's modulus of single-walled carbon nanotubes reveal that the Young's modulus of the single-walled carbon nanotubes decreases significantly with the increase of tube diameter. We demonstrated that the elastic modulus of a SWCNT is insensitive to its tube chirality and tube length. It is also considerable that both the bulk modulus and shear modulus also decreases linearly with increasing tube radius but the Poisson's ratio shows no such relation with the CNT diameter.

In Chapter 6, the effect of matrix material on elastic properties of CNT reinforced composites are studied using molecular dynamics simulations. In this technique, equilibrated structure for both amorphous polymer and nanocomposites models are obtained first, then 0.5% strain field is applied to all models. Elastic Modulus, bulk modulus, shear modulus and compressibility are evaluated for different matrix material like Polyethylene (PE), Polypropylene (PP), Polystyrene (PS), Polyamide 6 (PA6) and Polymethyl methacrylate (PMMA). Simulation result demonstrates that. CNT can significantly improve the elastic property of CNT reinforced composite in the direction parallel to the fiber axis. CNT also improves the elastic property of the composite in transverse direction but not as significant as that in the longitudinal direction. The effective Young's moduli of CNT-based composites found by MD simulations are compared with values obtained using rule-of-mixture. In two cases the simulation results

are also compared with experimentally available values. The results are in disagreement revealing the fact that rule-of-mixture is not an excellent approximate in estimating the overall response of the composite system since it assumes perfect bonding between fiber and matrix. MD simulation gives a close agreement to calculate Young's modulus of CNT based composite since the results are in good agreement with experimentally available data.

.7.2 Recommendations for Future Work

The following research problems can be considered as the possible extensions of the current work:

The research has focused, so far, on the properties of single CNTs in resin only. Much can be said in terms of the validity of these calculations as SWNTs, for instance, are often found in bundles when manufacturing nanocomposite materials. Thus, future modeling work should also focus on closing this gap.

In this study, no defects have been considered in modeling nanostructures. In reality, nanostructure contains point, line and volume defects as well as process induced defects and flaws. More detailed molecular models can be constructed by including as many types of defects as possible.

Alignment of nanotube is a major issue in preparing nanocomposites. It is generally found that in experimental study of nanocomposites, CNTs mostly remain dispersed inside the resin. The present study has only considered in-parallel continuous alignment of single-walled nanotubes. In this case, numerous improvements can still be made.

We also suggest attention be directed to the geometrical arrangement of the resin molecules in the resin system such as the orientation of the resin molecules around the nanotubes. In a broader manner, many curing resin systems can be examined in order to improve our knowledge of the effect of CNTs on resin systems.

LIST OF REFERENCES

1. Kroto H.W., Heath J. R., O'Brien S. C., Curl R. F., Smalley R.E., "C₆₀: Buckminsterfullerene", *Nature*, vol. 318, p. 162, 1985.
2. Iijima S., "Helical Microtubules of Graphitic Carbon", *Nature*, vol. 354, p. 56, 1991.
3. O Marietta-Tondin, "Molecular modeling of nanotube composite materials: interface formation, interfacial strength and thermal expansion", Ph.D. dissertation, The Florida State University, 2006.
4. M. Terrones, "Science and Technology of the Twenty-First Century: Synthesis, Properties and Applications of Carbon Nanotubes", *Annual Review in Materials Research*, vol. 33, p. 419, 2003.
5. K. Talukdar, A.K. Mitra, "Comparative MD simulation study on the mechanical properties of a zigzag single-walled carbon nanotube in the presence of Stone-Thrower-Wales defects", *Composite Structures*, vol. 92, p. 1701–1705, 2010.
6. Y. Han and J. Elliott, "Molecular dynamics simulation of the elastic properties of polymer/carbon nanotube composites", *Computational Material Science*, vol. 39, p. 315-323, 2007.
7. Schaffer J. P., Saxena A., Antolovich S. D., Sanders S. B., Warner T. H., "The Science and Design of Engineering Materials", McGraw Hill, NY, USA, 1995.
8. Jordan J., Jakob K.I., Tannenbaum R., Sharaf M.A., Jasiuk I., "Materials Science and Engineering A", vol. 393, p. 1, 2005.
9. P.K. Valavala, G.M. Odegard, "Modeling techniques for determination of Mechanical properties of polymer Nanocomposites", *Rev. Adv. Mater. Sci.*, vol. 9, p. 34-44, 2005.
10. M. Monthieux, V.L. Kuznetov, "Guest Editorial: Who should be given the credit for the discovery of carbon nanotubes?" *Carbon*, vol. 44, 2006.
11. L.V. Radushkevich, V.M. Lukyanovich, "O structure ugleroda, obrazujucesja pri termiceskom razlozenii okisi ugleroda na zeleznom kontakte", *Zurn Fisic Chim*, vol. 26, p. 88, 1952.
12. A. Oberlin, M. Endo, T. Koyama, "Filamentous growth of carbon through benzene decomposition", *Journal of Crystal Growth*, vol. 32, p. 335, 1976.
13. H. G. Tennent, "Carbon fibrils, method for producing same and compositions containing same", United States Patent #4663230, 1987.
14. Ebbesen T. W., Ajayan P. M., "Large-scale synthesis of carbon nanotubes", *Nature*, vol. 358, p. 220, 1992.

15. Iijima S., Ichihashi T., "Single-shell carbon nanotubes of 1-nm diameter", *Nature*, vol. 363, p. 603, 1993.
16. H.W. Zhang, J.B. Wang, X. Guo, "Predicting the elastic properties of single-walled carbon nanotubes", *Journal of the Mechanics and Physics of Solids*, vol. 53, p. 1929–1950, 2005.
17. P. Singh, R.M. Tripathi, A. Saxena, "Synthesis of carbon nanotubes and their biomedical application", *Journal of Optoelectronics and Biomedical Materials*, vol. 2, p. 91 -98, 2010.
18. Thess. A, Lee. R, Nikolaev. P, Diah. H, Petit. P, Robert. J, Xu. C, Fischer. J.E, Samalley. R.E, "Crystalline ropes of metallic nanotubes", *Science*, vol. 273, p. 483-487, 1996.
19. Cassel A, Raymakers J, Kong J, Dia H, "Large scale synthesis of single-walled carbon nanotubes", *J. Phys. Chem.B*, vol. 103, p. 6484-6492, 1999.
20. M. S. Dresselhaus, G. Dresselhaus, J. C. Charlier, E. Hernandez, "Electronic, thermal and mechanical properties of carbon nanotubes", *Phil. Trans. R. Soc. Lond.*, vol. 362, p. 2065–2098, 2005.
21. M.P. Allen, "Introduction to Molecular Dynamics Simulation", John von Neumann Institute for Computing, UK, NIC Series, vol. 23, p. 1-28, 2004.
22. Alder B. J., Wainwright T. E., *Journal of Chemical Physics*, vol. 27, p. 1208, 1957.
23. Rahman A., *Phys. Rev.*, vol. A136, p. 405, 1964.
24. Stillinger, F. H., Rahman, A. *J. Chem. Phys.* 60, p. 1545, 1974.
25. McCammon, J. A., Gelin, B. R., Karplus, M., *Nature (Lond.)*, vol. 267, p. 585, 1977.
26. D. Chandler, "Introduction to Modern Statistical Mechanics", Oxford University Press, NY, 1987.
27. R. E. Wilde, S. Singh, "Statistical Mechanics, Fundamentals and Modern Applications", John Wiley & Sons, Inc, New York, 1998.
28. Y. Jin, F.G. Yuan, "Simulation of elastic properties of single-walled carbon nanotubes", *Composites Science and Technology*, vol. 63, p. 1507–1515, 2003.
29. R. W. Hockney, "The potential calculation and some applications, *Methods in computational physics*", vol. 9, p.136, 1970.
30. W. C. Swope, H. C. Anderson, P. H. Berens, K. R. Wilson, "A computer simulation method for the calculation of equilibrium constants for the formation of physical cluster of molecules: applications to small water clusters", *Journal of chemical physics*, vol. 76, p. 637, 1982.
31. D. Beeman, "Some multistep methods for use in molecular dynamics calculations", *Journal of computational physics*, vol. 20, p. 130, 1976.
32. Allen MP, Tildesley DJ., "Computer simulations of liquids", Oxford University Press, NY, 1987.

33. <http://www.accelrys.com/products/mstudio>; Materials Studio; Accelrys (2006).
34. H.J.C. Berendsen, J.P.M. Postma, W.F. van Gunsteren, A. DiNola, J.R. Haak, “*Molecular dynamics with coupling to an external bath*”, J. Chem. Phys., vol. 81, p. 3684-3690, 1984.
35. S. Nosé, J. Chem. Phys. 81511; Mol. Phys., vol. 52, p. 255, 1984.
36. W. G. Hoover, “*Canonical dynamics: equilibrium phase space distribution*”, Phys. Rev. A vol. 31, p. 169, 1985.
37. H.C. Andersen, “*Molecular dynamics simulations at constant pressure and/or temperature*”, J. Chem. Phys., vol.72, p. 2384-2393, 1980.
38. M. Parrinello and A. Rahman, J. Appl. Phys., vol. 52, p. 7182, 1982.
39. H. Sun, “*Ab initio calculations and force field development for computer simulation of polysilanes*”, Macromolecules, vol. 28, p.701, 1995.
40. J. Yang, Y. Ren, A. Tian, H. Sun, “*COMPASS Force Field for 14 Inorganic Molecules, He, Ne, Ar, Kr, Xe, H₂, O₂, N₂, NO, CO, CO₂, NO₂, CS₂, and SO₂, in Liquid Phases*”, Journal of Physical Chemistry B, vol. 104, p. 4951-4957, 2000.
41. H. Sun, P. Ren, J.R. Fried, “*The COMPASS force field: parameterization and validation for phosphazenes*”, Computational and Theoretical Polymer Science, vol. 28, p. 229-246, 1998.
42. J. R. Maple, M. J. Hwang, T. P. Stockfisch, U. Dinur, M. Waldman, C. S. Ewig, A. T. Hagler, “*Derivation of class II force fields. i. methodology and quantum force field for the alkyl functional group and alkane molecules*”, Journal of Computational Chemistry, vol. 15, p.162, 1994.
43. H. Sun, “*Force field for computation of conformational energies, structures, and vibrational frequencies of aromatic polyesters*”, Journal of Computational Chemistry, vol. 15, p.752-768, 1994.
44. H. Sun, “*COMPASS: An ab-initio force-field optimized for condensed-phase applications – Overview with details on alkene and benzene compounds*”, Journal of physical chemistry B, vol. 102, p. 7338, 1998.
45. M. Waldman, A. T. Hagler, “*New Combining Rules for Rare Gas van der Waals Parameters*”, Journal of Computational Chemistry, vol. 14, p.1077, 1993
46. S.J.V. Frankland, V.M. Harik, G.M. Odegard, D.W. Brenner, T.S. Gates , “*The Stress-Strain Behavior of Polymer-Nanotube Composites from Molecular Dynamics Simulation*”, Composites Science and Technology, vol. 63, p. 1655–1661, 2003.
47. Fung CY. “*Foundations of solid mechanics*”, Englewood Cliffs (NJ): Prentice-Hall, 1965.
48. Nielsen OH, Martin RM., “*Quantum-mechanical theory of stress and force*”, Phys Rev B, vol. 32, p. 3780–379, 1995.

49. Vitek V, Egami T., “*Atomic level stresses in solids and liquids*”, Phys. Stat Solidi B: Basic Research, vol. 144, p. 145–156, 1987.
50. Tsai S.W., “*Composites design*”, Dayton OH, Think Composites Press, 1988.
51. Harik VM., “*Ranges of applicability for the continuum beam model in the mechanics of carbon nanotubes and nanorods*”, Solid State Commun, vol. 120, p. 331–335, 2001.
52. Lau KT, Hui D., “*The revolutionary creation of new advanced materials: carbon nanotube composites*”, Composites: Part B, vol. 33, p. 263–277, 2002.
53. Qian D, Wagner GJ, Liu WK, Yu MF, Ruoff RS, “*Mechanics of carbon nanotubes*”, Appl Mech Rev, vol. 55, p. 495–533, 2002.
54. Thostenson ET, Ren Z, Chou TW. “*Advances in the science and technology of carbon nanotubes and their composites: a review*”, Compos Sci Technol 2001; 61:1899–912.
55. Yakobson BI, Avouris P., “*Mechanical properties of carbon nanotubes*”, Carbon nanotubes. Berlin–Heidelberg: Springer Verlag, p. 287–327, 2001.
56. Qian D, Dickey EC, Andrews R, Rantell T., “*Load transfer and deformation mechanisms in carbon nanotube-polystyrene composites.*”, Appl Phys Lett , vol. 76, p. 2868–2870, 2000.
57. Schadler LS, Giannaris SC, Ajayan PM, “*Load transfer in carbon nanotube epoxy composites*”, Appl Phys Lett, vol. 73, p. 3842–3844, 1998.
58. Wanger HD, Lourie O, Feldman Y, Tenne R., “*Stress-induced fragmentation of multiwall carbon nanotubes in a polymer matrix*”, Appl Phys Lett, vol. 72, p.188–190, 1998.
59. Treacy MMJ, Ebbesen TW, Gibson JM, “*Exceptionally high young’s modulus observed for individual nanotubes*”, Nature, vol. 381, p. 678–680, 1996.
60. Wong EW, Sheehan PE, Lieber CM., “*Nanobeam mechanics: elasticity, strength, and toughness of nanorods and nanotubes*”, Science, vol. 277, p. 1971–1975, 1997.
61. Yu MF, Lourie O, Dyer MJ, Moloni K, Kelly TF, Ruoff RS., “*Strength and breaking mechanism of multi-walled carbon nanotubes under tensile load*”, Science, vol. 287, p. 637–640, 2000.
62. Krishnan A, Dujardin E, Ebbesen TW, Yianilos PN, Treacy MMJ., “*Young’s modulus of single walled nanotubes*”, Phys Rev B, vol. 58, p. 14013–14019, 1998.
63. Lu J P, “*Elastic Properties of Carbon Nanotubes and Nanoropes*”, Phys. Rev. Lett., vol. 79, p. 1297, 1997.
64. Yakobson B I, Brabec C J, Bernholc J, “*Nanomechanics of Carbon Tubes: Instabilities beyond Linear Response*”, Phys. Rev. Lett., vol. 76, p. 2511, 1996.
65. Robertson D H, Brenner D W, Mintmire J W, “*Energetics of nanoscale graphitic tubules*”, Phys. Rev. B, vol. 45, p. 12592, 1992.

66. Cornwell C F, Wille L T, “*Elastic properties of single-walled carbon nanotubes in compression*”, Solid State Commun., vol. 101, p. 555, 1997.
67. Hernandez E, Goze C, Bernier P, Rubio A, “*Elastic Properties of C and B_xC_yN_z Composite Nanotubes*”, Phys. Rev. Lett., vol. 80, p. 4502, 1998.
68. S´anchez-Portal D, Artacho E, Soler J M, Rubio A, Ordejón P, “*Ab initio structural, elastic, and vibrational properties of carbon nanotubes*”, Phys. Rev. B, vol. 59, p. 12678, 1999.
69. Van Lier G, Van Alsenoy C, Van Doren V, Geerlings P, “*Ab initio study of the elastic properties of single-walled carbon nanotubes and graphene*”, Chem. Phys. Lett., vol. 326, p. 181, 2000.
70. Peralta-Inga Z, Boyd S, Murray J S, O’Connor C J, Politzer P, “*Density Functional Tight-Binding Studies of Carbon Nanotube Structures*”, Struct. Chem., vol. 14, p. 431, 2003.
71. Xang X Y, Wang X, “*Numerical simulation for bending modulus of carbon nanotubes and some explanations for experiment*”, Composites B, vol. 35, p. 79, 2004.
72. Wang X, Zhang Y C, Xia X H, Huang C H, “*Effective bending modulus of carbon nanotubes with rippling deformation*”, Int. J. Solids Struct., vol. 41, p. 6429, 2004.
73. Cai H, Wang X, “*Effects of initial stress on transverse wave propagation in carbon nanotubes based on Timoshenko laminated beam models*”, Nanotechnology, vol. 17, p. 45, 2006.
74. Treacy M M J, Ebbesen T W, Gibson J M, “*Exceptionally high Young’s modulus observed for individual carbon nanotubes*”, Nature, vol. 381, p. 678, 1996.
75. Krishnan A, Dujardin E, Ebbesen T W, Yianilos P N, Treacy M M J, “*Young’s modulus of single-walled nanotubes*”, Phys. Rev. B, vol. 58, p. 14013, 1998.
76. Wong E W, Sheehan P E, Lieber C M, “*Nanobeam mechanics: elasticity, strength, and toughness of nanorods and nanotubes*”, Science, vol. 277, p. 1971, 1997.
77. Tomblor T W, Zhou C, Alexseyev L, Kong J, Dai H, Liu L, Jayanthi C S, Tang M, Wu S-Y, “*Reversible electromechanical characteristics of carbon nanotubes under local-probe manipulation*”, Nature, vol. 405, p. 769, 2000.
78. Ranjbartoreh A.R., Wang G, “*Consideration of mechanical properties of single-walled carbon nanotubes under various loading conditions*”, J Nanopart Res, vol. 12, p. 537–543, 2010.
79. L. Z. Liu, H. L. Gao, J. J. Zhao, J. P. Lu, “*Superelasticity of Carbon Nanocoils from Atomistic Quantum Simulations*”, Nanoscale Res Lett, vol. 5, p. 478–483, 2010.
80. Y. Jin, F.G. Yuan, “*Simulation of elastic properties of single-walled carbon nanotubes*”, Composites Science and Technology, vol. 63, p. 1507–1515, 2003.

81. T.T. Liu, X. Wang, “*Dynamic elastic modulus of single-walled carbon nanotubes in different thermal environments*”, Physics Letters A, vol. 365, p.144–148, 2007.
82. T. Natsuki , M. Endo, “*Stress simulation of carbon nanotubes in tension and compression*”, Carbon, vol. 42, p. 2147–2151, 2004.
83. Schaffer J. P., Saxena A., Antolovich S. D., Sanders, S. B. Warner T. H., “*The Science and Design of Engineering Materials*”, McGraw Hill, NY, USA, 1995.
84. S. B. Sane, T. Cagin, W. A. Goddard, W. G. Knauss, “*Molecular dynamics simulation to compute the bulk response of amorphous PMMA*”, Journal of Computer-Aided Materials Design, vol. 8, p. 87-106, 2001.
85. A. Adnan, C.T. Sun, H. Mahfuz, “*A molecular dynamics simulation study to investigate the effect of filler size on elastic properties of polymer nanocomposites*”, Composites Science and Technology, vol. 67, p. 348-356, 2007.
86. G. M. Odegard, T. C. Clancy, T. S. Gates, “*Modeling of the mechanical properties of nanoparticle/polymer composites*”, Polymer, vol. 46, p. 553-562, 2005.
87. J. Gou, Z. Liang, C. Zhang, B. Wang, “*Computational analysis of effect of single-walled carbon nanotube rope on molecular interaction and load transfer of nanocomposites*”, Composites: Part B, vol. 36, p. 524-533, 2005.
88. R. Zhu, E. Pan, A.K. Roy, “*Molecular dynamics study of the stress-strain behavior of carbon nanotube reinforced Epon 862 composites*”, Materials Science and Engineering A, vol. 447, p. 51-57, 2007.
89. A. Al-Ostaz, G. Pal, P. R. Mantena, A. Cheng, “*Molecular dynamics simulation of SWNT-polymer nanocomposite and its constituents*”, J Mater Sci, vol. 43, p. 164-173, 2008.
90. S.J.V. Frankland, V.M. Harik, G.M. Odegard, D.W. Brenner, T.S. Gates, “*The stress-strain behavior of polymer-nanotube composites from molecular dynamics simulation*”, Composites Science and Technology, vol. 63, p.1655-1661, 2003.
91. H. Yang, X. J. Zhao, Z. S. Li, F. D. Yan, “*Molecular dynamics simulations on crystallization of polyethylene/fullerene nanocomposites*”, The journal of chemical physics, vol. 130, 2009.
92. S.C. Chowdhury, T. Okabe, “*Computer simulation of carbon nanotube pull-out from polymer by the molecular dynamics method*”, Composites: Part A, vol. 38, p. 747–754, 2007.
93. S. H. Yang, Z. X. Wei, “*Molecular dynamics study of mechanical properties of carbon nanotube-embedded gold composites*”, Physica B, vol. 403, p. 559–563, 2008.
94. www.wikipedia.org, the free web based encyclopedia accessed on 26-08-2011.
95. www.polymerprocessing.com, accessed on 26-08-2011.

96. T. Mulder, V. A. Harmandaris, A. V. Lyulin, N. F. A. Van der Vegt, B. Vorselaars, M. A. J. Michels, “*Equilibration and Deformation of Amorphous Polystyrene: Scale-jumping Simulational Approach*”, *Macromol. Theory Simul.*, vol. 17, p. 290–300, 2008.
97. J. Joshi, R. Lehman, T. Nosker, “*Selected Physical Characteristics of Polystyrene/High Density Polyethylene Composites Prepared from Virgin and Recycled Materials*”, *Journal of Applied Polymer Science*, vol. 99, p. 2044–2051, 2006
98. P. G. Galanty, G. A. Bujtas, “*Modern Plastics Encyclopedia*” vol. 92, p. 23-30, McGraw Hill, 1992.
99. www.engr.utk.edu, accessed on 26-08-2011
100. D. Hossain, M.A. Tschopp, D.K. Ward, J.L. Bouvard, P. Wang, M.F. Horstemeyer, “*Molecular dynamics simulations of deformation mechanisms of amorphous polyethylene*”, *Polymer*, vol. 51, p. 6071-6083, 2010.
101. Plastics Pipe Institute (PPI), “*Engineering Properties of Polyethylene*”, The Society for the Plastics Industry, Inc., 1993.
102. Van Krevelen DW, “*Properties of polymers*”, 3rd edition, Amsterdam, Elsevier; 1990.
103. www.boedeker.com, accessed on 30-08-2011
104. N. H. Ladizesky, I. M. Ward, “*Determination of Poisson's ratio and Young's modulus of low-density polyethylene*”, *Journal of Macromolecular Science, Part B*, vol. 5, 1971.
105. Thostenson ET, Chou TW, “*Aligned multi-walled carbon nanotube reinforced composites: processing and mechanical characterization*”, *J Phys D: Appl Phys*, vol. 35, p. 77–80, 2002.
106. Ji XL, Jing JK, Jiang W, Jiang BZ, “*Tensile modulus of polymer nanocomposites*”, *Polym Eng Sci*, vol. 42, p. 983–93, 2002.
107. Zou Y, Feng Y, Wang L, Liu X, “*Processing and properties of MWNT/HDPE composites*”, *Carbon*, vol. 42, p. 271–277, 2004.
108. S. Kanagaraj, Fátima R. Varanda, Tatiana V. Zhil'tsova, Mónica S.A. Oliveira, Jose' A.O. Simões, “*Mechanical properties of high density polyethylene/carbon nanotube composites*”, *Composites Science and Technology*”, vol. 67, p. 3071–3077, 2007.
109. C. Maier, T. Calafut, “*Polypropylene: the definitive user's guide and databook*”, William Andrew, Norwich, NY, 1998.
110. H. Peter Frank, “*Polypropylene*”, Gordon and Breach Science Publishers, NY, 1968.
111. M. Ganß, B. K. Satapathy, M. Thunga, R. Weidisch, P. Pötschke, D. Jehnichen, “*Structural interpretations of deformation and fracture behavior of polypropylene/multi-walled carbon nanotube composites*”, *Acta Materialia*, vol. 56, p. 2247–2261, 2008.
112. Liao K., Li S., “*Interfacial characteristics of a carbon nanotube-polystyrene composite system*”, *Applied physics letters*, vol. 79, p. 4225, 2001.

113. Gou J., Minaie B., Wang B., Liang Z., Zhang C., “*Computational and experimental study of interfacial bonding of single-walled nanotube reinforced composites*”, Computational Materials Science, vol. 31, p. 225, 2004.
114. S. J. V. Frankland, A. Caglar, D. W. Brenner, M. Griebel, “*Molecular simulation of the influence of chemical cross-links on the shear strength of carbon nanotube-polymer interfaces*”, Journal of physical chemistry, vol. 106, p. 3046, 2002.
115. Q. Zheng, Q. Xue, K. Yan, L. Hao, Q. Li, X. Gao, “*Investigation of Molecular Interactions between SWNT and Polyethylene/Polypropylene/ Polystyrene/Polyaniline Molecules*”, J. Phys. Chem. C, vol. 111, p. 4628-4635, 2007.
116. M. Yang, V. Koutsos, M. Zaiser, “*Interactions between Polymers and Carbon Nanotubes: A Molecular Dynamics Study*”, J. Phys. Chem. B, vol. 109, p. 10009-10014, 2005.